(1)

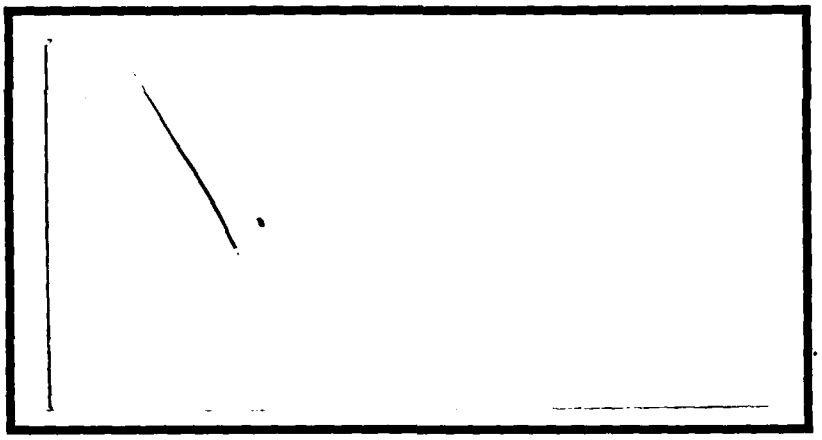

DEPARTMENT OF THE AIR FORCE

AIR UNIVERSITY

AIR FORCE INSTITUTE OF TECHNOLOGY

Wright-Patterson Air Force Base, Ohio

(1)

AFIT/GAE/AA/88D-30

THE EFFECTS OF LOADING HISTORY AND CLOSURE ON THE FATIGUE CHARACTERISTICS OF HEAT TREATED Ti-6Al-2Sn-4Zr-6Mo

THESIS

Jerardo A. Pérez
Captain, USAF

AFIT/GAE/AA/88D-30

Approved for public release; distribution unlimited

AFIT/GAE/AA/88D-30

THE EFFECTS OF LOADING HISTORY AND CLOSURE ON THE FATIGUE CHARACTERISTICS OF HEAT TREATED Ti-6Al-2Sn-4Zr-6Mo

THESIS

Presented to the Faculty of the School of Engineering

of the Air Force Institute of Technology

Air University

In Partial Fulfillment of the

Requirements for the Degree of

Master of Science in Aeronautical Engineering

Jerardo A. Pérez

Captain, USAF

December 1988

Preface

The primary goal of this study was to examine the fatigue characteristics of heat treated Ti-6Al-2Sn-4Zr-6Mo (Ti 6246) and how they were affected by loading history and crack closure. The fatigue properties of Ti 6246 improved as a result of the additional heat treatment. Thus, this material would be well suited for current applications of standard Ti 6246 for which the fatigue characteristics are critical.

A secondary objective, although not mentioned as such in this study, was to validate the operability of AFIT's newly acquired laser interferometric displacement gage (IDG). The completion of my thesis using this new IDG would not have been possible without the assistance of George Hartman, University of Dayton Research Institute, and Jay Anderson, AFIT's Aero/Astro Engineering Lab. I would also like to thank Jay Jira, Jim Larsen, and Ted Nicholas from AFWAL/MLLN for their assistance. Also, I am grateful for the guidance and support of my faculty advisor, Dr. S. Mall.

I would also like to thank my father and mother, [redacted] for their moral support. Lastly, I could not have completed my work without the understanding and patience my wife [redacted] and [redacted] daughters, [redacted] gave me during the times I needed it most.

Table of Contents

List of Figures

List of Tables

Abstract

The main objective of this study was to investigate the effects of loading history and crack closure on the fatigue threshold properties of heat treated Ti-6Al-2Sn-4Zr-6Mo. The crack closure measurements taken by a clip gage, strain gage mounted on the back face (BFS), and laser interferometric displacement gage (IDG) were compared. Also, the effects of heat treating on the fatigue characteristics of Ti 6246 were discussed.

Two different types of tests were run using compact test specimens at a test frequency of 30 hz. The first type of test included holding R, the loading ratio, constant throughout the test. Two tests of this type were conducted, the ASTM decreasing K and varying ΔK tests. Since no experimental data for additionally heat treated Ti 6246 was found, the ASTM decreasing K tests established the reference lines used in the remainder of this study. Next, the effects of overloads on the fatigue threshold were examined using the varying ΔK test. Here, K_{max} was dropped instantaneously after an overload condition while maintaining a constant R for the test. If threshold was not reached, the test was repeated with a larger K_{max} drop after the overload than before.

The second type of test utilized a varying R. For these

constant K_{max} tests, K_{max} was held constant while K_{min} was gradually increased. Thus, a constant plastic zone size ahead of the crack tip resulted. All the tests in this study were run at low R values so that the effects of crack closure could be examined.

The results from these tests indicated that additionally heat treating Ti 6246 did improve its fatigue threshold characteristics. Also, out of the three measurements techniques used, the IDG measured the highest closure loads. Further, with the constant K_{max} test under tensile cyclic loading, threshold could not be reached for R less than 0.5 as desired for closure studies.

Other results included the effects of loading history and closure on the fatigue threshold behavior of heat treated Ti 6246. The ΔK_{th} was found to be dependent on R, loading history, and crack closure. The $\Delta K_{eff,th}$, on the other hand, was relatively constant for the ASTM decreasing K and constant K_{max} tests. However, since the threshold data for the varying ΔK tests did not coincide with the other tests, $\Delta K_{eff,th}$ should not be considered a material property until further research involving the effects of overloads is conducted.

The Effects of Loading History and Closure on the Fatigue Characteristics of Heat Treated Ti-6Al-2Sn-4Zr-6Mo

I. Introduction

Overview

The quest for speed and performance during the Jet Age of the 1950's demanded new material technology for the production of aircraft. Corrosion resistance, a high melting point, and, most importantly, a high strength-to-weight ratio have prompted the use of titanium alloys by the aircraft industry. Today, titanium alloys have been used extensively in air frames and gas turbine engines, particularly the discs and fan blades of the compressor unit. Since gas turbine engines are subjected to high cycle vibration, the fatigue crack propagation and threshold characteristics of titanium alloys have become important.

Despite all the research conducted thus far, an accurate means of predicting fatigue life has yet to be developed. A threshold stress intensity range, ΔK_{th}, is currently used as the design parameter for high cycle fatigue. However, ΔK_{th} is highly dependent on stress ratios, loading histories, and crack closure. Thus, information on ΔK_{th} and the factors influencing it is needed.

Background

A common tool for studying fatigue crack propagation

characteristics has long been the double-logarithmic plot of crack growth rate versus the stress intensity range. The plot can be broken down into three main regions. Region A shown in Figure 1 represents the stress intensity range for the fatigue threshold, ΔK_{th}, where the crack will no longer propagate. At the other end of the plot, region C represents the stress intensity range for the critical crack growth, ΔK_{Ic}, where the specimen will fail immediately without any need for load cycling.

The Paris-Erdogan (1:528) equation is used to model region B as a straight line. The form of the equation most commonly used is:

$$\frac{da}{dN} = C(\Delta K)^n \qquad (1)$$

where da/dN represents the crack growth rate, ΔK is the stress intensity range, and C and n are material constants which need to be determined. Unfortunately, this equation is only valid for region B. Also, even though it is approximated as such, region B is not a straight line.

New designs are incorporating the concept of pre-existing flaws which could cause cracks early in the component's service life. So, ΔK_{th} has become the critical parameter when designing the fatigue life of a component. If service loads are maintained at and below those calculated from ΔK_{th}, then the life of the component can be extended. However, ΔK_{th} has been found to be dependent on various factors including stress ratios, loading histories, crack closure, and specimen geometry.

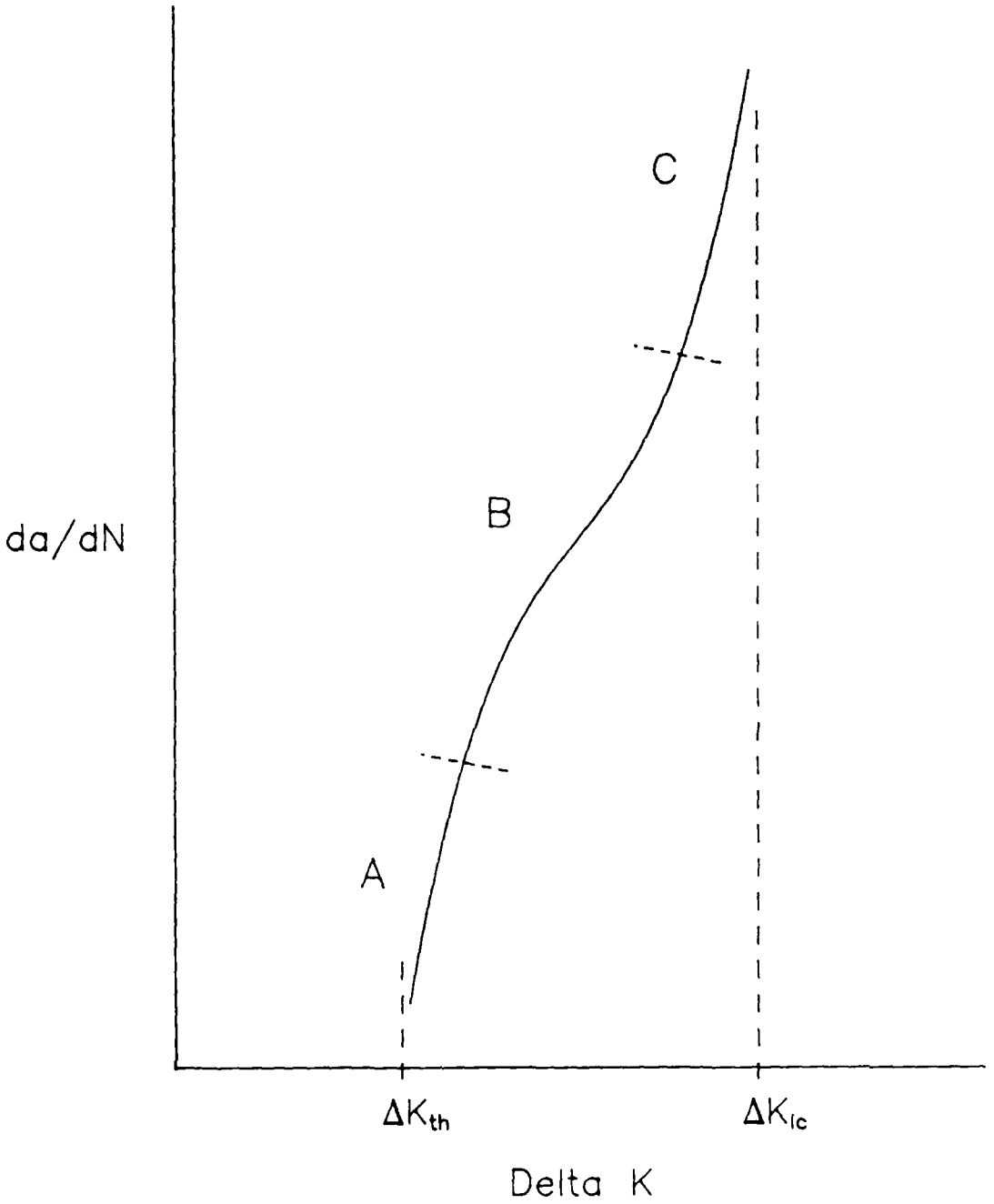

Figure 1. Typical Crack Growth Curve

The stress ratio for cyclic fatigue can be expressed as:

$$R = \frac{K_{min}}{K_{max}} \qquad (2)$$

where K_{min} is the minimum stress intensity and K_{max} is the maximum stress intensity of a loading cycle. Previous studies (2:80; 3:238; 4:49) have shown that the da/dN plot will shift to the left as R increases (Figure 2).

Secondly, loading histories can affect ΔK_{th} simply by altering the size of the plastic zone ahead of the crack tip. Once the crack grows beyond the damaged area created by an overload, the crack growth rate returns to its expected values.

Lastly, ΔK_{th} is highly dependent on closure. Crack propagation will occur only if the stress intensity range, ΔK, is above the effective threshold range, $\Delta K_{eff,th}$, as shown in Figure 3. The closure load is taken into account when using effective stress intensity ranges, ΔK_{eff}. Any load below the crack opening stress intensity, K_{op}, does not contribute to crack propagation since the crack will remain closed. So, even under an external tensile load, the crack can be closed and will not propagate.

Objectives

The objective of this study is to determine the effects of loading histories and crack closure on the fatigue threshold characteristics of additionally heat treated Ti-6Al-2Sn-4Zr-6Mo (Ti 6246). Next, this study will compare the closure loads as

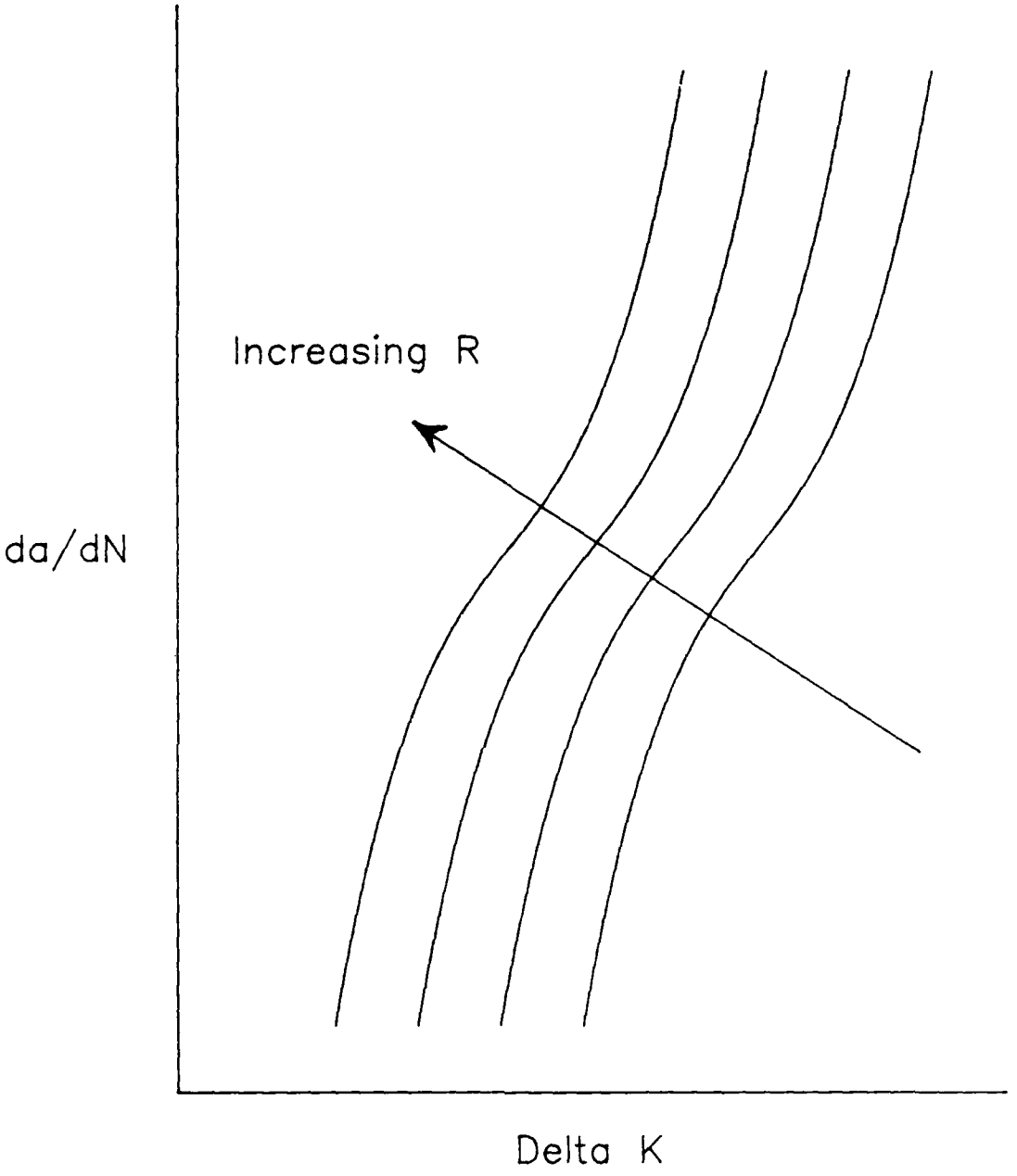

Figure 2. Crack Growth Curve's Dependence on R

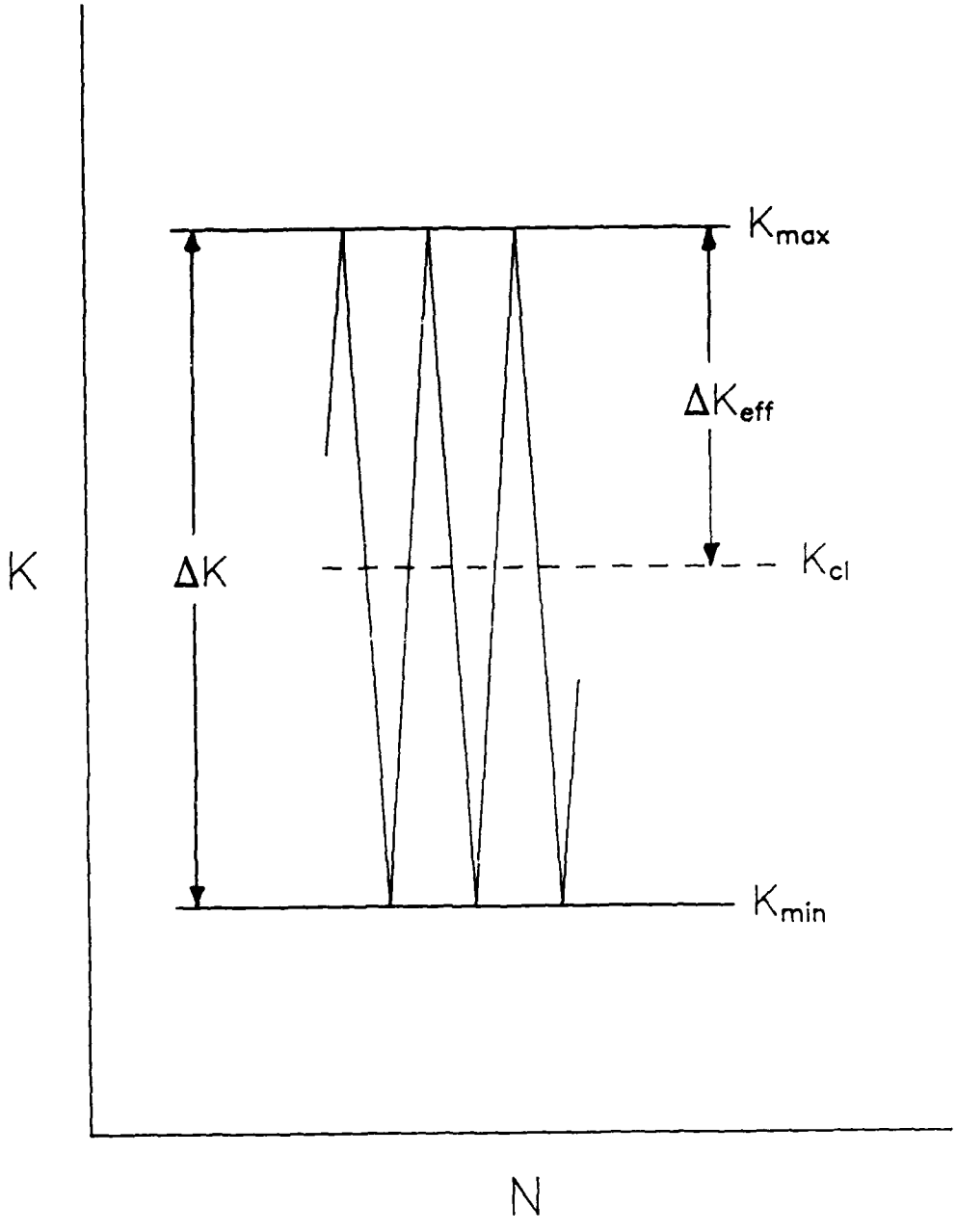

Figure 3. Nomenclature for the Stress Intensity Factors

measured by a clip gage, back face strain gage, and a laser interferometric displacement gage. The effects of the additional heat treatment on the fatigue threshold behavior of Ti 6246 will also be discussed.

Two types of tests will be conducted using compact test specimens. The first type of test is where the load ratio is held constant throughout the test. Two tests fell under this category. First, the standard load shedding test as described by the ASTM was included (5:907). Here, K_{max} is decreased exponentially until the fatigue threshold crack growth rate ($da/dN < 10^{-10}$ m/cycle) is reached (Figure 4). The second constant R test involved instantaneously dropping the stress intensity range, ΔK, similar to the test developed by Castro and others (6:308-309; 7:822). After running at a prior ΔK, K_{max} is decreased while K_{min} is increased such that the mean stress intensity, K_{mean}, is a percentage lower than the previous K_{mean} (Figure 5).

The second type of test used a constant K_{max} while linearly increasing the K_{min} (6:307-308; 7:820-822). Since K_{max} is held constant, R steadily increases as the test progresses as shown in Figure 6. The load ratio at threshold must be below 0.5 for closure to be measured.

These tests were selected because they provide different loading histories for studying the fatigue threshold. The closure created by these different loading histories and its effects on the fatigue threshold will also be examined. Since no previous experimental data was found for the heat treated

Ti 6246 used in this research, the ASTM decreasing K tests will establish the reference lines used for the remainder of this study. Further, the results from these tests will be used to determine the effects of the additional heat treatment on the fatigue characteristics of Ti 6246.

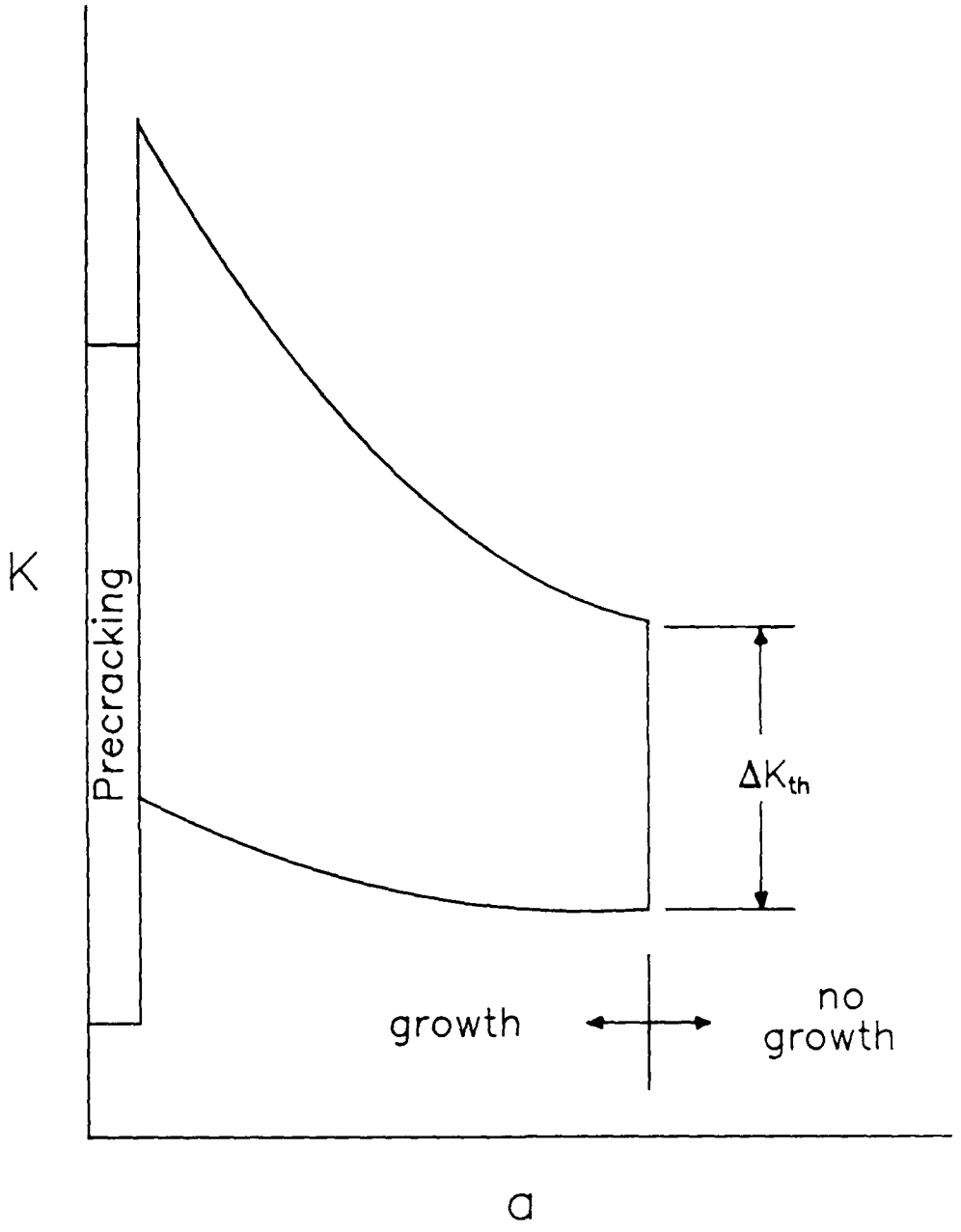

Figure 4. Standard ASTM Decreasing K Test

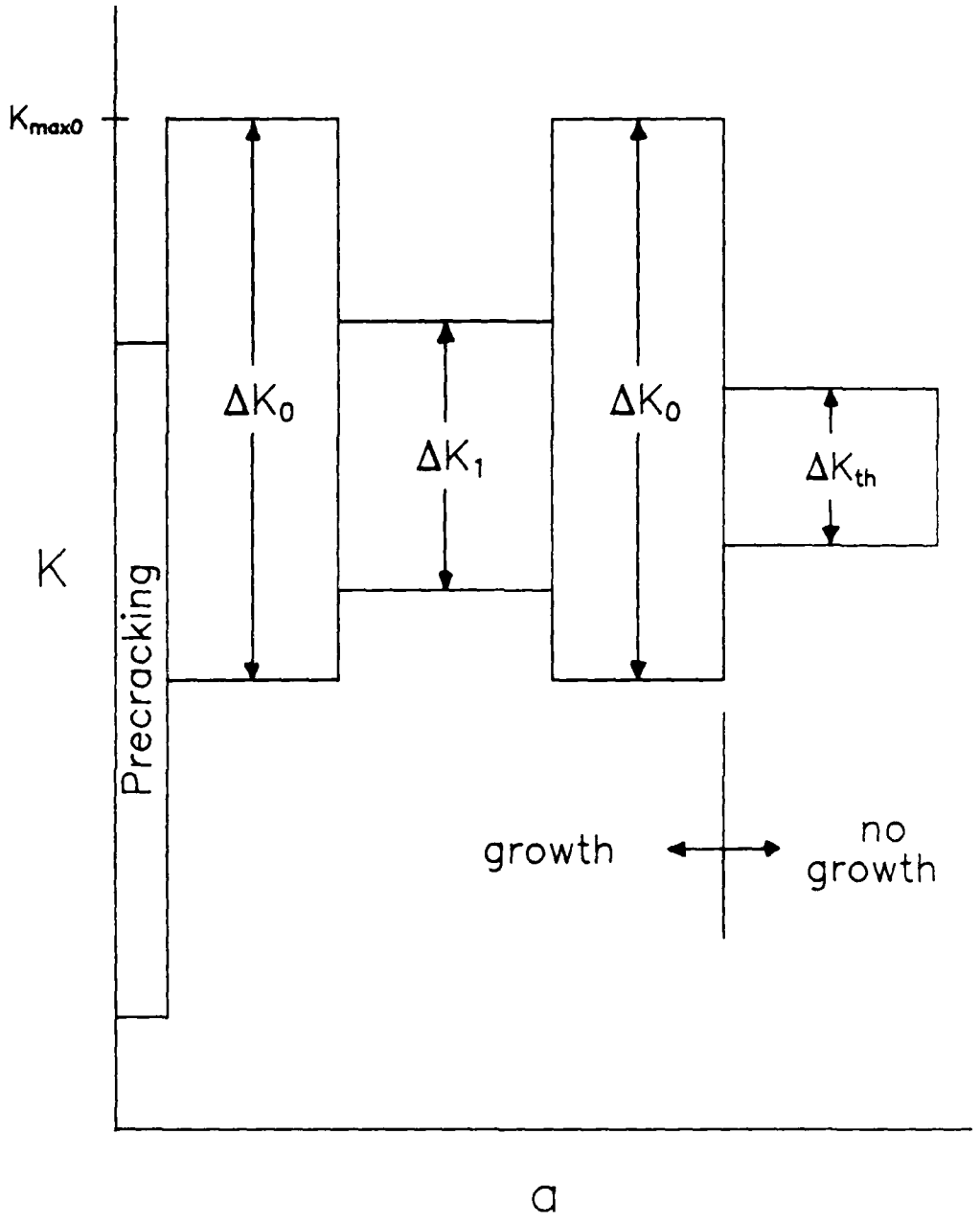

Figure 5. Varying ΔK Test with Constant R

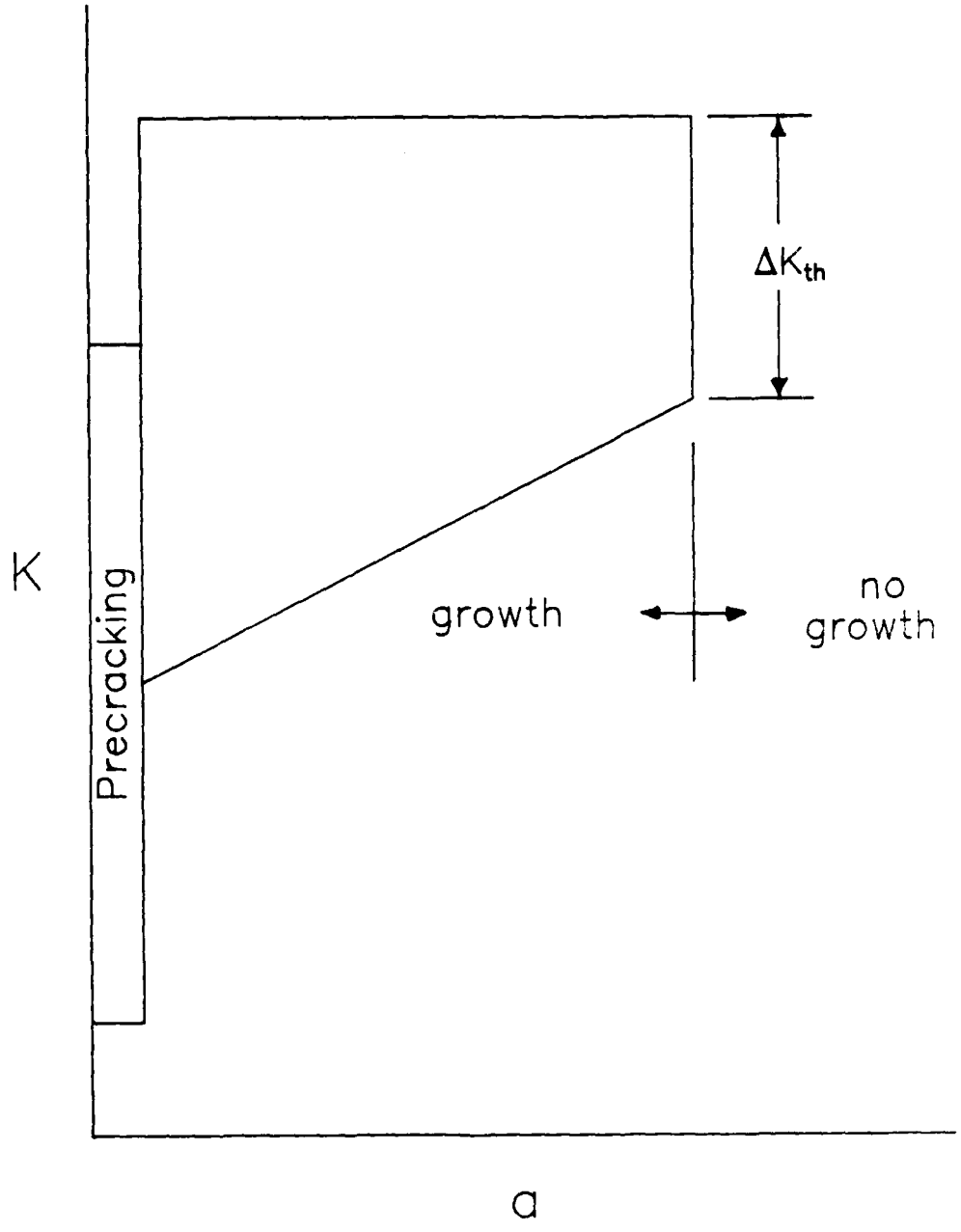

Figure 6. Constant K_{max} Test with Linearly Increasing K_{min}

II. Theory ~ History

Presently, the Paris-Erdogan equation is the most commonly used tool design engineers have when considering fatigue. But, this equation has various limitations. The Paris-Erdogan equation models region B of Figure 1 as a straight line even though it is curved. Also, it does not include the fatigue threshold. Since a majority of designs use the ΔK_{th} as the limiting parameter, an accurate means of determining fatigue threshold becomes important.

Factors Influencing Fatigue Threshold

Research has shown that ΔK_{th} is not a constant material property. Instead, ΔK_{th} is dependent on numerous factors including load ratio, loading history, and crack closure.

Load Ratio (R). Many studies have found ΔK_{th} to be dependent on R (2:80 ; 3:238 ; 4:49). As shown in Figure 2, the crack propagation curve shifts to the left as R increases. Thus, ΔK_{th} decreases with increasing R (8:125 ; 9:73).

Walker and Beevers (10:145) found that the crack growth curves almost converged at higher ΔK values. However, at stress intensities closer to ΔK_{th}, the crack growth rate was significantly dependent on R.

Using surface-flaw specimens made of Ti 6246, Jira and others (11:626-629) ran several load shedding threshold tests. By holding R constant throughout each test, they determined that ΔK_{th} decreased with increasing R. Thus, if ΔK_{th} is to be

used as a design parameter, its dependence on R must be taken into account.

Loading History. Another important variable in determining ΔK_{th} is the loading history of the specimen. Overloads in terms of a prior maximum stress intensity and an initial stress intensity range have been used to study the effects of loading history.

Ogawa and others (12:875, 877) studied the effects of single and multiple overloads on ΔK_{th} using steel. At a constant R during and after the overload, they found that ΔK_{th} linearly increased with an increasing overload K_{max}. Multiple overloads were found to produce a larger increase in ΔK_{th} than single overloads.

As a contrast, Döker and Marci (13:190) found that ΔK_{th} decreased with an increasing overload K_{max}. Castro and others (6:313 ; 7:828) had similar results. However, neither group maintained a constant R throughout a given test. Threshold was intentionally measured at $R > 0.7$ to avoid any closure effects (6:309 ; 7:823).

Thus, it would appear that the effects of an overload on ΔK_{th} vary depending on whether R remains constant throughout the test or not. Similar tests need to be conducted to confirm this observation.

Loading history effects on ΔK_{th} can also be examined in terms of a gradual change in the prior ΔK. Castro and others (6:307-308 ; 7:820-822) ran several such tests using an Inconel 617 Alloy. The K_{max} was held constant while K_{min} was

increased. By holding K_{max} constant, the plastic zone size ahead of the crack tip also remained constant. In the first test, K_{min} was increased gradually so that the amount of ΔK decrease was small from one increment to the next. The subsequent tests used larger increases in K_{min}. Again, ΔK_{th} decreased as the constant K_{max} value increased. The ΔK_{th} also decreased as the amount of ΔK difference between incremented K_{min} steps increased. In other words, the ΔK_{th} values were highest for a gradual increase in K_{min} (6:310 ; 7:824).

Mall and others (14:5-6) conducted tests with constant K_{max}. In their study, K_{min} was either increased or decreased linearly for each test. The results indicated that ΔK_{th} was higher for tests where K_{min} was decreased linearly.

So, it is evident that loading history influences the ΔK_{th} values. Therefore, these effects must also be included if ΔK_{th} is to be a fatigue design parameter.

Closure. Elber (15:231-232) was the first to consider the effects of fatigue crack closure under cyclic tensile loading. In his tests, Elber compared a zero-width saw cut, which was commonly used to model a fatigue crack, with an actual crack. Unlike the zero-width saw cut, the fatigue crack did not remain open throughout the zero-to-tensile loading cycle. Instead, the fatigue crack remained closed for a significant portion of the loading cycle. Since the crack must be fully open before it can propagate, the amount of load needed to overcome closure effects must be taken into account.

As can be seen in Figure 7, closure can be measured using

a load displacement relation. The non-linear portion of the plot signifies the presence of closure. Thus, the load at which this relation is no longer linear is the closure load.

Presently, there are three elements which contribute to crack closure. The effects of plasticity, asperity, and oxides must be considered when studying closure. Although asperity and oxides keep the crack tip from closing at zero load, they must still be classified as closure effects when studying fatigue.

Elber stated that closure was caused by "the permanent tensile plastic deformation left in the wake of the propagating crack" (16:44). As shown in Figure 8, the crack is surrounded by a plastic wake formed from previous monotonic plastic zones. Since the tensile deformation in the plastic wake cannot be supported by the surrounding elastic field at zero load, compressive stresses normal to the crack surfaces are introduced. Thus, these compressive stresses close the fatigue crack at zero load. The applied external load must be greater than the compressive stresses at the crack surfaces to initiate propagation.

Another factor contributing to plasticity induced closure is the cyclic or reverse plastic zone (17:17). Once unloaded, the compressive stresses within the monotonic plastic zone near the crack tip exceed the compressive yield strength of the material. This additional deformation occurring at the crack tip is referred to as reverse plasticity. The resulting cyclic plastic zone is approximately one-fourth the size of the

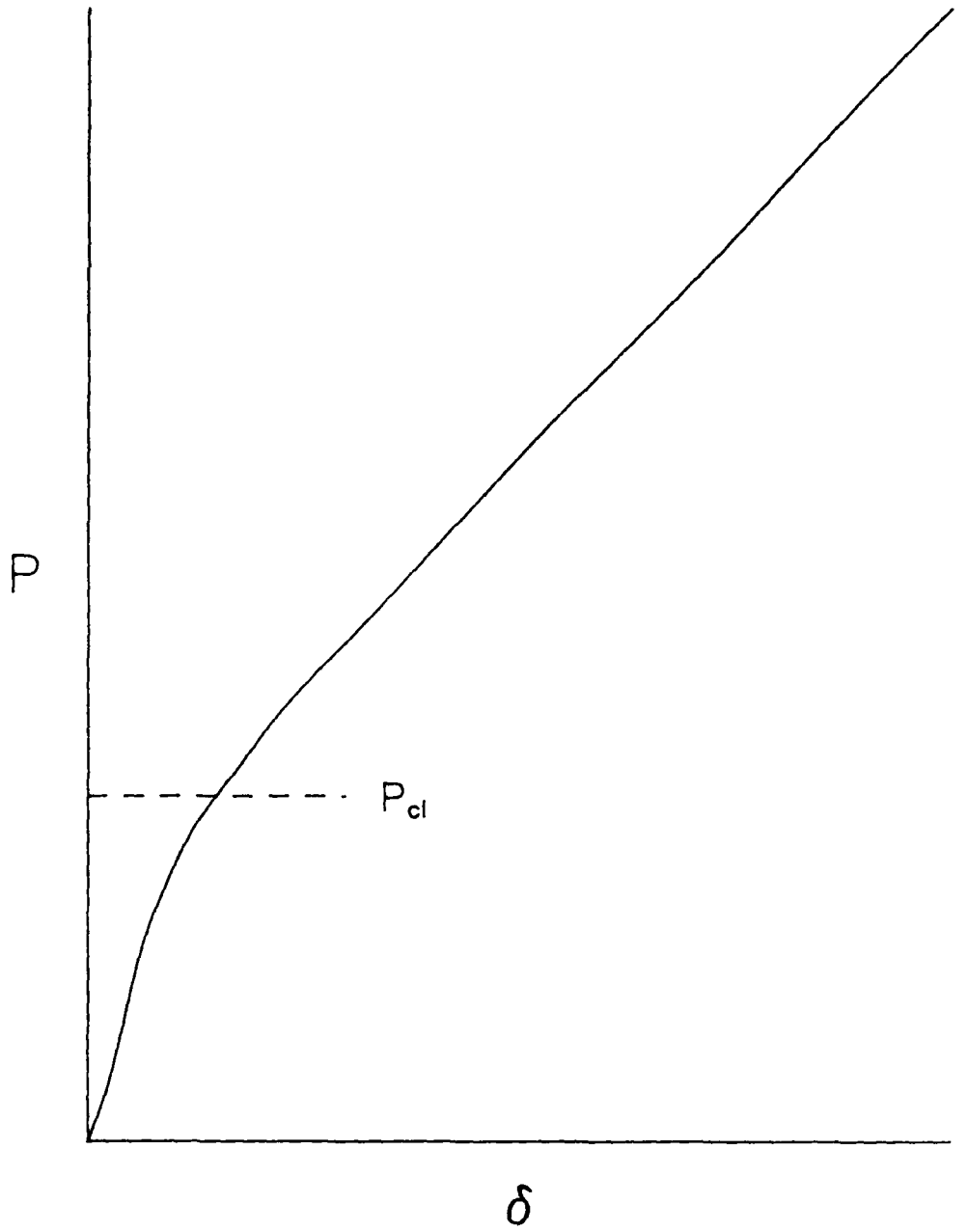

Figure 7. Typical Load Displacement Diagram

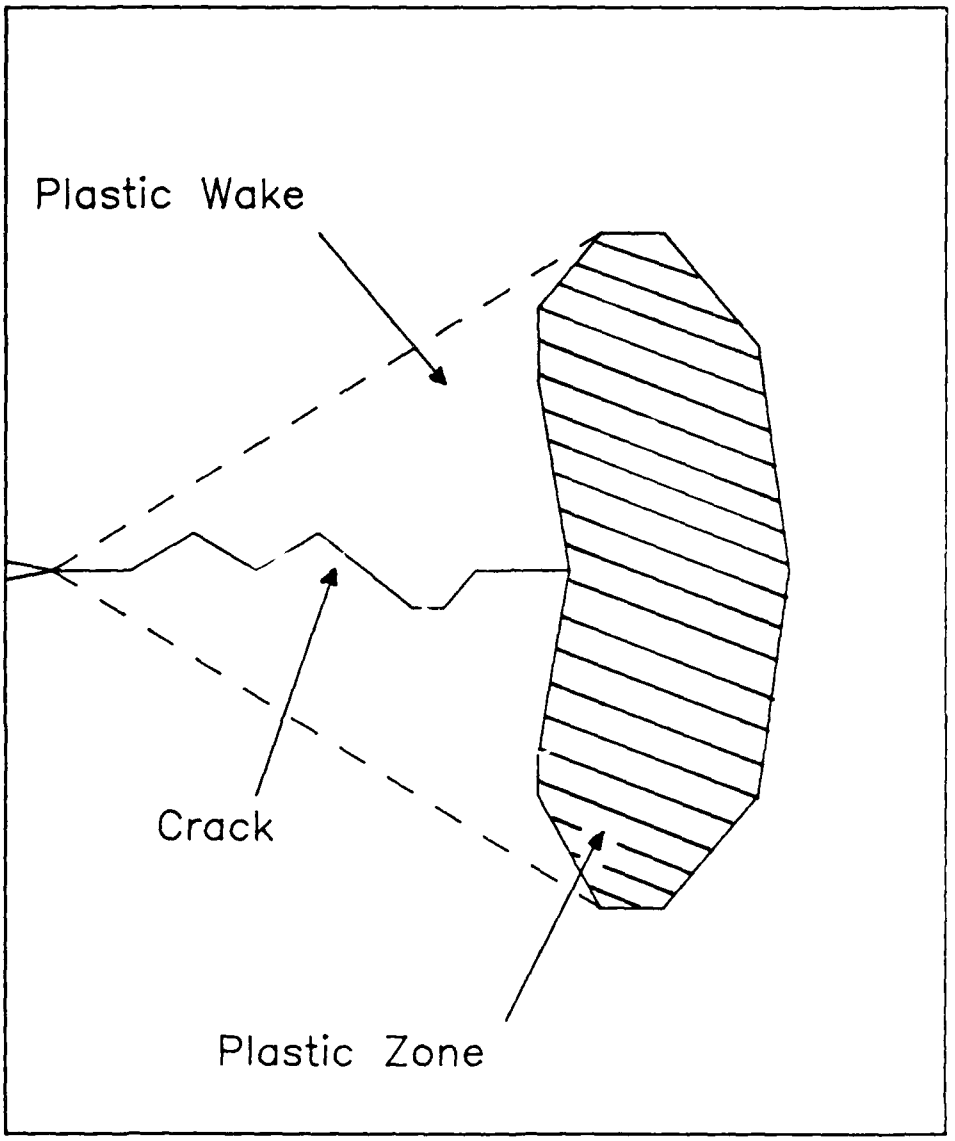

Figure 8. Plastic Wake of a Fatigue Crack

monotonic plastic zone.

Walker and Beevers (10:140-145) introduced asperity, the second closure mechanism. They concluded that fatigue crack closure in commercial titanium was caused by the non-planar crack geometry rather than plasticity. Mode II (in-plane shear) displacement during crack growth causes the mating surfaces to become misaligned. The crack surfaces will then make contact before the minimum load is reached. Aside from the meandering of the crack path, Sadananda (18:149-150) found that crack tip branching and secondary cracking also contribute to asperity.

Asperity is classified as a closure effect because it increases the minimum load at which the crack surfaces make contact. Thus, the crack is "closed" at a higher load than would have been produced by plasticity. In any event, the effective range of the loading cycle required to propagate the crack is reduced. Banerjee (17:28) noted that asperity was usually observed at low crack growth rates ($da/dN < 10^{-10}$ m/cycle).

Oxide induced closure will be the last closure mechanism discussed. Many studies (19:439 ; 20:310 ; 21:752 ; 12:875) have shown that certain materials when exposed to a corrosive environment will form oxidation layers on the crack surfaces. So, the crack surfaces will make contact at a higher load than the minimum load of the cycle due to the interference of these oxidation layers. By raising the closure load, the effective range of the loading cycle is reduced. Like asperity, oxide

induced closure occurs at low crack growth rates.

Döker and Peters (22:278-279) looked at the effects of a corrosive environment on the fatigue threshold characteristics of a Ti-6Al-4V alloy. When exposed to a NaCl solution, the titanium alloy showed the same ΔK_{th} as measured in air for similar loading conditions. Asperity induced closure was found to be the dominant closure mechanism. Thus, even in a corrosive environment, oxidation did not contribute to the crack closure measured. The dominant closure mechanism for Ti 6246 is expected to be asperity as well.

Factors Influencing Closure

Now that closure has been defined, the factors influencing it must be examined. Studies thus far have indicated that closure is primarily dependent on the load ratio and measurement location. Since measurement techniques will be discussed in the next section, only closure's dependence on R will be addressed here.

Schmidt and Paris (2:84-85) were first to describe the closure's dependence on R. They stated that closure would be eliminated at high load ratios, $R \geq 0.5$. Similarly, Guerra-Rosa and others (3:236) concluded that "crack closures can be significantly avoided if stress ratios R are very high (≥ 0.8)." They also found that K_{cl}, the stress intensity for which the crack is closed, increased linearly with increasing load ratios for $R < 0.8$.

On the other hand, Döker and Bachmann (23:254, 258-259) found that closure was present even at high load ratios. Using

Ti-6Al-4V in air, they determined that at:

$$R = 0.1, \quad K_{op} = 0.44\ K_{max} \tag{3}$$

$$R = 0.5, \quad K_{op} = 0.64\ K_{max} \tag{4}$$

$$R = 0.75, \quad K_{op} = 0.77\ K_{max} \tag{5}$$

where R is the load ratio, K_{op} is the stress intensity factor at which the crack opens, and K_{max} is the maximum stress intensity of a cycle.

Thus, there is a contradiction in the literature with regards to closure. One possible explanation for the difference in the closure data at high R could be the accuracy of the measurement device used. Döker and Bachmann (23:252-256) used a direct current potential drop method with an accuracy of 10^{-2} mm. Closure loads measured by this method were determined to be higher than those measured by either a clip gage or strain gage.

Measuring Closure

As was noted above, closure is dependent on the measurement technique used. Macha and others (24:213 ; 25:195) noted that the accuracy in determining the closure load was also dependent on the measurement location. The advantages and disadvantages of three commonly employed techniques for crack closure measurement methods; the clip gage, strain gage, and interferometric displacement gage (IDG), will be discussed.

The clip gage is presently the most commonly used device when monitoring crack growth. However, the load displacement plots generated from the clip gage data are sensitive to the

friction in the system and misalignment of the grips. Either of these conditions can distort the data or cause hysteresis. Since the closure load is determined from the load displacement diagram as previously discussed, a bad plot can lead to bad closure measurements. Another problem is the clip gage's "distant" location relative to the crack tip. Thus, its closure load measurements are not very accurate (23:254 ; 26:151).

On the other hand, clip gages are convenient to use. Also, many automated systems use a clip gage as the controlling device for measuring crack lengths. Lastly, thickness averaged closure behavior as well as thickness averaged crack lengths are obtained from a clip gage.

Strain gages mounted on the back face (BFS) of the specimen can be used to eliminate some of the problems presented by the clip gage. A BFS load displacement plot does not have hysteresis since the friction of the system and misalignment of the grips do not affect the data collected. However, like the clip gage, the BFS has a "distant" measurement location. Further, BFS yields thickness averaged data, as in the case of the clip gage.

The newest of the techniques is the IDG. There are several advantages in using the IDG. First, an IDG has very high accuracy, 0.01 microns when used with a helium neon laser (27:24). Next, the IDG can have a gage length as short as 25 microns (28:76). A short gage length is advantageous in measuring displacements near the crack tip. An IDG is also a

non-contact gage which is insensitive to temperature. Lastly, since the indents used by the IDG can be placed anywhere along the crack path, the measurement location is flexible.

Ashbaugh (25:195) showed that the indents must be placed within 10% of the specimen's width (0.1W) from the crack tip for accurate closure measurements. Distances further than 0.1W yielded the same closure loads as measured by the clip gage and BFS. So, thickness averaged data can only be acquired at distances greater than 0.1W. Nevertheless, many studies (25:190-191 ; 23:254 ; 26:151) indicated that the IDG was better at measuring crack closure than either the clip gage and BFS.

Effective Stress Intensity Range

Since ΔK_{th} has been shown to be an inadequate design parameter for fatigue threshold, a new criterion must be examined. Schmidt and Paris (2:83) were first to incorporate K_{cl} as an attempt to redefine ΔK as a material constant. For low load ratios where $K_{min} \leq K_{cl}$:

$$\Delta K_{eff} = K_{max} - K_{cl} \tag{6}$$

where the ΔK_{eff} is the effective stress intensity range, K_{max} is the maximum stress intensity in a cycle, and K_{cl} is the stress intensity below which the crack is closed. Figure 3 is a graphical representation of Eq (6).

Experimenting with a Ti-6Al-4V alloy, Döker and Marci (13:189-190) showed that ΔK_{eff} was a material constant independent of the loading conditions. Their conclusions were

valid for $R \geq 0.5$ where ΔK_{eff} was relatively constant. For $R \leq 0.5$, the difficulty in accurately determining K_{cl} hampered their results.

Döker and Bachmann (23:254-255) worked at R = 0.1, 0.5, and 0.75 on Ti-6Al-4V. For the given load ratios, they plotted ΔK_{eff} versus ΔK and developed the general expression

$$\Delta K_{eff} = 0.65\ \Delta K \tag{7}$$

where ΔK_{eff} and ΔK are the same as previously designated.

Similarly, Mall and others (14:7) found that ΔK_{eff} was a material property. Surface-flaw specimens made of Ti 6246 were used for their tests. Constant K_{max} tests were conducted using either a linearly increasing or decreasing K_{min}. These tests allowed R to be varied throughout the test. By applying Eq (6), they consolidated the crack growth curves from both test types into one ΔK_{eff} curve.

Jira and others (11:633) also did research on surface-flaw specimens made of Ti 6246. A series of load shedding threshold tests were conducted utilizing two different specimen geometries. Four different initial loads were run for R = 0.5, 0.1, and -0.1. Despite the test variations, the ΔK_{eff} crack growth curve was still found to be constant.

Thus, ΔK_{eff} has been shown to be constant irregardless of R, loading history, or specimen geometry. This study will attempt to verify those results for $R < 0.5$ where closure strongly affects ΔK_{eff} using compact test specimens made of additionally heat treated Ti 6246.

Heat Treating Ti-6Al-2Sn-4Zr-6Mo

Presently, there is no information on the fatigue threshold characteristics of additionally heat treated Ti 6246. Chesnutt and others (29:341) did tests on Ti 6246 at fatigue crack propagation rates higher than threshold. They also tested other titanium alloys. These $\alpha+\beta$ alloys generally displayed a change in fatigue crack propagation rates upon being heat treated. The crack growth curve as shown in Figure 1 shifted to the right for the heat treated specimens. Thus, heat treated materials exhibited a higher ΔK_{th}.

In a similar study, Rhodes and Paton (30:40-44) found that heat treated Ti-6Al-4V had a higher fatigue crack propagation (FCP) resistance. They believed that the two main factors increasing the FCP resistance were an increase in the volume fraction of the primary α phase and an increase in the interface phase width. They defined interface phase as the microstructural feature occurring at the interphase boundaries of the α and β phases in titanium alloys as a result of a slow cooling rate after being heat treated.

By increasing the volume fraction of the primary α, the strength of the β phase would also increase. The stronger β phase would increase crack resistance by forcing the crack to branch along the interfaces. Further, a wider interface phase would produce secondary cracks ahead of the crack tip by inhibiting the transfer of slip between α and β phases. These secondary cracks would absorb some of the energy required to propagate the fatigue crack.

Rhodes and Paton (30:19-26) also noted that the effects of heat treating on FCP resistance were more pronounced at higher ΔK values. At lower ΔK values, fracture was caused by cleavage through the α phase. An increase in secondary cracking and interface cracking at higher ΔK values increased the FCP resistance. Thus, the separation of the crack growth curves between the additionally heat treated and standard specimens was greater at higher ΔK values.

Recently, Larsen (31) stated that interface phase was no longer considered a contributor to the FCP resistance experienced by additionally heat treated Ti 6246. Interface phase was found to be an artifact from the polishing procedure used to prepare the specimens for the Transmission Electron Microscope (TEM). Instead, roughness induced closure becomes more prominent for these specially heat treated specimens thereby improving the fatigue characteristics.

One factor contributing to asperity is an increased grain size. Brown and Smith (32:336) discovered that ΔK_{th} increased with an increase in grain size. The photographs in Figure 9 display the difference in the microstructure caused by the additional heat treatment of Ti 6246. As can be seen, Ti 6246 which had an additional heat treatment has a much larger grain size.

The most important factor leading to an increase in roughness induced closure for the additionally heat treated specimens is the alignment of the α platelets into large colonies. The α phase in standard Ti 6246 is divided into

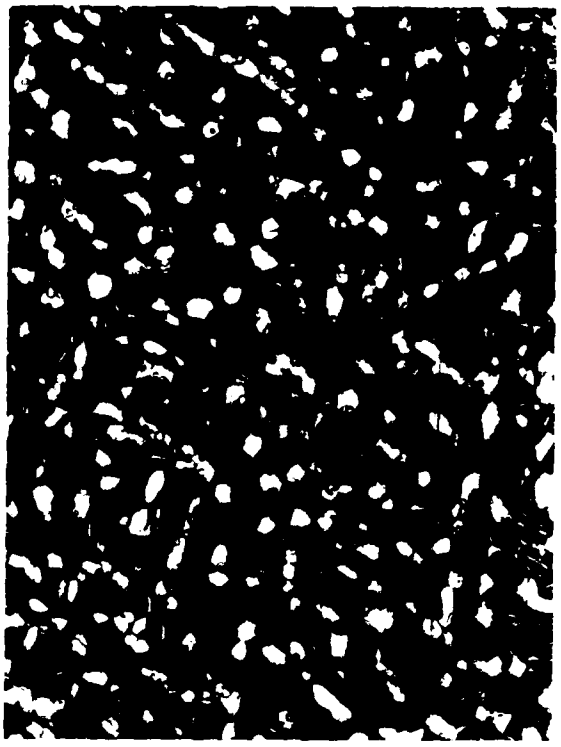

Standard Heat Treatment

(x400)

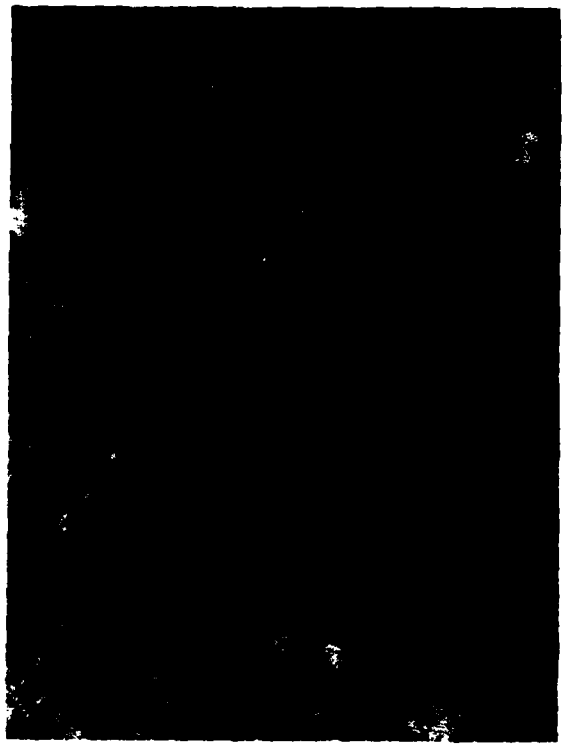

Additional Heat Treatment

(x50)

Figure 9. Microstructures of Ti 6246 Specimens

equiaxed particles and short platelets as seen in Figure 9a. However, after an additional heat treatment, only long α platelets exist. The α platelets comprising a single grain grow in the same orientation. Thus, a propagating crack will either be deflected along the grain boundary or across the platelets of the grain. The resulting crack surface will have larger asperities due to the jagged crack path.

Larsen and others (33:905-908) have performed crack growth tests on surface-flaw specimens made of standard Ti 6246. The data from these tests was then compared to trend lines for compact test specimens. These trend lines for compact test specimens were generated using data collected from several constant R tests. As expected, the ΔK_{eff} plots for both specimens types correlated very well. Figure 10 contains the trend lines for ΔK at R values of 0.1 and 0.5. ΔK_{eff} crack growth curves for the same R values can be found in Figure 11. This study will use the trend lines in Figures 10 and 11 to compare the fatigue characteristics of additionally heat treated and standard Ti 6246.

As discussed above, the ΔK_{th} values for the Ti 6246 which underwent an additional heat treatment are expected to be larger than those obtained from materials which has not been additionally heat treated. Similarly, the ΔK and ΔK_{eff} crack growth curves are expected to shift to the right for the additionally heat treated Ti 6246. This study will attempt to confirm these speculations as well as determine the effects of closure and loading history on the ΔK_{th}.

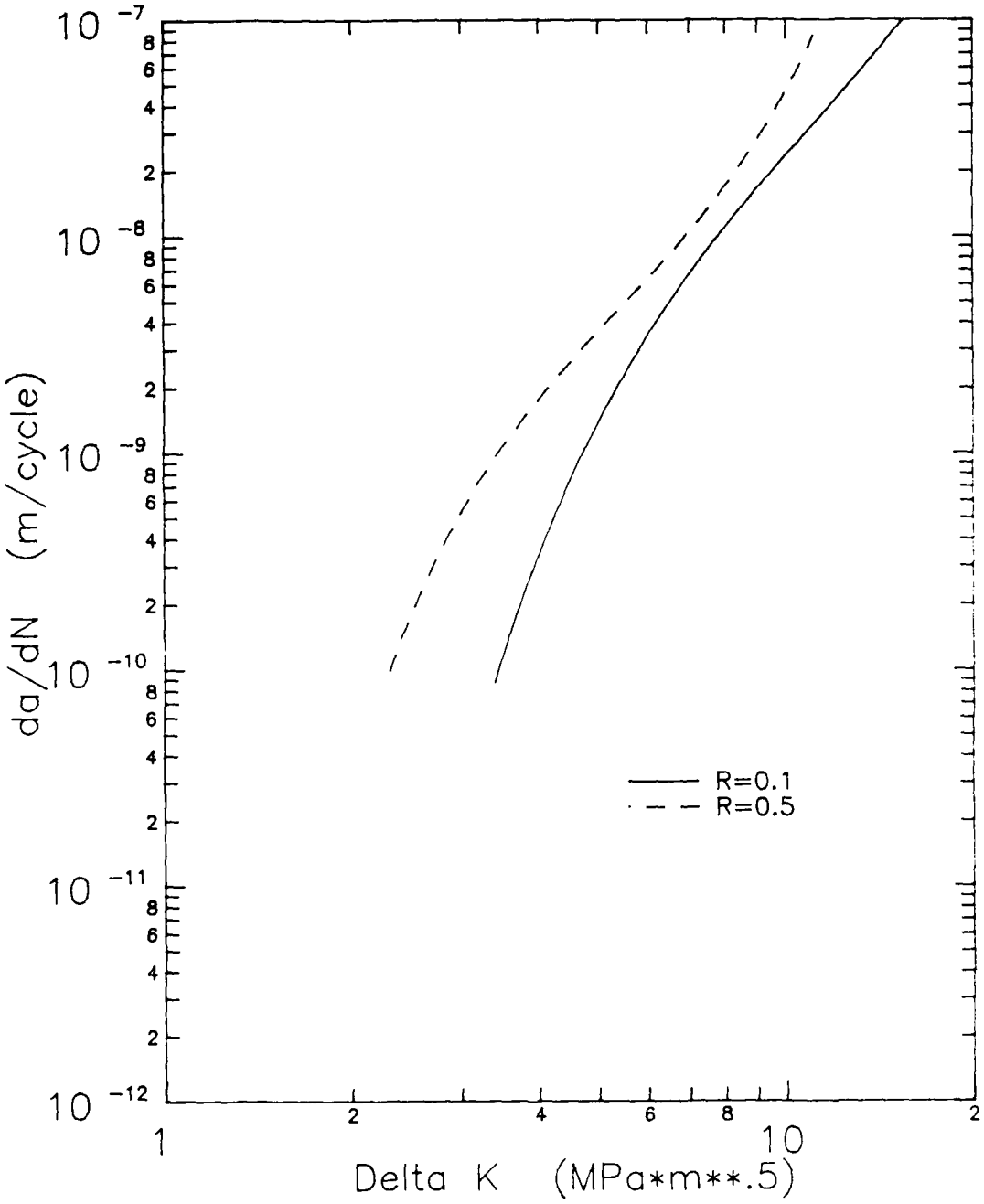

Figure 10. ΔK Crack Growth Curves for Standard Ti 6246 (33:905–906)

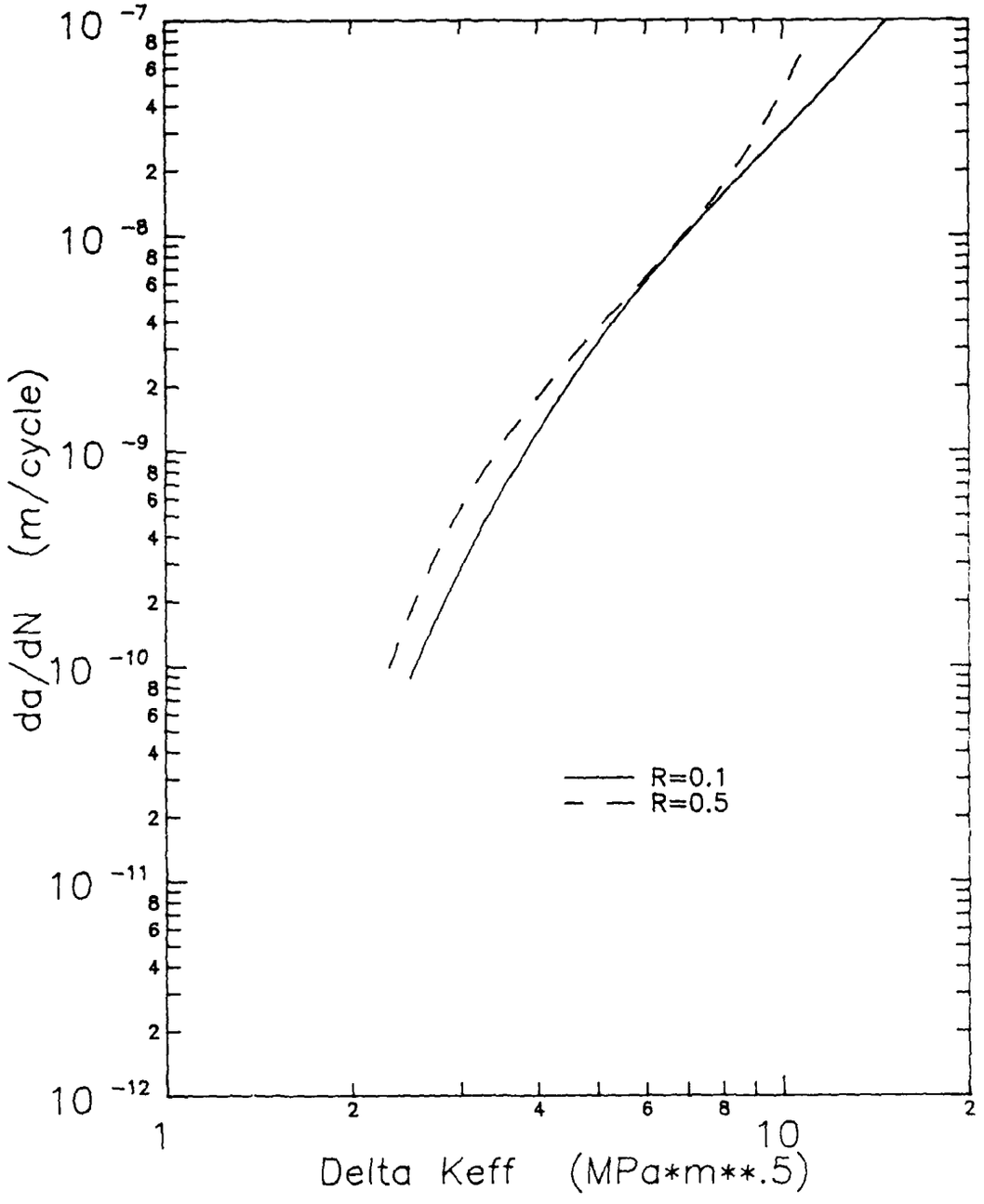

Figure 11. ΔK_{eff} Crack Growth Curve for Standard Ti 6246 (33:908)

III. Test Procedures

Specimen Preparation

All tests were conducted using the titanium alloy Ti-6Al-2Sn-4Zr-6Mo (Ti 6246). Refer to Table I for a complete chemical breakdown of this alloy. Titanium alloys are used in aircraft air frames and gas turbine engines. Due to the high cycle vibration experienced by these engines, fracture mechanics is the primary design criterion when predicting the service life of these components.

The alloy was cast and isothermally forged at 913°C into circular disks known as pancakes. Each pancake was approximately 500 mm in diameter and 50 mm thick. The material then underwent a series of heat treatments. First, it was heat treated at 921°C for two hours and air cooled. Next, the material was water quenched after being heat treated to 824°C for two hours. Following eight hours at 593°C , it was air cooled. Most other titanium alloys are then machined to specifications. However, the Ti 6246 used for this study was additionally heat treated at 971°C for 2 1/4 hours and furnace cooled at a rate of 38°C/hour to improve its fatigue characteristics. After the material reached 593°C , it was removed from the furnace and allowed to air cool. To complete the process, the alloy was heat treated to 593°C for eight hours again and air cooled. The material has a yield strength of 1158 MPa and an ultimate strength of 1230 MPa. This titanium alloy is essentially isentropic.

Table I. Chemical Composition of Ti-6Al-2Sn-4Zr-6Mo

ELEMENT	WEIGHT PERCENT
Al	6.33
B	0.01
C	0.02
Cu	0.01
Fe	0.12
H	0.0017
Mo	5.76
Zr	3.93
N	0.01
O	0.10
Si	0.09
Sn	2.07
Ti	Remainder
Y	0.001

The material was subsequently machined into 9.6 mm thick compact test specimens as shown in Figure 12a. The clip gage mounts were placed at the load line in an attempt to get more accurate closure load measurements. In order to use the laser interferometric displacement gage (IDG), all specimens were polished down to a one micron mirror finish.

After polishing, strain gages were mounted to the center of the back face of the specimens. Appendix A contains the specifications for the strain gages used in this study. Next, all specimens were identically precracked according to ASTM requirements (5:905-906). A precrack 4 mm long was grown at a constant $R = 0.1$ and initial $K_{max} = 12$ MPa$\sqrt{m}$. The precracking was completed when the fatigue threshold ($da/dN < 10^{-10}$ m/cycle) was reached. Thus, the final K_{max} from precracking was always kept lower than the initial K_{max} for the subsequent tests as prescribed by the ASTM (5:906). So, the effects of precracking and its plastic zone are negligible.

As a final preparation before testing, microhardness indents were placed at the crack tip. As shown in Figure 12b, the pyramidally shaped indents were placed on opposite sides of the crack so they could produce the proper interference fringe patterns required by the IDG. The size and orientation of the indents determine the quality and quantity of fringe patterns produced. For this study, the best fringe patterns were produced by indents 33 microns wide and 100 microns apart. On the average, the indents were positioned 50 microns behind the crack tip.

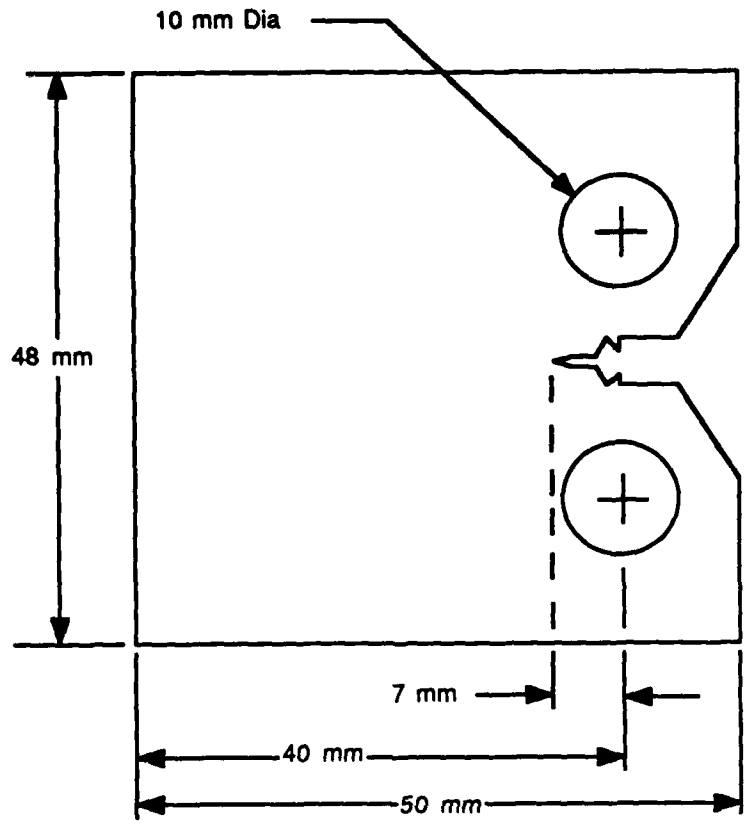

a. Compact Test Specimen with Clip Gage Mounts at Load Line

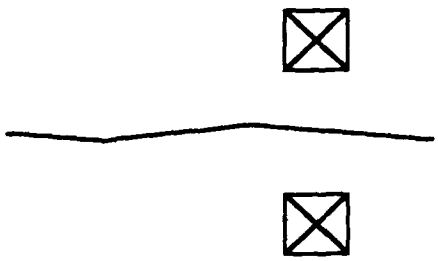

b. Microhardness Indents for IDG

Figure 12. Compact Test Specimen and IDG Indents

Test Setup

The tests for this study were conducted on an MTS machine at room temperature (23°C) in laboratory air at a test frequency of 30 hz. The testing system was fully automated and controlled by an IBM AT computer. Three measurement techniques; clip gage, back face strain gage (BFS), and IDG, were interfaced to the computer through an analog to digital board.

Inputs from the load cell and clip gage are used by the computer to control the tests. The compliance for determining the crack length is calculated using the slope of the linear portion of the load displacement diagram shown in Figure 7. Saxena and Hudak (34:459) developed the equations used for computing the crack lengths in CT specimens with measurements taken from the displacement measured at the load line as:

$$\frac{a}{W} = 1.002 - 4.0632(U_x) + 11.242(U_x)^2 - 106.04(U_x)^3 + 464.33(U_x)^4 - 650.68(U_x)^5 \quad (8)$$

with

$$U_x = \frac{1}{\left(\frac{BEV}{P}\right)^{1/2} + 1} \quad (9)$$

where a is the crack length, W is the specimen width, B is the specimen thickness, E is Young's Modulus, P is the load, and V is the displacement measured by the clip gage. The a/W values predicted from Eq (8) fall within ± 0.0005 of the actual values.

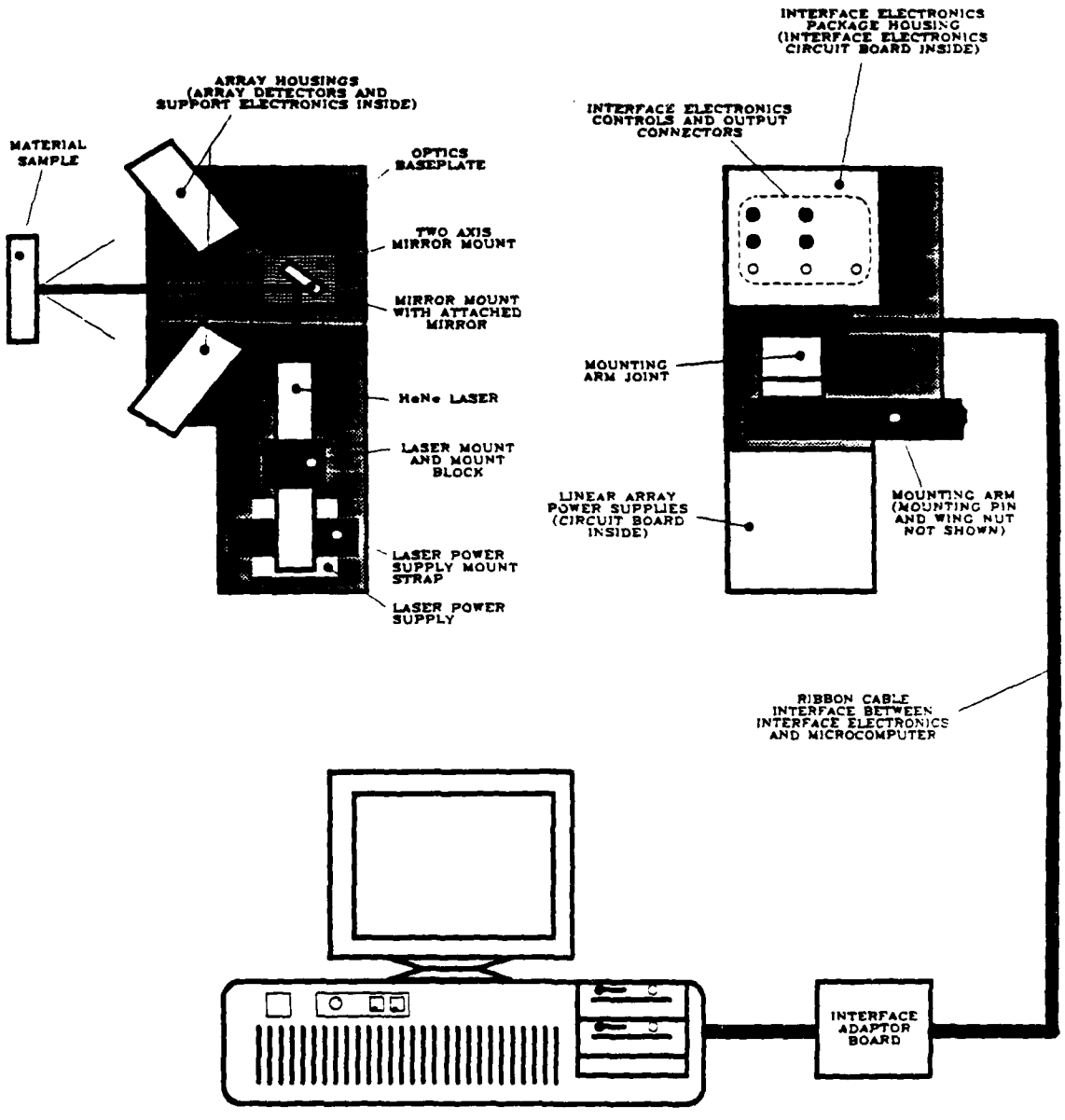

Figure 13. IDG Setup (35:29)

Presently, both the IDG and BFS are used for determining the closure load. According to Hartman and Nicholas (27:25), the IDG system used for this study has an accuracy of 0.01 microns when used with a helium neon laser. The IDG setup is illustrated in Figure 13. This accuracy is achieved by using two linear detector chips to record the motion of the fringe patterns produced by the microhardness indents on the specimen surface. The linear-array detector chips consist of 1024 detector elements spaced 13 microns apart along its 13.3 mm axis. By sequentially scanning the detectors, the fringe patterns are digitized into voltage versus time sweeps representing the light intensity across each array. The relative displacement of the indents and respective loads are stored in the computer along with the other data from the clip gage and BFS.

Test Plan

To analyze the effects of loading history and crack closure on the fatigue threshold of additionally heat treated Ti 6246, two different types of tests were run. The constant R tests included the ASTM decreasing K test and the varying ΔK test. The second type of test, constant K_{max} test, did not maintain a constant R throughout the test. A summary of all the tests conducted in this study is given in Table II.

ASTM Decreasing K Test. The ASTM decreasing K test is a load shedding test used to determine the ΔK_{th} ($da/dN < 10^{-10}$ m/cycle) and reference crack growth curves for a specified

loading condition (Figure 3). As outlined in the ASTM (5:907), R is held constant while K_{max} is exponentially decreased according to the following equation:

$$K = K_o \exp [C(a-a_o)] \quad (10)$$

where K_o is the initial stress intensity, a_o is the initial crack length, a is the final crack length, and C is the normalized K-gradient (-0.08/mm).

Since no data was available on this material, two decreasing K tests were run to set reference crack growth curves for the rest of the tests. As indicated in Table II, one test was started at K_{max} = 12 MPa$\sqrt{m}$ at R = 0.1. The second test had the initial conditions of R = 0.5 and K_{max} = 5 MPa$\sqrt{m}$.

Varying ΔK Test. The second test with a constant R was the varying ΔK test as shown in Figure 5. This test is similar to the one conducted by Castro and others (6:308-309 ; 7:822) with the exception of holding R constant. After running at an initial constant ΔK_o at a given stress ratio, K_{max} is decreased and K_{min} is increased instantaneously while still maintaining the same stress ratio. The resulting ΔK_1 is held constant until the data indicates whether threshold has been reached. If not, the specimen is loaded to the initial ΔK_o. Then, the ΔK is dropped such that $\Delta K_2 < \Delta K_1$. This testing procedure is repeated until ΔK_{th} is encountered.

Table II contains the details of the four tests run to study the effects of loading histories on ΔK_{th}. At R = 0.1, the first two tests were started at K_{max} = 10 and 20 MPa$\sqrt{m}$.

Table II. Summary of Test Plan

SPECIMEN	TEST TYPE	INITIAL CONDITIONS	FINAL CONDITIONS	REMARKS
84-337	ASTM Decr K Test	R=0.1 K_{max}=12 MPa$\sqrt{m}$	R=0.1 K_{max}=6.4 MPa$\sqrt{m}$	Fig. 4
84-338	Const K_{max} Incr K_{min}	R=0.1 K_{max}=7 MPa$\sqrt{m}$	R=0.54 K_{max}=7 MPa$\sqrt{m}$	Fig. 6
84-339	Const K_{max} Incr K_{min}	R=0.1 K_{max}=6.5 MPa$\sqrt{m}$	R=0.56 K_{max}=6.5 MPa$\sqrt{m}$	
84-340	Varying ΔK Test	R=0.1 K_{max}=10 MPa$\sqrt{m}$	R=0.1 K_{max}=6.3 MPa$\sqrt{m}$	Fig. 5
	Varying ΔK Test	R=0.1 K_{max}=20 MPa$\sqrt{m}$	R=0.1 K_{max}=6.3 MPa$\sqrt{m}$	
84-341	Varying ΔK Test	R=0.5 K_{max}=10 MPa$\sqrt{m}$	R=0.5 K_{max}=7.4 MPa$\sqrt{m}$	Fig. 5
	Varying ΔK Test	R=0.5 K_{max}=20 MPa$\sqrt{m}$	R=0.5 K_{max}=10.6 MPa$\sqrt{m}$	
84-342	ASTM Decr K Test	R=0.5 K_{max}=25 MPa$\sqrt{m}$	R=0.5 K_{max}=5.6 MPa$\sqrt{m}$	Fig. 4
	ASTM P_{max} Test	R=0.5 P_{max}=0.33 KN	R=0.5 K_{max}=8.7 MPa$\sqrt{m}$	

Thus, ΔK_o was equal to 9 and 18 MPa$\sqrt{m}$, respectively. The last two tests were conducted at the same K_{max} values as before but at R = 0.5. The resulting ΔK_o for these tests were 5 and 10 MPa$\sqrt{m}$. Thus, each test will yield two ΔK values, one signifying crack growth and the other representing no crack growth. The difference between subsequent drops ($\Delta K_2 - \Delta K_1$) used to differentiate between crack growth and no growth was set arbitrarily equal to 0.2 MPa$\sqrt{m}$.

Constant K_{max} Test. The final test type included in this study was the constant K_{max} test. For this test, K_{max} was held constant while K_{min} was linearly increased. So, K_{min} was gradually increased until threshold crack growth was obtained (Figure 6). In order to study the effects of closure, the final load ratio at threshold should be less than 0.5. Castro and others (6:307-308 ; 7:820-822) ran the same tests but at higher R values (> 0.5). In doing so, they did not have to account for closure in their work.

In an attempt to keep the final load ratios small (< 0.5), two tests were run at low K_{max} values of 7 and 6.5 MPa$\sqrt{m}$. As shown in Table II, both tests were initiated at R = 0.1.

Data Reduction

The analysis of the data included determining the closure loads and calculating crack growth rates. As previously mentioned, the crack closure for a loading cycle was determined using a load displacement diagram as shown in Figure 7. Basically, the closure load represents the value for which the

load displacement curve is no longer linear. The standard deviation method of determining closure was used in this study. First, a straight line is fit to the linear portion of the curve. The closure load is then computed as the point where the data is two or more standard deviations away from the linearly fit line.

ASTM (5:919-925) recommends reducing the crack growth data using an incremental polynomial method. The procedure involves fitting a second order polynomial to a subset of data points, usually seven, where the crack extension, Δa_{reg}, is greater than ten times the measurement precision. The values for da/dN and ΔK are calculated for the midpoint of this subset using the polynomial fit. The procedure is repeated for successive data subsets by including the next point and dropping the first.

However, when studying short crack lengths and near threshold crack propagation rates, many data points are collected with very little crack extension. So, data from these studies could not be reduced accurately using ASTM's procedure. Thus, Larsen (36:238-241) developed a modified procedure to accommodate for small crack lengths and near threshold crack propagation rates. His modified incremental method fits a second order polynomial to all the data falling within either a prescribed Δa_{reg} which is still ten times the measurement precision or a user defined number of points per subset. If the Δa generated from the user defined subset is not greater than Δa_{reg}, the program will increase the number of points in the subset until $\Delta a \geq \Delta a_{reg}$. Then, the next da/dN

and ΔK values are generated by incrementing an amount Δa_{inc} ($[1/6]\Delta a_{reg}$) before doing another fit. This study used Larsen's modified approach for data reduction.

IV. Results and Discussions

The fatigue threshold behavior of additionally heat treated Ti 6246 will be discussed using the results of the tests conducted in this study. First, the ASTM decreasing K tests will establish the reference lines for the remaining tests in this study since no such data for this particular alloy is presently available. The effect of heat treatment on the fatigue properties will also be discussed. Both the varying ΔK and the constant K_{max} tests will be used to determine how the crack closure and loading history might affect the fatigue threshold characteristics of Ti 6246. The effectiveness of the three measurement techniques; clip gage, BFS, and IDG, will also be discussed.

All the specimens used in this study were precracked at $R = 0.1$ with a $K_{max} = 12$ MPa$\sqrt{m}$ until the fatigue threshold ($da/dN < 10^{-10}$ m/cycle) was reached. In accordance with ASTM guidelines, the final K_{max} from precracking was always kept lower than the initial K_{max} of the subsequent tests (5:906). By following this procedure, the effects of precracking and its plastic zone were eliminated.

Once a test was running, the IDG indents were kept within 3 mm of the crack tip. Thus, for every 3 mm of crack growth, a new set of indents was placed on the specimen surface approximately 50 microns behind the crack tip.

Comparison of Measurement Techniques

As discussed previously, three different gages were used to measure the crack closure from the recorded load and displacement data. The closure stress intensity, K_{cl}, was then computed from the measured closure loads. The ΔK_{eff} was calculated using this K_{cl} in Eq (6). So, if K_{cl} was large, the corresponding ΔK_{eff} would be small.

Figure 14 shows the ΔK_{eff} crack curves for the ASTM decreasing K test at R = 0.1 from the data obtained by the IDG and clip gage. Unfortunately, the strain gage amplifier was not delivered in time to get BFS data for this particular test. As can be seen in Figure 14, the IDG measured consistently smaller values of ΔK_{eff} than the clip gage throughout the test. Looking at Table III, the IDG measured the $\Delta K_{eff,th}$ of 3.29 MPa$\sqrt{m}$ as compared to 3.65 MPa$\sqrt{m}$ for the clip gage. Clearly, the IDG provided the lowest ΔK_{eff} and thus the highest closure loads than the clip gage.

To complete the comparison, Figure 15 includes the ΔK_{eff} crack curves from all three measurement techniques for the constant K_{max} = 7 MPa$\sqrt{m}$ test. Again, the smallest ΔK_{eff} was computed using the IDG data. For the constant K_{max} test, the fatigue threshold (da/dN < 10^{-10} m/cycle) was reached for R > 0.5. So, very little or no closure was expected. As can be seen in Table III, both the clip gage and BFS measured no closure since $\Delta K_{th} = \Delta K_{eff,th}$ = 3.50 MPa$\sqrt{m}$. However, the IDG indicated that a small amount of closure was present since $\Delta K_{eff,th}$ = 3.22 MPa$\sqrt{m}$. Thus, the IDG measured the highest

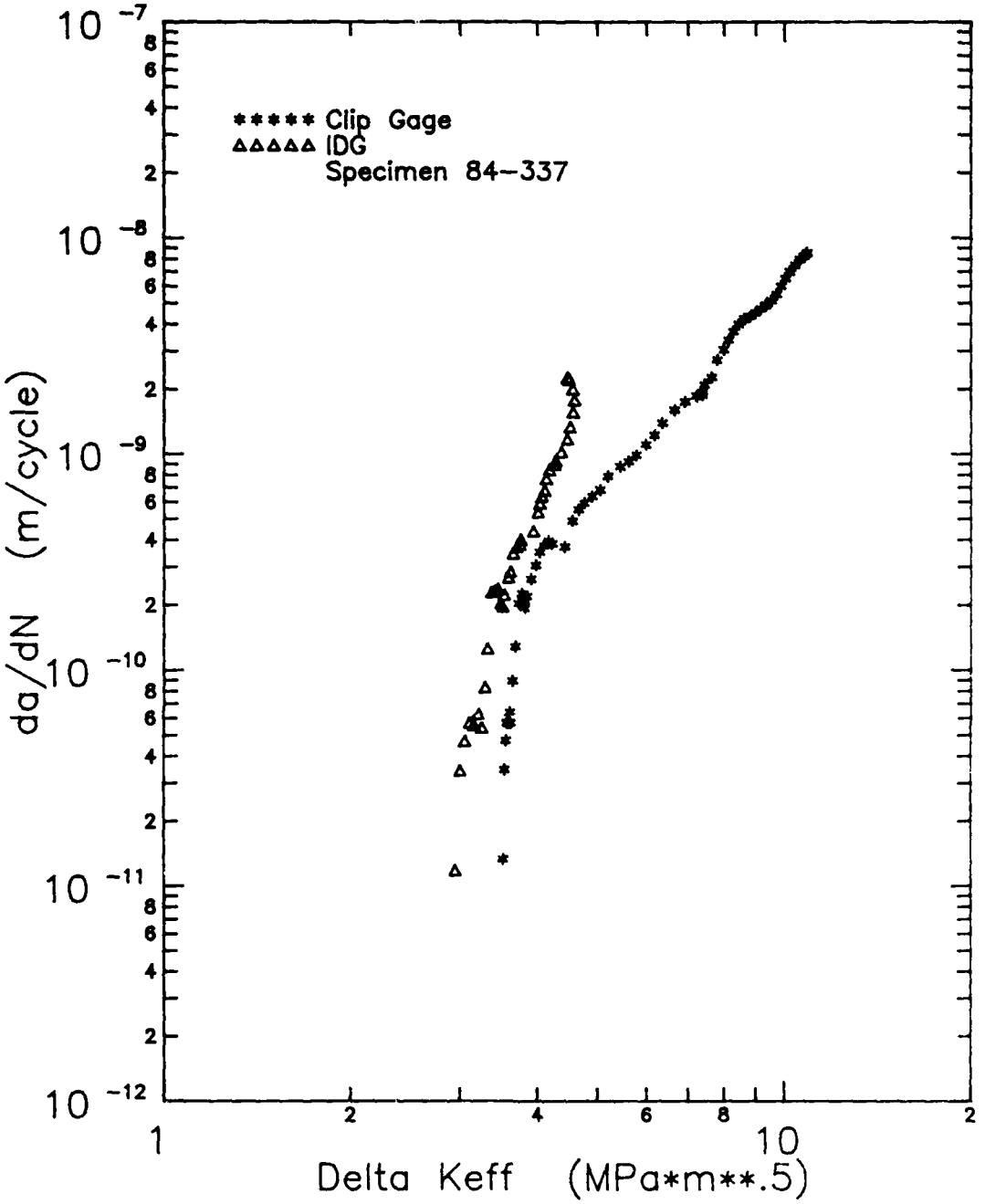

Figure 14. ΔK_{eff} Crack Growth Curves for the ASTM Decreasing K Test with R=0.1

III. Threshold Data for the ASTM Decreasing K , Constant P_{max} and Constant K_{max} Tests

Test	ΔK_{th} (MPa$\sqrt{m}$)	$\Delta K_{eff,th}$ (MPa$\sqrt{m}$)			R_{th}
		Clip	BFS	IDG	
ASTM Dec K R=0.1	5.89	3.65	N/A	3.29	0.1
ASTM Dec K R=0.5	2.86	2.72	2.86	2.72	0.5
Const Pmax R=0.5	2.86	2.70	2.86	2.65	0.5
Const Kmax 7 MPa$\sqrt{m}$	3.50	3.50	3.50	3.22	0.5
Const Kmax 6.5 MPa$\sqrt{m}$	3.25	3.25	N/A	3.18	0.5

Notes:

1. The R_{th} values represent the loads ratio at threshold.
2. The constant Pmax test was a continuation of the ASTM decreasing K test at R = 0.5. Thus, the constant Pmax test is not a threshold test since it establishes crack growth after threshold has been reached.

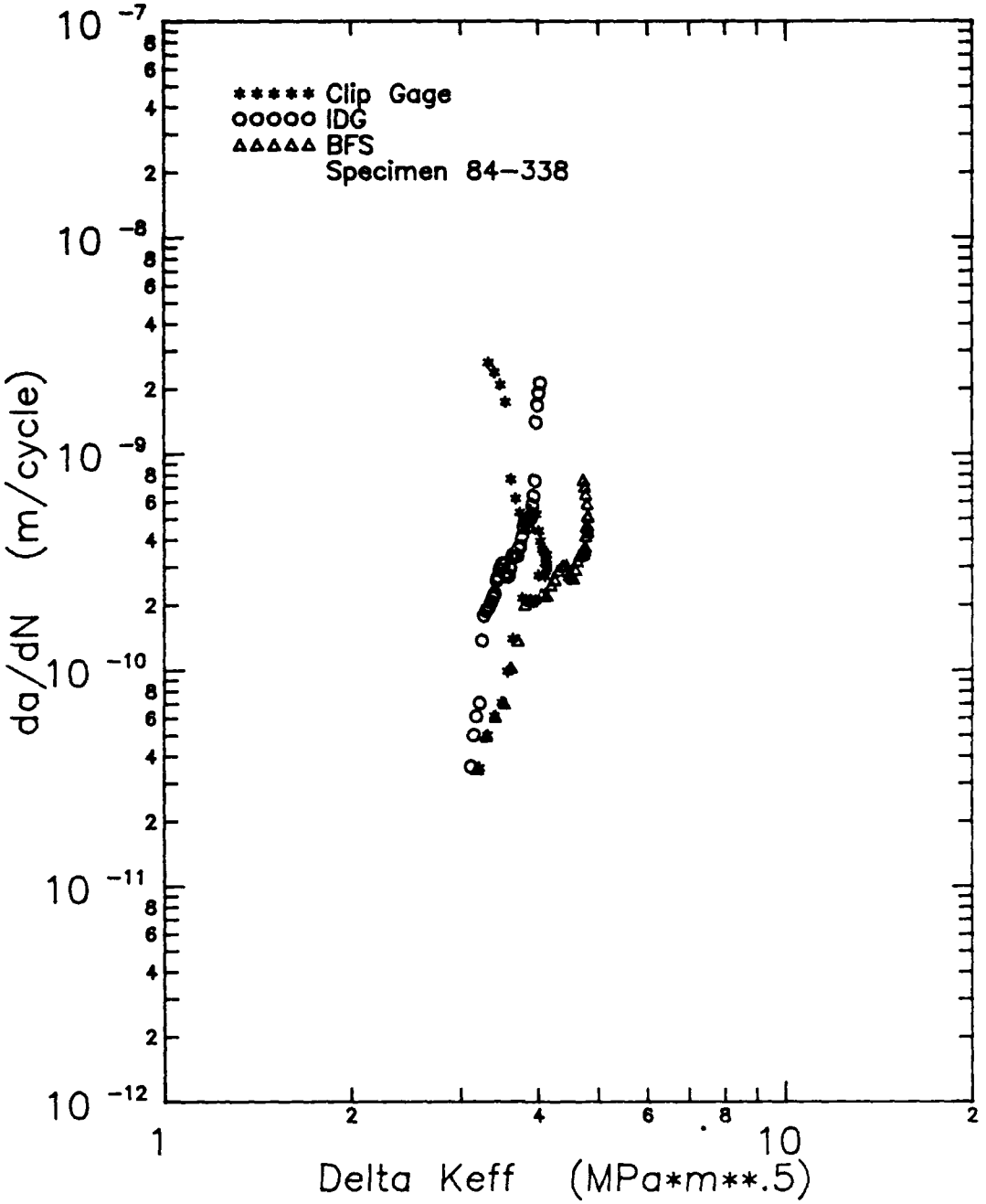

Figure 15. Crack Growth Curves for the Constant K_{max}=7 MPa*m**.5 Test

closure loads of the three techniques used in this study.

A similar trend for closure load measurements can be seen in the ΔK_{eff} crack curves plotted for the other tests in Appendix B. The actual closure loads measured are displayed in the load histories contained in Appendix C. Since the IDG was still able to measure closure at the higher load ratios, the ΔK_{eff} data discussed in the remainder of this study will be based on the IDG data.

ASTM Decreasing K Tests

The test control of the load shedding rate and data collection for the ASTM decreasing K tests (Figure 4) was fully automated. Data was recorded at intervals of Δa = 0.025 mm. By using the most recent fifteen data points, the control program calculated the current crack growth rate. Knowing the da/dN and the cycling frequency of 30 hz, the time needed to get the desired crack extension was then computed.

The ASTM decreasing K tests were run on specimens 84-337 and 84-342 for R = 0.1 and 0.5, respectively. The measured crack length histories and computed crack growth rates as a function of cycles for these tests are included in Appendices D and E. Since there was little or no closure measured throughout the test, the ΔK was approximately equal to the ΔK_{eff} for the ASTM decreasing K test at R = 0.5. This result can be verified by looking at the load history in Appendix C. So, only the ΔK_{eff} crack growth relation was plotted in Figure 16 for R = 0.5. Both the ΔK and ΔK_{eff} curves are shown for R = 0.1 since the

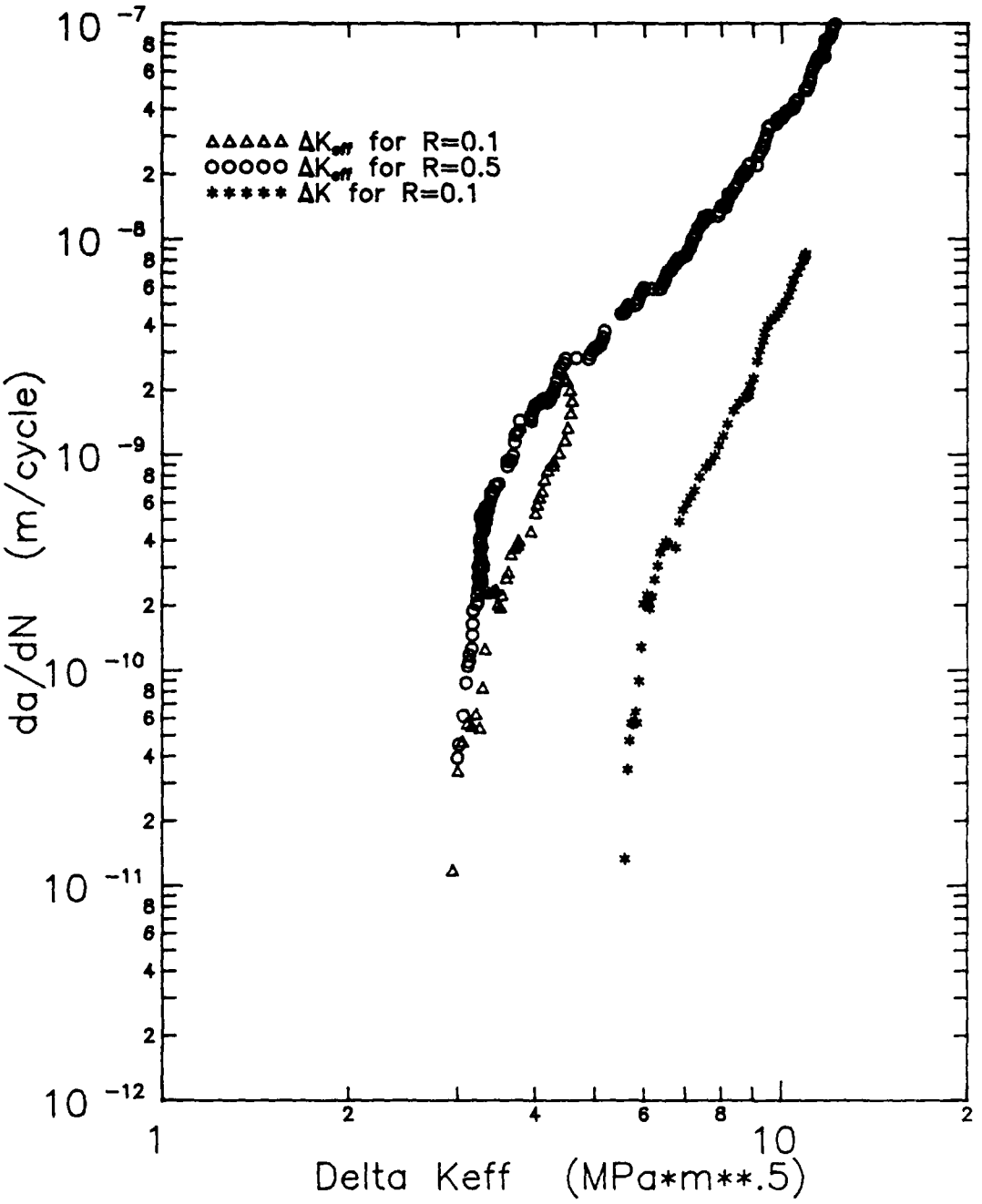

Figure 16. Crack Growth Curves for the ASTM Decreasing K Tests

closure measured for that test was significant. As can be seen in Figure 16, the ΔK crack growth relations were highly dependent on R. The curves shifted to the left as the load ratio increased. Similarly, from Table III, the ΔK_{th} varied from 5.89 to 2.86 MPa$\sqrt{m}$ for R = 0.1 and 0.5, respectively. However, the ΔK_{eff} curves for both tests had approximately the same with $\Delta K_{eff,th}$ = 3.29 MPa$\sqrt{m}$ for R = 0.1 and 2.72 MPa$\sqrt{m}$ for R = 0.5 when taking the data at da/dN = 10^{-10} m/cycle. To ensure that the threshold was reached, the tests were allowed to run to lower crack growth rates than the threshold condition as shown in Figure 16. So, by taking closure into account with ΔK_{eff}, the R dependence of the data was eliminated. For the ASTM decreasing K test at R = 0.1, IDG data was not taken until after da/dN < $5x10^{-9}$ m/cycle. Thus, the ΔK_{eff} crack curve which was computed using the closure loads measured by the IDG started at a lower crack growth rate than the ΔK crack curve for R = 0.1 as shown in Figure 16.

After the ASTM decreasing K test was completed, a constant P_{max} test at R = 0.5 was run on specimen 84-342 to ensure the threshold data collected was correct. In Figure 17, the ΔK_{eff} crack growth curve for the constant P_{max} test was about the same as the curve for the ASTM decreasing K test. especially at threshold. The $\Delta K_{eff,th}$ values of 2.65 and 2.72 MPa$\sqrt{m}$ shown in Table III for the constant P_{max} test and the ASTM decreasing K test, respectively, only varied 2.6%. Thus, these results verify the accuracy and repeatability of the data using the test setup and testing procedures in this study.

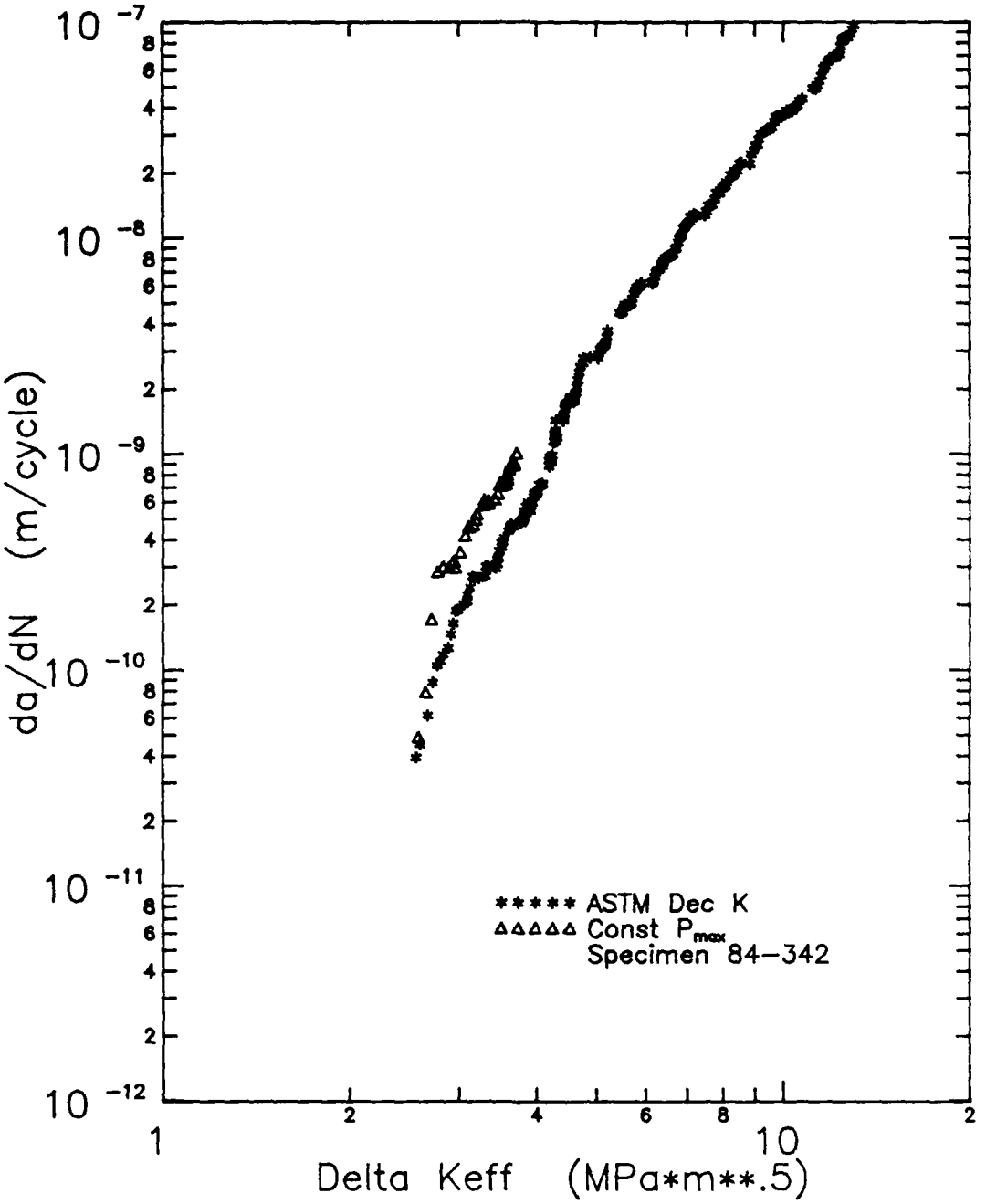

Figure 17. ΔK_{eff} Crack Growth Curves for the ASTM Decreasing K and Constant P_{max} Tests for the IDG at R=0.5

Now that the trend lines for the heat treated Ti 6246 have been established, a comparison with the fatigue behavior of a similar alloy that did not undergo the additional heat treatment can be discussed. As expected, the additional heat treatment improved the fatigue characteristics of Ti 6246 as shown in Figures 18 and 19. The ΔK crack growth relations shifted to the right as a result of the heat treatment. The ΔK_{th} increased from 3.39 to 6.08 MPa$\sqrt{m}$ at R = 0.1. Further, at R = 0.5, the ΔK_{th} increased from 2.30 to 2.86 MPa$\sqrt{m}$ due to the heat treatment. By looking at Figure 19, it was apparent that the additional heat treatment also increased the amount of closure present since the change in ΔK_{eff} was more dramatic for the heat treated Ti 6246. Also, for higher ΔK_{eff} values, the effects of heat treatment were negligible. However, at threshold, the $\Delta K_{eff,th}$ increased from 2.58 to 3.29 MPa$\sqrt{m}$ at R = 0.1 for the heat treated alloy. Similarly, at R = 0.5, the $\Delta K_{eff,th}$ increased from 2.30 to 2.72 MPa$\sqrt{m}$.

Varying ΔK Tests

The second set of constant R tests, the varying ΔK tests (Figure 5), were conducted on specimens 84-340 and 84-341. Two tests with K_{max0} = 10 and 20 MPa$\sqrt{m}$ were run on each specimen at two load ratios. To prevent any effects of a larger previous overload, the tests with K_{max0} = 10 MPa$\sqrt{m}$ were run first on both specimens.

To establish the crack growth rate for a particular ΔK, twenty data points were taken at intervals of Δa = 0.025 mm.

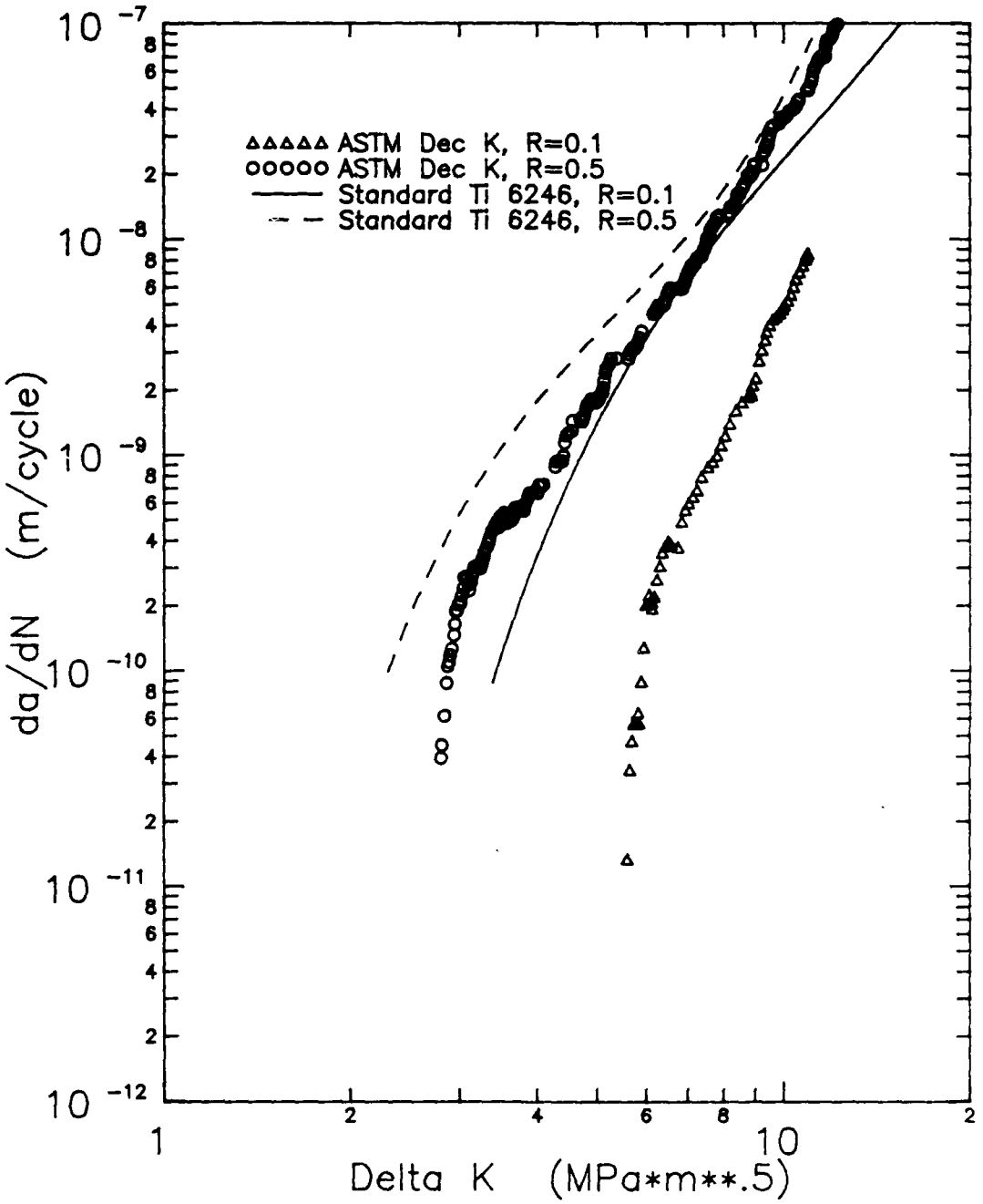

Figure 18. Effects of Heat Treatment on ΔK Crack Growth Curves for Ti 6246

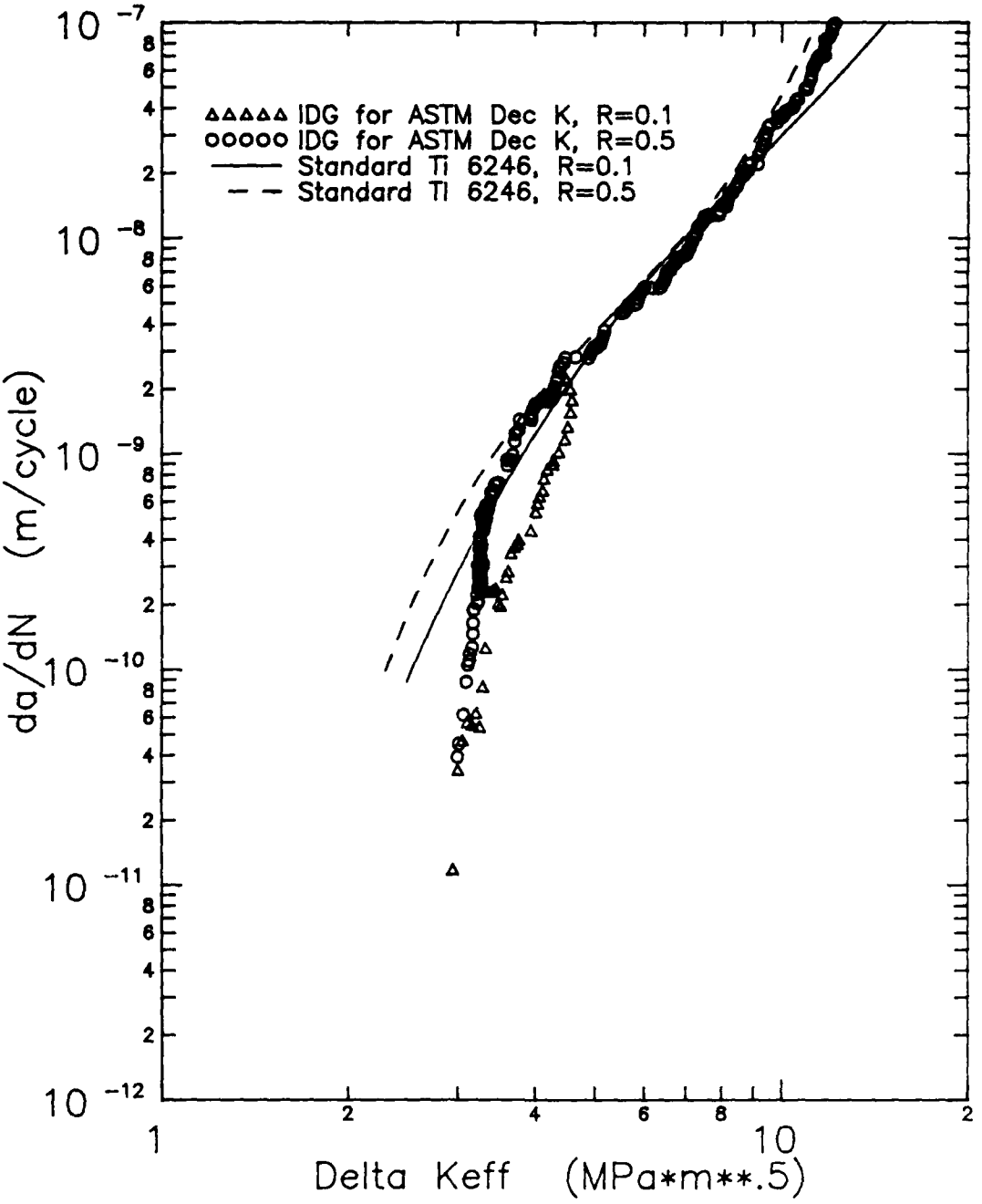

Figure 19. Effects of Heat Treatment on ΔK_{eff} Crack Growth Curves for Ti 6246

Once twenty or more data points were collected, the subsequent load drop was manually entered since these tests were not fully automated.

For comparison purposes, the amount of closure present during a loading cycle was calculated using the following equation:

$$\%K_{cl} = \frac{\Delta K - \Delta K_{eff}}{\Delta K} \times 100\% \qquad (11)$$

where K_{cl} is the closure stress intensity, ΔK is the stress intensity range, and ΔK_{eff} is the effective stress intensity range. By using Eq (11), the closure load can be represented as a percentage of the applied load range.

The first varying ΔK test run was at R = 0.1 and 10 MPa$\sqrt{m}$ overload. To minimize the number of ΔK drops required to complete the test, the $\Delta K_{eff,th}$ from the ASTM decreasing K test was estimated to be the threshold for this test. So, a total of three drops were needed to determine the threshold range. The threshold range shown in Table IV sets the upper limit of the ΔK where crack growth was still detected and the lower limit of no growth. By comparing the growth and no growth conditions, the closure load remained constant at about 60% of the applied load range. However, for the ASTM decreasing K test at R = 0.1, the closure load was only 44% of the load range at threshold. So, the overload condition increased the amount of closure present when compared to a

Table IV. Results from the Varying ΔK Tests

		Growth		No Growth	
		ΔK	ΔKeff	ΔK	ΔKeff
R = 0.1 Kmaxo=10	Clip	5.85	3.71	5.66	3.15
	BFS		4.42		4.32
	IDG		2.29		2.26
R = 0.1 Kmaxo=20	Clip	5.86	2.35	5.63	2.34
	BFS		3.06		3.02
	IDG		2.22		2.11
R = 0.5 Kmaxo=10	Clip	3.88	3.93	3.68	3.76
	BFS		3.96		3.75
	IDG		3.66		2.94
R = 0.5 Kmaxo=20	Clip	5.43	5.35	5.26	3.49
	BFS		5.40		3.73
	IDG		4.13		2.74

Note: The units for the stress intensities are MPa$\sqrt{m}$.

loading history with a gradual change as was the case for the ASTM decreasing K test.

For K_{max0} = 20 MPa$\sqrt{m}$ at R = 0.1, the threshold range was reached within the first two ΔK drops. Again, looking at Table IV, the closure load represented 62% of the applied load range. Thus, doubling the overload only slightly increased the closure present.

As shown in Table IV, the varying ΔK tests at R = 0.1 had approximately the same ΔK and ΔK_{eff} at the growth and no growth for both overload conditions. Therefore, the overload conditions at this low load ratio did not have much effect on the threshold data.

Specimen 84-341 was used to run the same ΔK tests at R = 0.5. Again, only two ΔK drops were needed to get the threshold range for K_{max0} = 10 MPa$\sqrt{m}$. But, the no growth condition was found in the first drop instead of the last. Since the ΔK overload should eliminate any previous load histories up to that point, the order in which growth and no growth is established for the threshold range should not matter.

For R = 0.5, no significant closure measurements were expected. However, as shown in Figure 20, after the overload was applied there was a significant amount of closure present. From Table IV, the closure load for the growth and no growth conditions was 6% and 20% of the applied load range, respectively. Although the change in ΔK between growth and no growth was only 0.2 MPa$\sqrt{m}$, the change in ΔK_{eff} was 0.72 MPa$\sqrt{m}$

due to the introduction of higher closure load for the no growth condition.

A similar trend was seen for the test at R = 0.5 and K_{max0} = 20 MPa$\sqrt{m}$ as shown in Figure 21. For the growth condition, the closure load represented 20% of the applied load range. The amount of closure present increased to 48% of the applied range for the no growth condition after the overload of 20 MPa$\sqrt{m}$. Unlike the varying ΔK tests at R = 0.1, the amount of closure present after the overload increased dramatically when increasing the K_{max0} from 10 to 20 MPa$\sqrt{m}$ for R = 0.5 . Also, for R = 0.5, increasing the overload increased the ΔK at which growth was established from 3.88 to 5.43 MPa$\sqrt{m}$. Similar results were found for the no growth condition with ΔK increasing from 3.68 to 5.26 MPa$\sqrt{m}$. Like the test with K_{max0} = 10 MPa$\sqrt{m}$, the change in ΔK_{eff} between growth and no growth was 1.39 MPa$\sqrt{m}$ even though the change in ΔK was only 0.2 MPa$\sqrt{m}$.

According to the data presented in Table IV, the results of these tests confirmed the work done by Ogawa and others (12:875, 877). Their study concluded that the ΔK_{th} increased with an increasing overload if R was held constant throughout the test. However, other researchers (13:190 ; 6:313 ; 7:828) found that ΔK_{th} decreased for an increasing overload when R was not held constant. Thus, the ΔK_{th} produced from overloading the material was also dependent on whether R was held constant throughout the test or not.

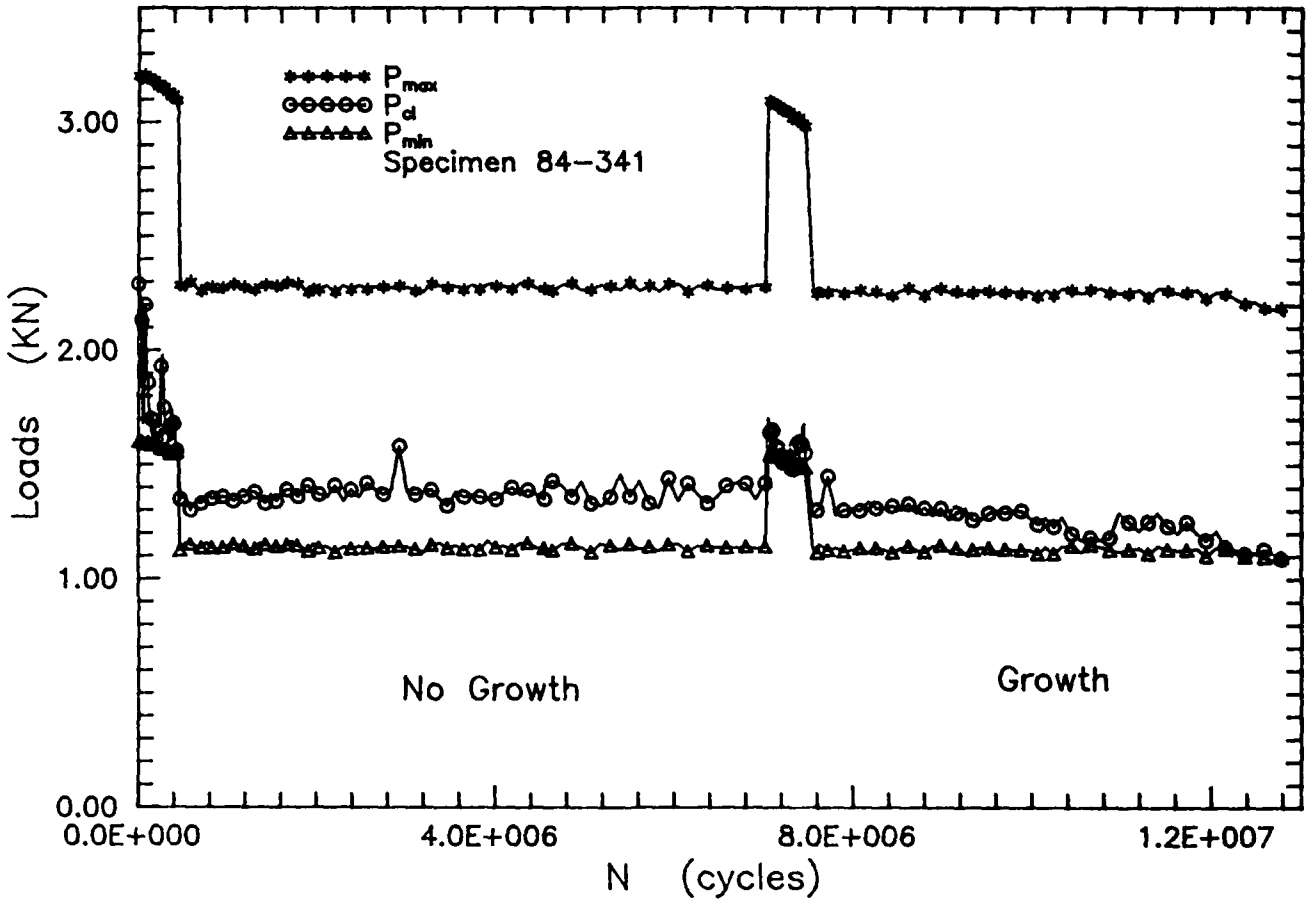

Figure 20. Load History for Varying ΔK Test with Closure from IDG for R=0.5 and K_{max0}=10 MPa*m**.5

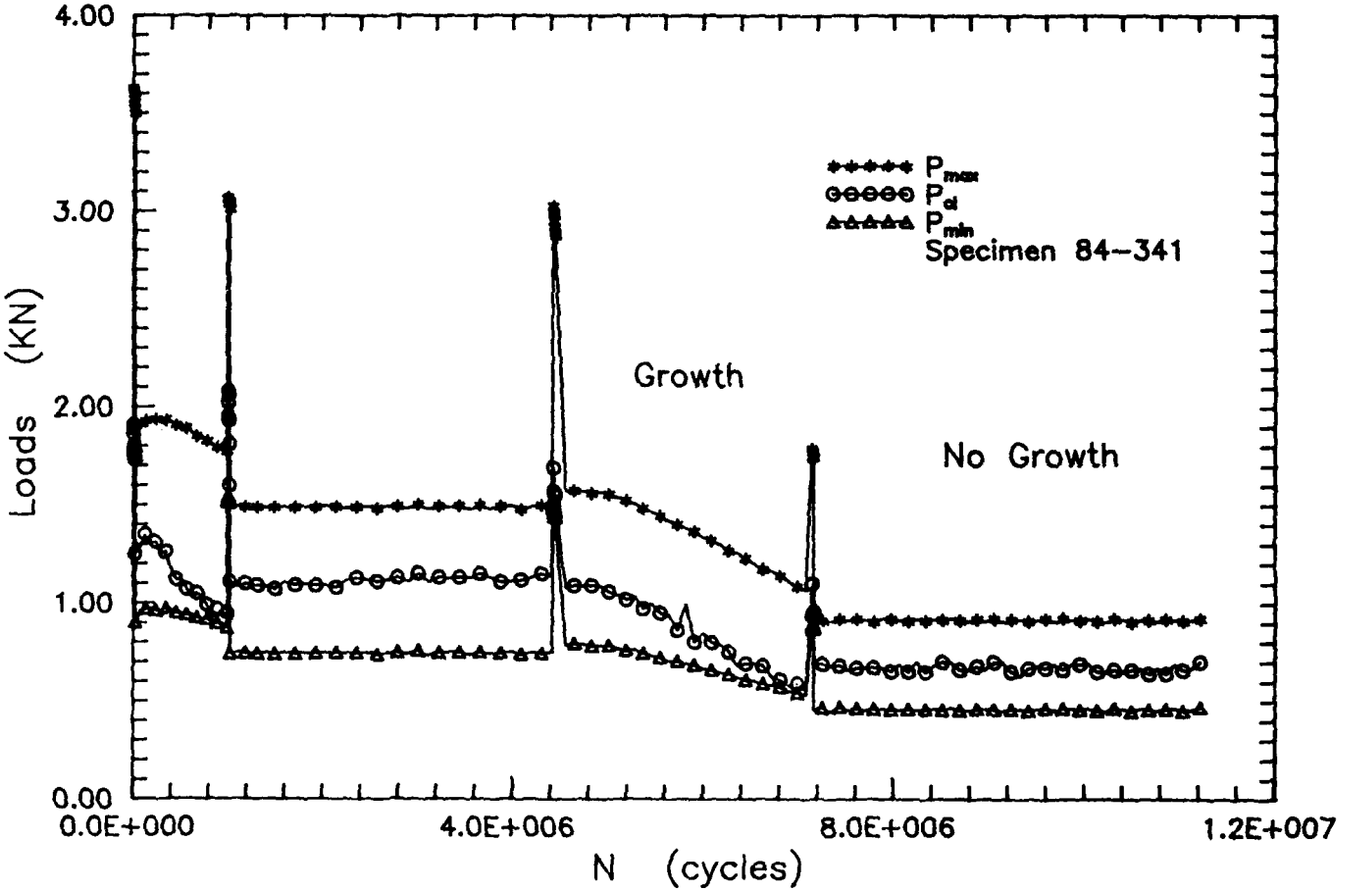

Figure 21. Load History for Varying ΔK Test with Closure from IDG for R=0.5 and K_{max0}=20 MPa*m**.5

Constant K_{max} Tests

The second type of test involved holding K_{max} constant while R was allowed to vary. The control of the constant K_{max} tests was fully automated. Data was collected following the same procedure outlined for the ASTM decreasing K tests.

The ΔK_{eff} crack growth relations are shown in Figure 15 and Appendix B for the constant K_{max} = 7 and 6.5 MPa$\sqrt{m}$ tests, respectively. The load histories for both tests are contained in Appendix C.

Both tests began at R = 0.1 with low K_{max} values in an attempt to reach threshold below R = 0.5 so that the closure effects could be examined. Figure 22 contains the ΔK crack growth curves for the constant K_{max} = 6.5 and 7 MPa$\sqrt{m}$ tests along with the reference lines generated by the ASTM decreasing K tests at R = 0.1 and 0.5. As can be seen in the diagram, both constant K_{max} tests began on the R = 0.1 curve and ended at or just beyond the R = 0.5 curve. Since K_{max} is held constant, as K_{min} is linearly increased, the load ratio will also increase linearly. Thus, the fatigue threshold for both constant K_{max} tests was reached at R = 0.5.

The constant K_{max} = 7 MPa$\sqrt{m}$ test was run on specimen 84-338. The initial ΔK of 6.3 MPa$\sqrt{m}$ was close to the ΔK_{th} of 6.08 MPa$\sqrt{m}$ obtained by the ASTM decreasing K test at R = 0.1, the crack length history in Figure 23 graphically depicts a total crack extension of 2.15 mm. A da/dN of approximately 5×10^{-10} m/cycle can be seen in Figure 24 as threshold was reached. If K_{max} is held constant, the corresponding ΔK_{eff} was

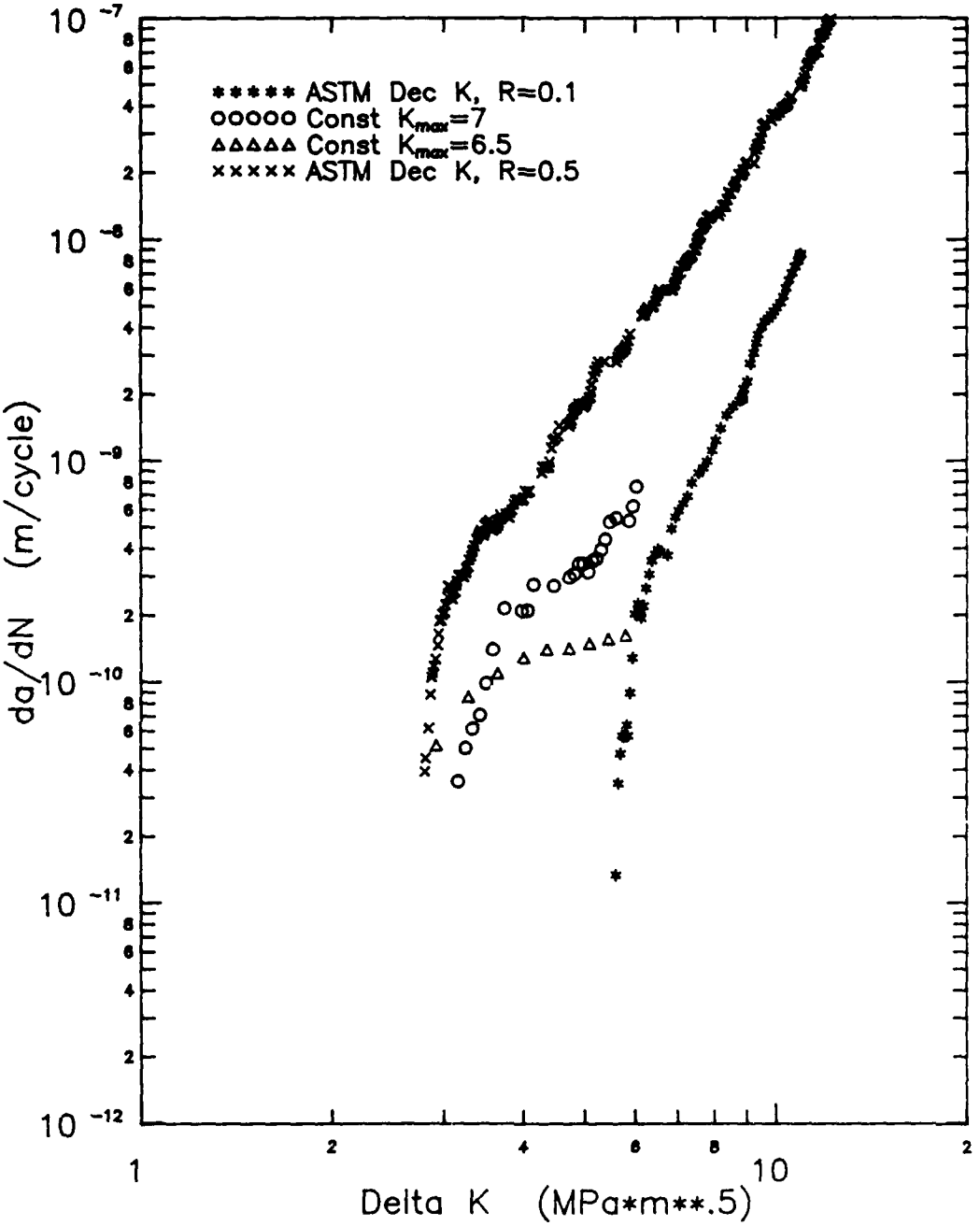

Figure 22. ΔK Crack Growth Curves

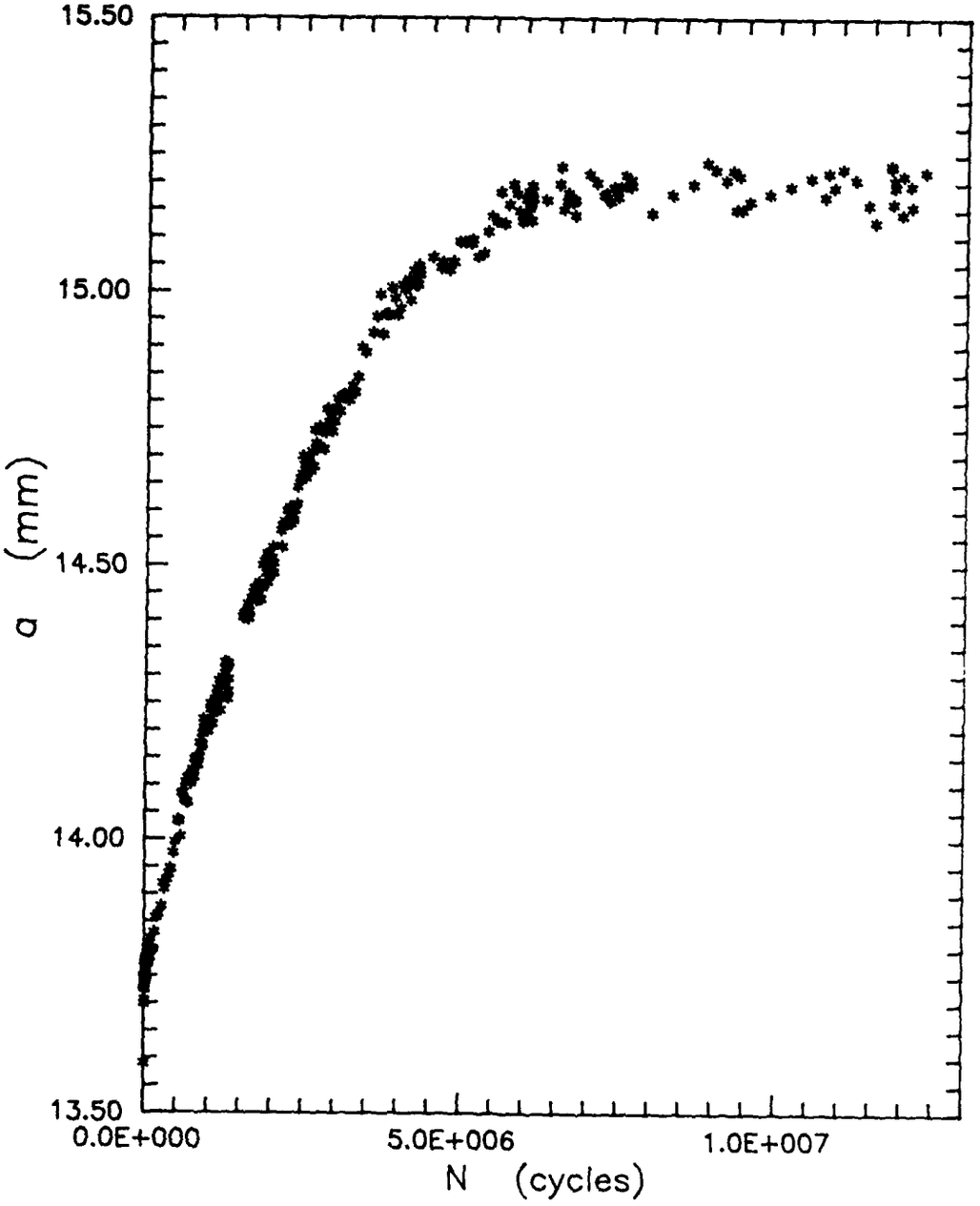

Figure 23. Crack Length History for the Constant K_{max}=7 MPa*m**.5 Test

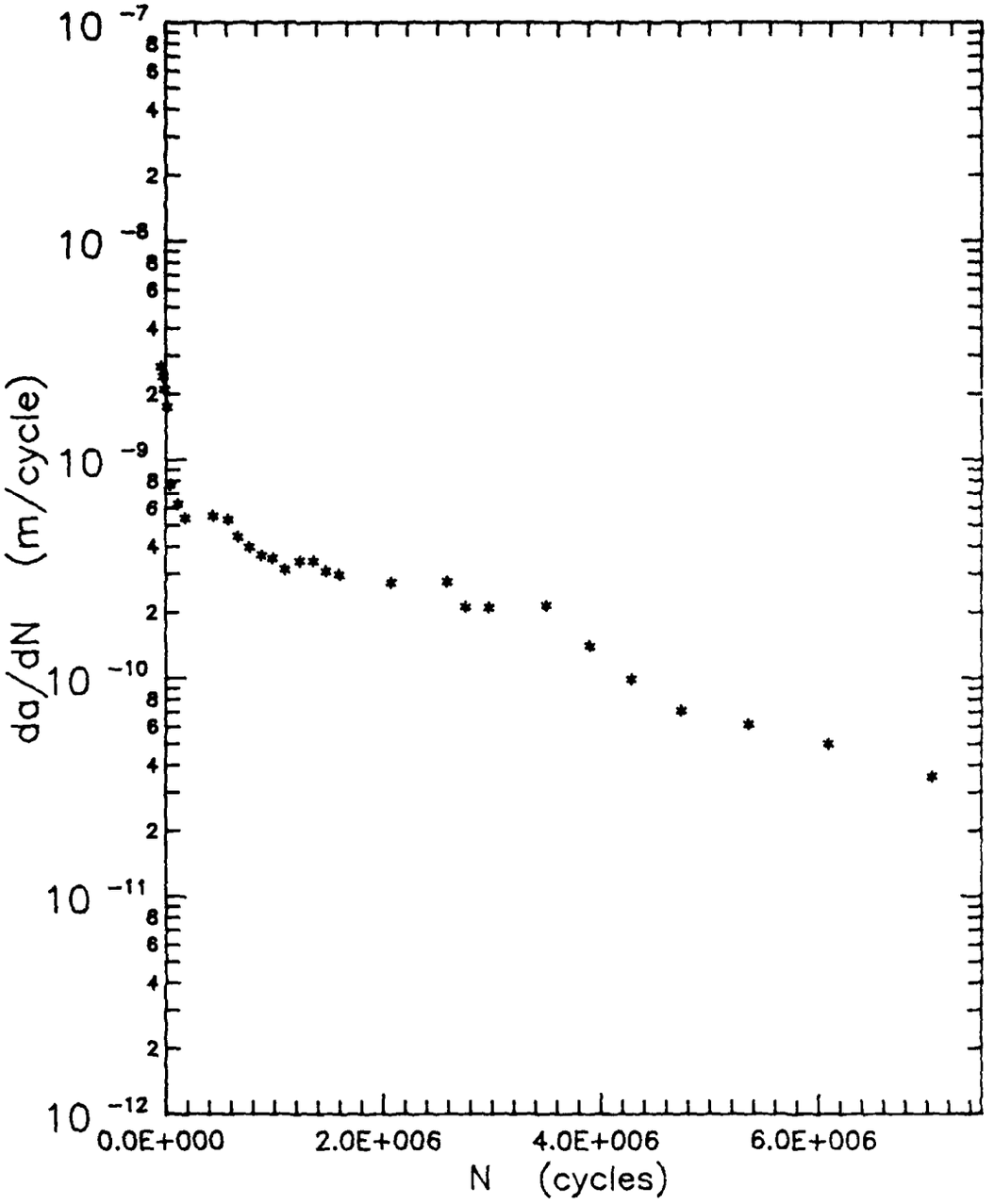

Figure 24. Crack Growth Rates for the Constant K_{max}=7 MPa*m**.5 Test

anticipated to be relatively constant for small variations in R since the closure load was also expected to be constant. So, the resulting da/dN should have been constant until $K_{min} > K_{cl}$ or $R \geq 0.5$. However, Figure 24 illustrates a gradual decrease in da/dN with increasing R. So, it is evident that the closure load was not constant at lower R values for a constant K_{max}.

As already noted, the R at threshold for specimen 84-338 was equal to 0.5. In an attempt to find threshold at a lower R, a second test was run with K_{max} = 6.5 MPa$\sqrt{m}$ using specimen 84-339. Unfortunately, the fatigue threshold was again reached at R = 0.5. Thus, for tensile cyclic loading using Ti 6246, it was not possible to reach threshold at $R < 0.5$ for the constant K_{max} tests.

As shown in Table III, the ΔK_{th} decreased from 3.45 to 3.25 MPa$\sqrt{m}$ for the constant K_{max} = 7 and 6.5 MPa$\sqrt{m}$, respectively. The $\Delta K_{eff,th}$, on the other hand, remained relatively constant for both tests only varying 1.2%. Thus, ΔK_{th} was sensitive to the load history while $\Delta K_{eff,th}$ was not.

Closure

Döker and Bachmann (23:254, 258-259) stated that closure was present up to R = 0.75. In Eqs (3) and (4) discussed earlier, they proposed that K_{cl} was linearly related to K_{max}. Knowing that K_{cl}/K_{max} is the same as P_{cl}/P_{max}, the values of P_{cl} were plotted against P_{max} in Figure 25. Since the equations were limited to constant R, only the ASTM decreasing K and varying ΔK tests were considered for this comparison.

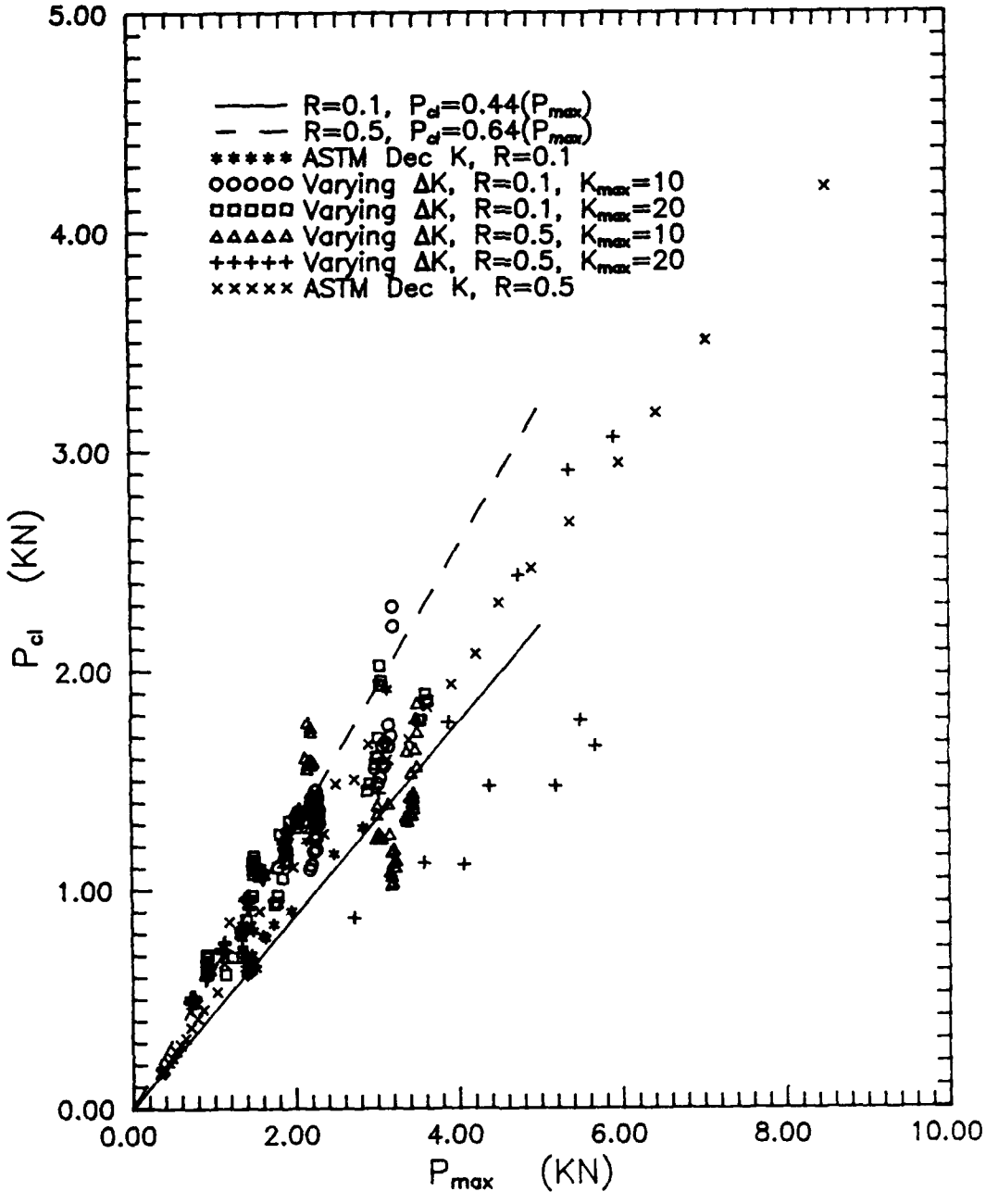

Figure 25. Comparison of Closure Equations with Test Results

Also, Döker and Bachmann (23:258) concluded that the BFS and clip gage were inadequate for measuring closure accurately. So, the closure as measured by the IDG was plotted against their equations. Figure 25 illustrates that the closure measurements collected in this study were not linearly related to K_{max}. The K_{cl} in this study was also found to be dependent on the loading history.

Döker and Bachmann (23:254-255) presented Eq (7) in the same paper. Again, they proposed that ΔK_{eff} was linearly dependent on ΔK for constant R tests. Figure 26 contains the results of the tests conducted in this study as compared to the theoretical relationship. As before, the ΔK_{eff} data collected in this study did not follow the linear relationship represented by Eq (7).

Effective Stress Intensity Threshold

Previous studies (14:7 ; 11:633) concluded that $\Delta K_{eff,th}$ could be considered a material property independent of R, loading history, and specimen geometry for standard Ti 6246. So, the $\Delta K_{eff,th}$ values for the ASTM decreasing K and constant K_{max} tests conducted in this study are compared in Figure 27. First, the ΔK_{th} was found to be dependent on R and loading history. As R increased in the ASTM decreasing K tests, the ΔK_{th} decreased dramatically from 5.89 to 2.86 MPa$\sqrt{m}$. Also, by decreasing the K_{max} in the loading history for the constant K_{max} tests, the ΔK_{th} was found to decrease. However, the $\Delta K_{eff,th}$ data was relatively constant. A mean $\Delta K_{eff,th}$ of

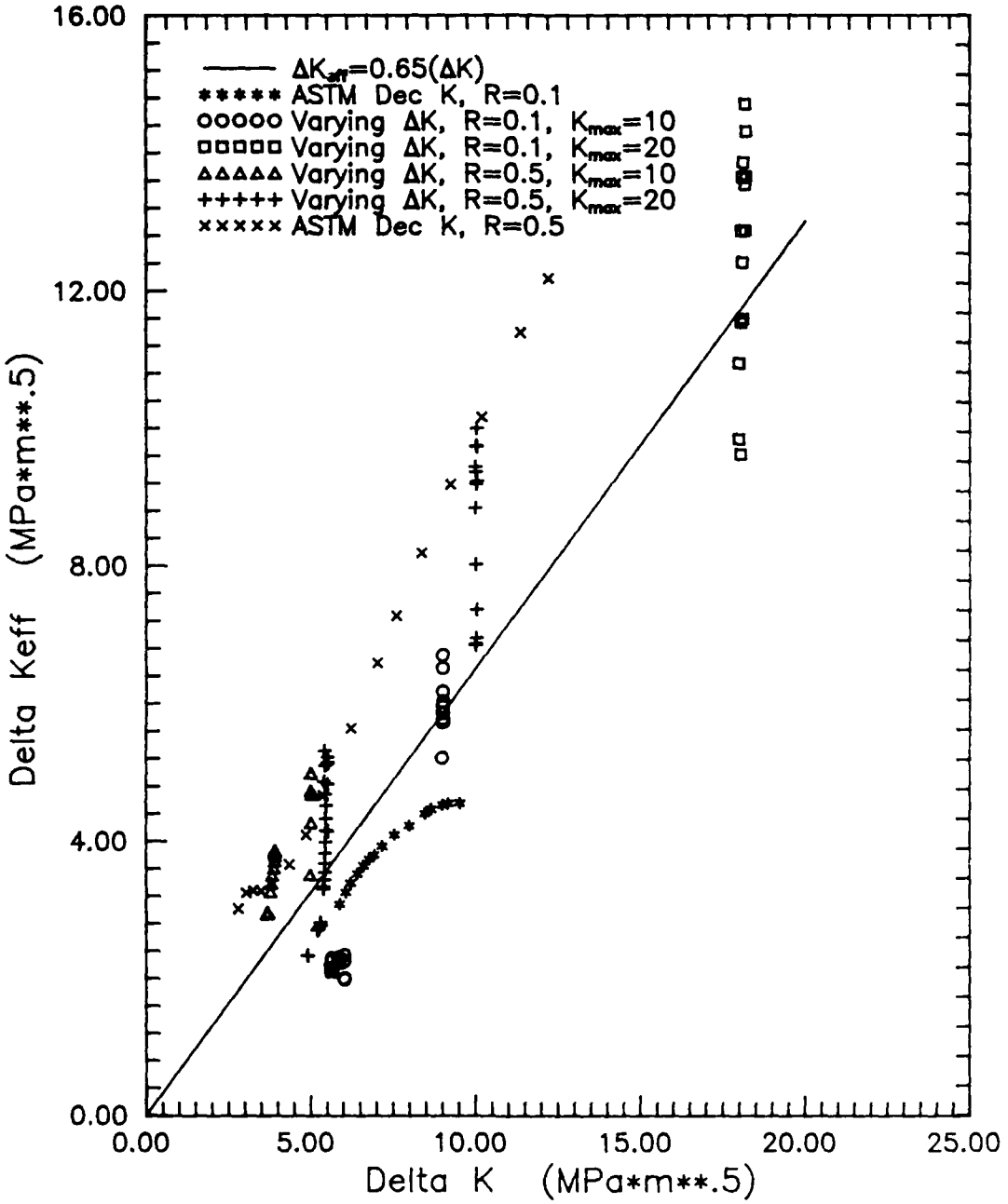

Figure 26. Comparison of $\Delta K_{eff}=0.65(\Delta K)$ with Test Results

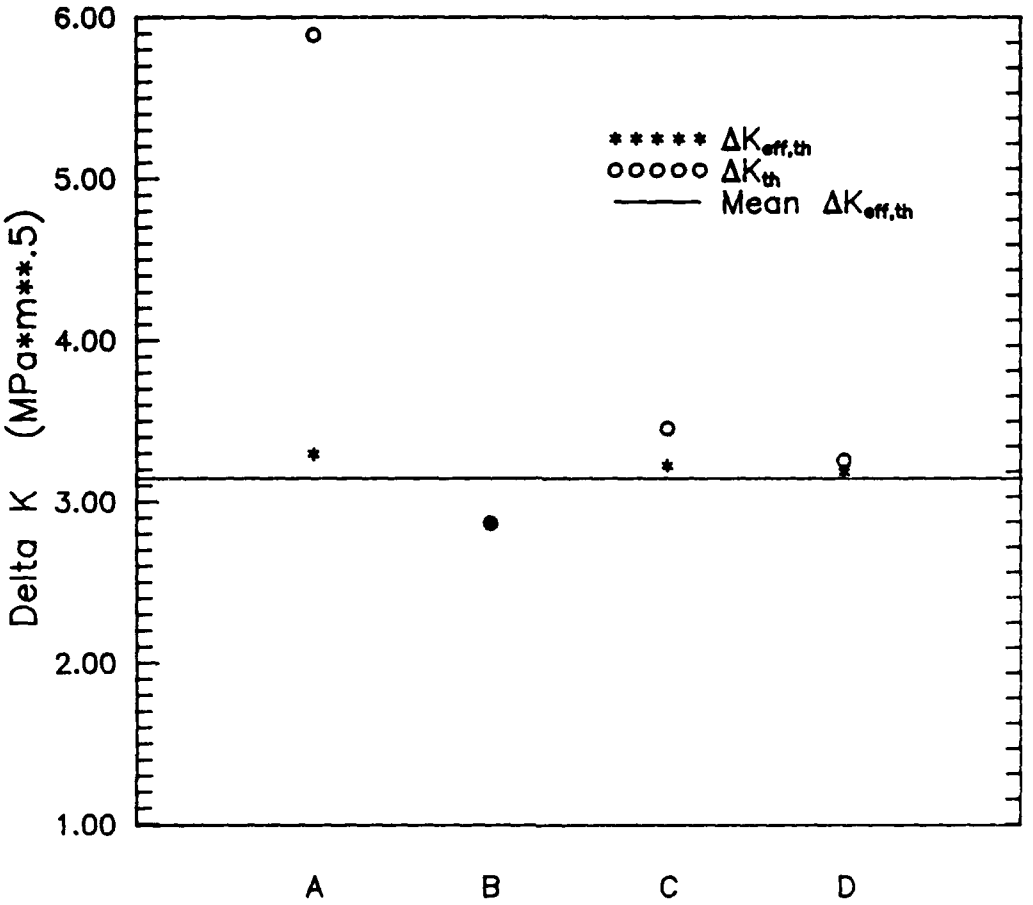

Specimens:
A = 84–337, ASTM Dec K, R=0.1
B = 84–342, ASTM Dec K, R=0.5
C = 84–339, Const K_{max}=7 MPa*m**.5
D = 84–342, Const K_{max}=6.5 MPa*m**.5

Figure 27. Threshold Stress Intensities for the ASTM Decreasing K and Constant K_{max} Tests

3.14 MPa$\sqrt{m}$ for these four tests was plotted as the straight line in Figure 27. The largest deviation from the mean $\Delta K_{eff,th}$ was the ASTM decreasing K test which varied 8.9%. The other three tests, on the other hand, deviated less than 5% from the mean $\Delta K_{eff,th}$.

Figure 28 shows the threshold data for the varying ΔK tests. The large difference for the growth and no growth conditions for the tests run at R = 0.5 was due to the amount of closure present after the overload as discussed earlier. For the R = 0.1 tests, the ΔK and ΔK_{eff} data remained relatively constant. But, for the R = 0.5 tests, ΔK increased with an increased overload. The change in ΔK_{eff} between the growth and no growth conditions increased from 0.72 to 1.39 MPa$\sqrt{m}$ as the overload increased for R = 0.5. The mean $\Delta K_{eff,th}$ from the ASTM decreasing K and constant K_{max} tests is also shown in Figure 28. Using this reference line, it is clear that $\Delta K_{eff,th}$ did not remain constant for the varying ΔK tests. Actually, the $\Delta K_{eff,th}$ varied as much as 30% from the mean $\Delta K_{eff,th}$ value.

The main difference between these tests was the overloads used in the varying ΔK tests. Both the ASTM decreasing K and constant K_{max} tests involved gradual changes in ΔK. Thus, $\Delta K_{eff,th}$ can not be considered a material property since it was not constant for different loading histories. Further, the $\Delta K_{eff,th}$ was found to be sensitive to overload conditions.

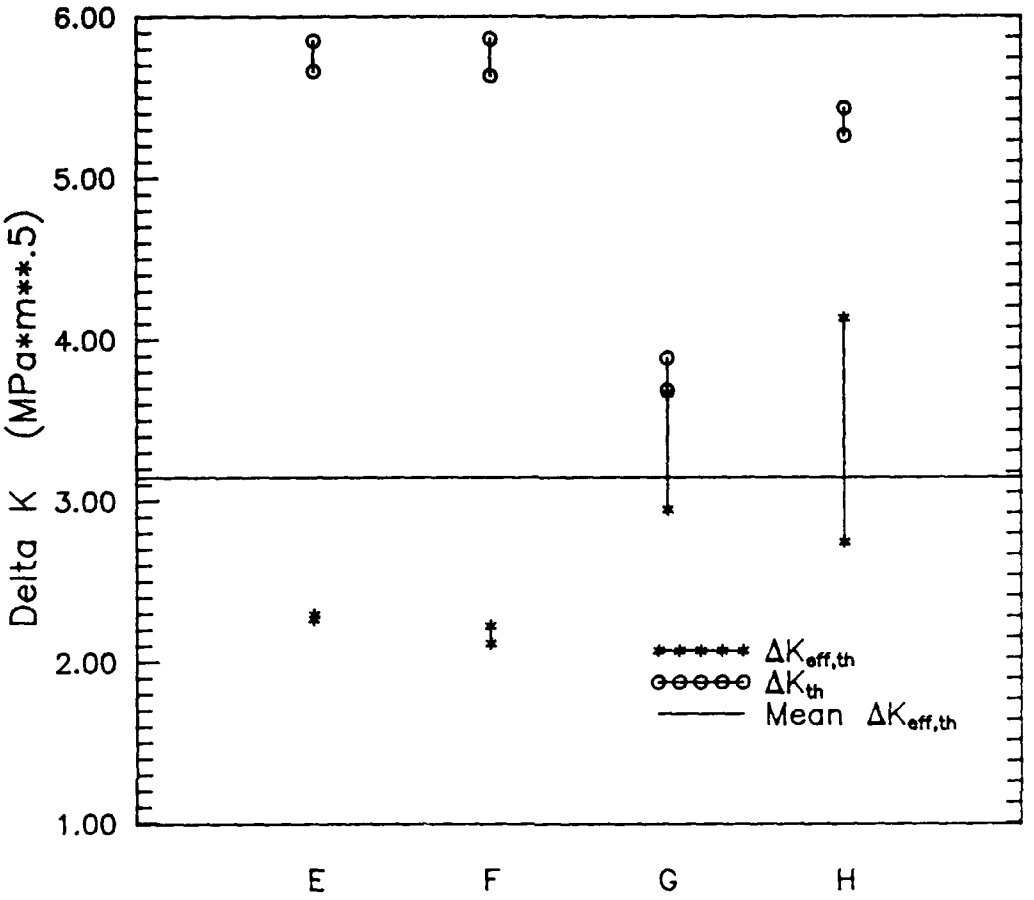

Specimens:
E = 84-340, Varying ΔK, R=0.1, K_{max}=10 MPa*m**.5
F = 84-340, Varying ΔK, R=0.1, K_{max}=20 MPa*m**.5
G = 84-341, Varying ΔK, R=0.5, K_{max}=10 MPa*m**.5
H = 84-341, Varying ΔK, R=0.5, K_{max}=20 MPa*m**.5

Figure 28. Threshold Stress Intensities for the Varying ΔK Tests

V. Conclusions

This study was conducted to determine the effects of crack closure and loading history on heat treated Ti 6246. Three measurement techniques; clip gage, BFS, and IDG, were used to record the closure loads. A comparison of heat treated and standard Ti 6246 was also discussed.

To accomplish the objectives, two types of tests were used. Maintaining R constant throughout the test was the first test type. The ASTM decreasing K test was used to establish reference lines for the remainder of the study since no experimental data was available for this alloy. The second test holding R constant was the varying ΔK test where the effects of overloads were examined. The last test type involved varying R. A constant K_{max} test with a gradually increasing K_{min} was the only test run under this category.

Based on the results, the following conclusions were made:

1. Out of the three measurement techniques used, the IDG yielded the highest closure loads.

2. Heat treating Ti 6246 at 971°C for 2 1/4 hours and furnace cooling at a rate of 38°C/hour improved its fatigue characteristics.

3. Applying tensile cyclic loading only, threshold could not be reached at $R < 0.5$ for the constant K_{max} test using this heat treated Ti 6246.

4. The ΔK_{th} decreased for an increasing load ratio, R.

5. For testing with overload conditions, ΔK_{th} increased with an increasing K_{max} if R was held constant throughout the test.

6. The K_{cl} was dependent on R and loading history. For the varying ΔK tests, K_{cl} increased with an increasing overload.

7. $\Delta K_{eff,th}$ was approximately constant for the ASTM decreasing K and constant K_{max} tests. However, the varying ΔK tests yielded different effective stress intensity thresholds. Thus, $\Delta K_{eff,th}$ was found to be sensitive to overloads and should not be considered a material property until more research involving overload effects is conducted.

VI. Recommendations

Since the IDG was found to be more accurate at measuring the closure loads, it is recommended that the program used to control the testing should employ the IDG data collected rather the clip gage's data. So, the compliance equations for calculating the crack length need to be changed to use the crack opening displacements measured by the IDG. Lastly, varying ΔK tests for several R values need to be conducted to establish how $\Delta K_{eff,th}$ is related to overloads.

Bibliography

1. Paris, P. and Erdogan, F. "A Critical Analysis of Crack Propagation Laws," Journal of Basic Engineering, 85: 528-534 (December 1963).

2. Schmidt, R. A. and Paris, P. C. "Threshold for Fatigue Crack Propagation and the Effects of Load Ratio and Frequency," Progress in Flaw Growth and Fracture Toughness Testing, ASTM STP 536. 79-94. Philadelphia: American Society for Testing and Materials, 1973.

3. Guerra-Rosa, L. and others. "Influence of Plastic Zone Size on Closure Phenomenon at Fatigue Thresholds in Steels," Fatigue 84. 231-239. Warley, United Kingdom: Engineering Materials Advisory Services LTD., 1984.

4. Döker, H. and others. "A Comparison of Different Methods of Determination of the Threshold for Fatigue Crack Propagation," Fatigue Thresholds: Fundamentals and Engineering Applications. 45-57. Warley, United Kingdom: Engineering Materials Advisory Services LTD., 1982.

5. Annual Book of ASTM Standards, E647-86a. 899-926. Philadelphia: American Society for Testing and Materials, 1986.

6. Castro, D. E. and others. "A Generalized Concept of a Fatigue Crack," Fatigue of Engineering Materials and Structures, 10: 305-314 (1987).

7. Castro, D. E. and others. "Threshold and Nonpropagation of Fatigue Cracks Under Service Loading," Fracture Mechanics: Nineteenth Symposium, ASTM STP 969. 818-829. Philadelphia: American Society for Testing and Materials, 1988.

8. Radon, J. C. "Fatigue Crack Growth in the Threshold Region," Fatigue Thresholds: Fundamentals and Engineering Applications. 113-132. Warley, United Kingdom: Engineering Materials Advisory Services LTD., 1982.

9. Cadman, A. J. and others. "Effect of Test Technique on the Fatigue Threshold ΔK_{TH}," Fatigue Thresholds: Fundamentals and Engineering Applications. 59-75. Warley, United Kingdom: Engineering Materials Advisory Services LTD., 1982.

10. Walker, N. and Beevers, C. J. "A Fatigue Crack Closure Mechanism in Titanium," Fatigue of Engineering Materials and Structures, 1: 135-148 (1979).

11. Jira, J. R. and others. "Effects Of Closure on Fatigue Crack Growth of Small Surface Cracks in a High Strength Titanium Alloy," Mechanics of Fatigue Crack Closure, ASTM STP 982. 617-635. Philadelphia: American Society for Testing and Materials, 1988.

12. Ogawa, T. and others. "The Effects of Loading History on Fatigue Crack Growth Threshold," Fatigue 87. 869-878. Warley, United Kingdom: Engineering Materials Advisory Services LTD., 1987.

13. Döker, H. and Marci, G. "Threshold Range and Opening Stress Intensity Factor in Fatigue," International Journal of Fatigue, 5: 187-191 (October 1983).

14. Mall, S. and others. "A Comparison of Different Test Techniques on Fatigue Threshold Behavior of Surface Flaws in a Titanium Alloy," to be presented at the Seventh International Conference in Fracture, Houston, April 1989.

15. Elber, W. "The Significance of Fatigue Crack Closure," Damage Tolerance in Aircraft Structures, ASTM STP 486. 230-242. Philadelphia: American Society for Testing and Materials, 1971.

16. Elber, W. "Fatigue Crack Closure Under Cyclic Tension," Engineering Fracture Mechanics,, 2: 37-45 (1970).

17. Banerjee, S. A Review of Crack Closure, August 1983 - December 1983. AFWAL-TR-84-4031. Dayton OH: University of Dayton, April 1984.

18. Sadananda, K. "Factors Governing Near-Threshold Fatigue Crack Growth," Fatigue 84. 543-553. Warley, United Kingdom: Engineering Materials Advisory Services LTD., 1984.

19. Kwon, J. H. and others. "Atmospheric Influence on Fatigue Crack Growth Mechanisms," Fatigue 84. 435-443. Warley, United Kingdom: Engineering Materials Advisory Services LTD., 1984.

20. Kendall, J. M. and Knott, J. F. "The Influence of Microstructure and Temperature on Near-Threshold Fatigue Crack Growth in Air and Vacuum," Fatigue 84. 307-317. Warley, United Kingdom: Engineering Materials Advisory Services LTD., 1984.

21. Dias, A. and others. "Influence of Crack Closure on Fatigue Crack Propagation and Threshold," Fatigue 87. 749-758. Warley, United Kingdom: Engineering Materials Advisory Services LTD., 1987.

22. Döker, H. and Peters, M. "Fatigue Threshold Dependence on Material, Environment and Microstructure," Fatigue 84. 275-285. Warley, United Kingdom: Engineering Materials Advisory Services LTD., 1984.

23. Döker, H. and Bachmann, V. "Determination of Crack Opening Load by Use of Threshold Behavior," Mechanics of Fatigue Crack Closure, ASTM STP 982. 247-259. Philadelphia: American Society for Testing and Materials, 1988.

24. Macha, D. E. and others. "On the Variation of Fatigue-Crack-Opening Load with Measurement Location," Experimental Mechanics, 19: 207-213 (June 1979).

25. Ashbaugh, N. "Effects of Load History and Specimen Geometry on Fatigue Crack Closure Measurements," Mechanics of Fatigue Crack Closure, ASTM STP 982. 186-196. Philadelphia: American Society for Testing and Materials, 1988.

26. Sharpe, W. D., Jr. and Grandt, Capt A. F., Jr. "A Laser Interferometric Technique for Crack Surface Displacement Measurement," ISA ASI 74230: 147-154 (1974).

27. Hartman, G. and Nicholas, T. "An Enhanced Laser Interferometer for Precise Displacement Measurements," Experimental Techniques, 11: 24-26 (February 1987).

28. Sharpe, W. N., Jr. "Interferometric Surface Strain Measurement," International Journal of Nondestructive Testing, 3: 59-76 (1971).

29. Chesnutt, J. C. and others. "Fatigue Crack Propagation in Titanium Alloys," Fatigue 84. 341-350. Warley, United Kingdom: Engineering Materials Advisory Services LTD., 1984.

30. Rhodes, C. G. and Paton, N. E. Mechanical Behavior of Titanium Alloys, 1 February 1976 - 31 January 1979. Contract N00014-76-C-0598. Thousand Oaks CA: Rockwell International Science Center, April 1979 (AD-A068810).

31. Larsen, J. M., Materials Research Engineer. Personal Interview. Materials Laboratory Air Force Wright Aeronautical Laboratories, AFWAL/MLLN, Wright-Patterson Air Force Base, OH, 19 October 1988.

32. Brown, C. W. and Smith, G. C. "The Effect of Microstructure and Texture on the Fatigue Crack Growth Threshold in Ti-6Al-4V," Fatigue Thresholds: Fundamentals and Engineering Applications. 329-343. Warley, United Kingdom: Engineering Materials Advisory Services LTD., 1982.

33. Larsen, J. M. and others. "Crack Opening Displacement Measurements on Small Cracks," Fracture Mechanics: Eighteenth Symposium, ASTM STP 945. 896-912. Philadelphia: American Society for Testing and Materials, 1988.

34. Saxena, A. and Hudak, S. J., Jr. "Review and Extension of Compliance Information for Common Crack Growth Specimens." International Journal of Fracture, 14: 453-468 (October 1978).

35. Mate Laser Interferometer Technical Reference Manual, Version 2.10. Dayton; University of Dayton Research Institute, Structural Integrity Division, Automated Materials Characterization Group. Undated.

36. Larsen, J. M. The Effects of Slip Character and Crack Closure on the Growth of Small Fatigue Cracks in Titanium Alloys. PhD dissertation. Carnegie Mellon University, Pittsburgh PA, September 1987.

Appendix A: Strain Gage Specifications

A strain gage was placed on the center of the back face of each specimen used in this study. The specifications of the strain gages used are as follows:

Manufacturer: Measurements Group, Inc.
Micro-Measurements Division
Raleigh, North Carolina

Gage Type: EA-06-250BF-350

Resistance: 350.0 Ω ± 0.15%

The strain gage amplifier used was also made by the same manufacturer. For this study, the filter on the amplifier was set on the wide band frequency. An excitation voltage of five volts was used. Lastly, the gain was set on x1000.

Appendix B: Effective Stress Intensity Plots

The figures included in this appendix show the ΔK_{eff} crack growth relations for the tests run in this study. Some of these plots are located in Chapter IV of this thesis.

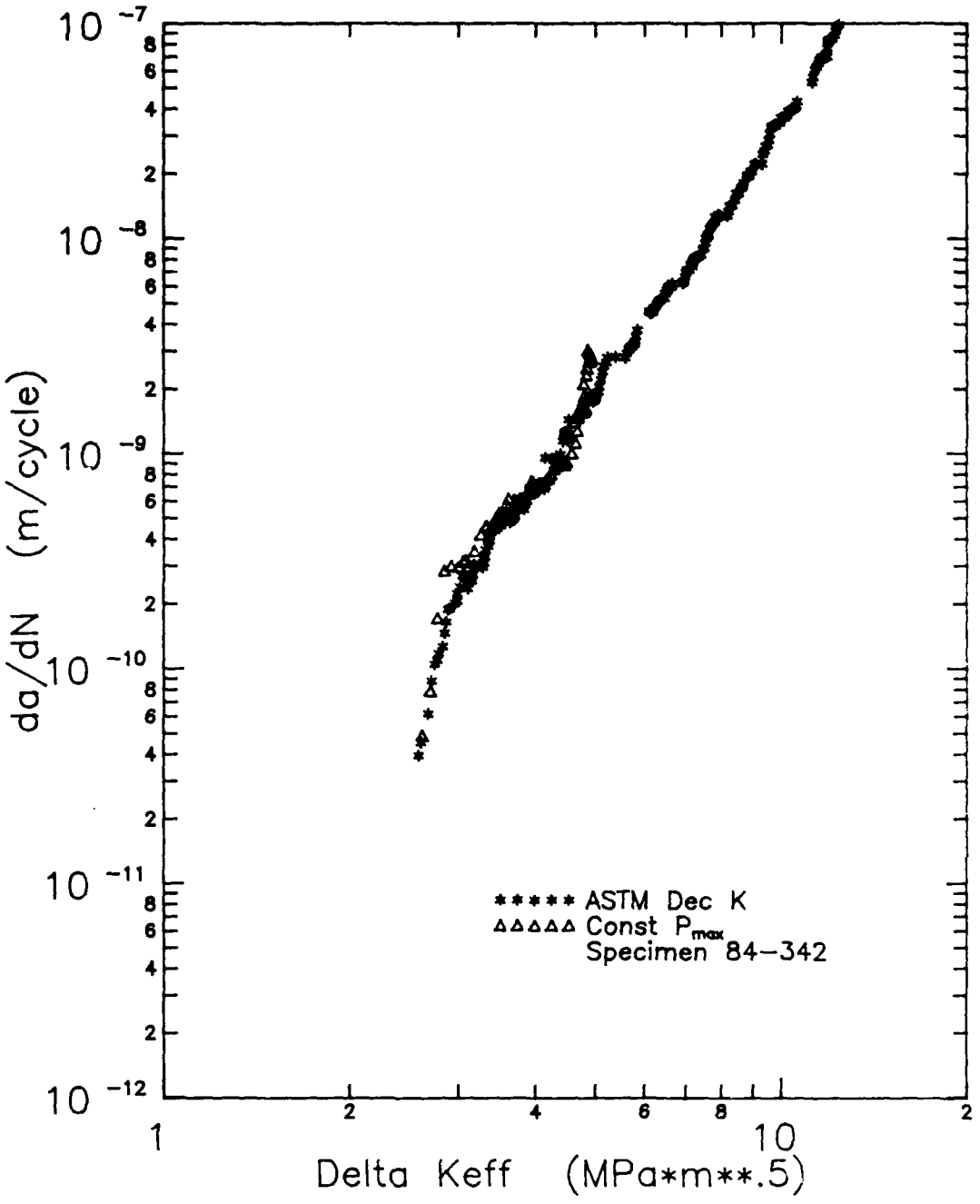

Figure 29. ΔK_{eff} Crack Growth Curves for the ASTM Decreasing K and Constant P_{max} Tests for the Clip Gage at R=0.5

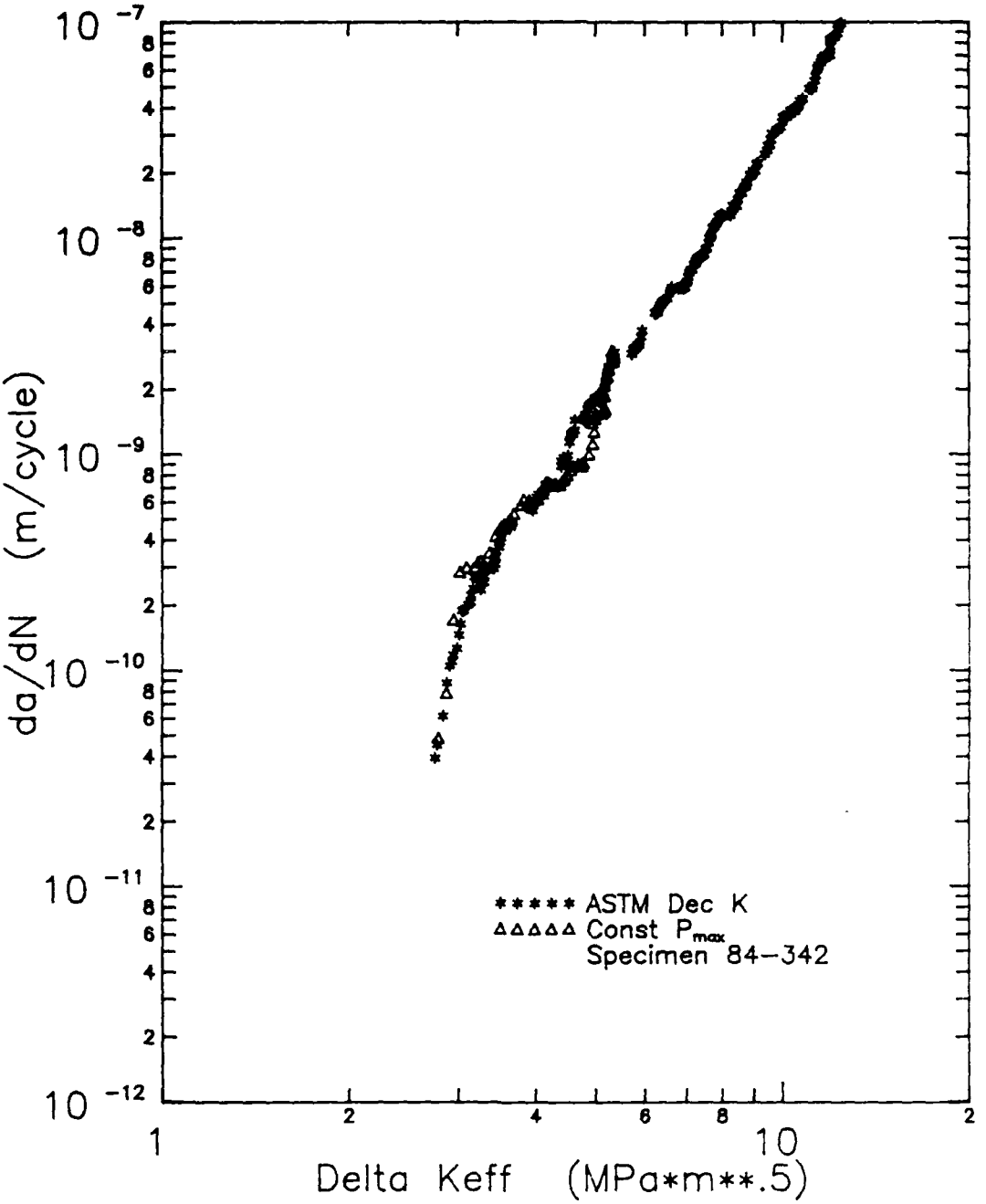

Figure 30. ΔK_{eff} Crack Growth Curves for the ASTM Decreasing K and Constant P_{max} Tests for the BFS at R=0.5

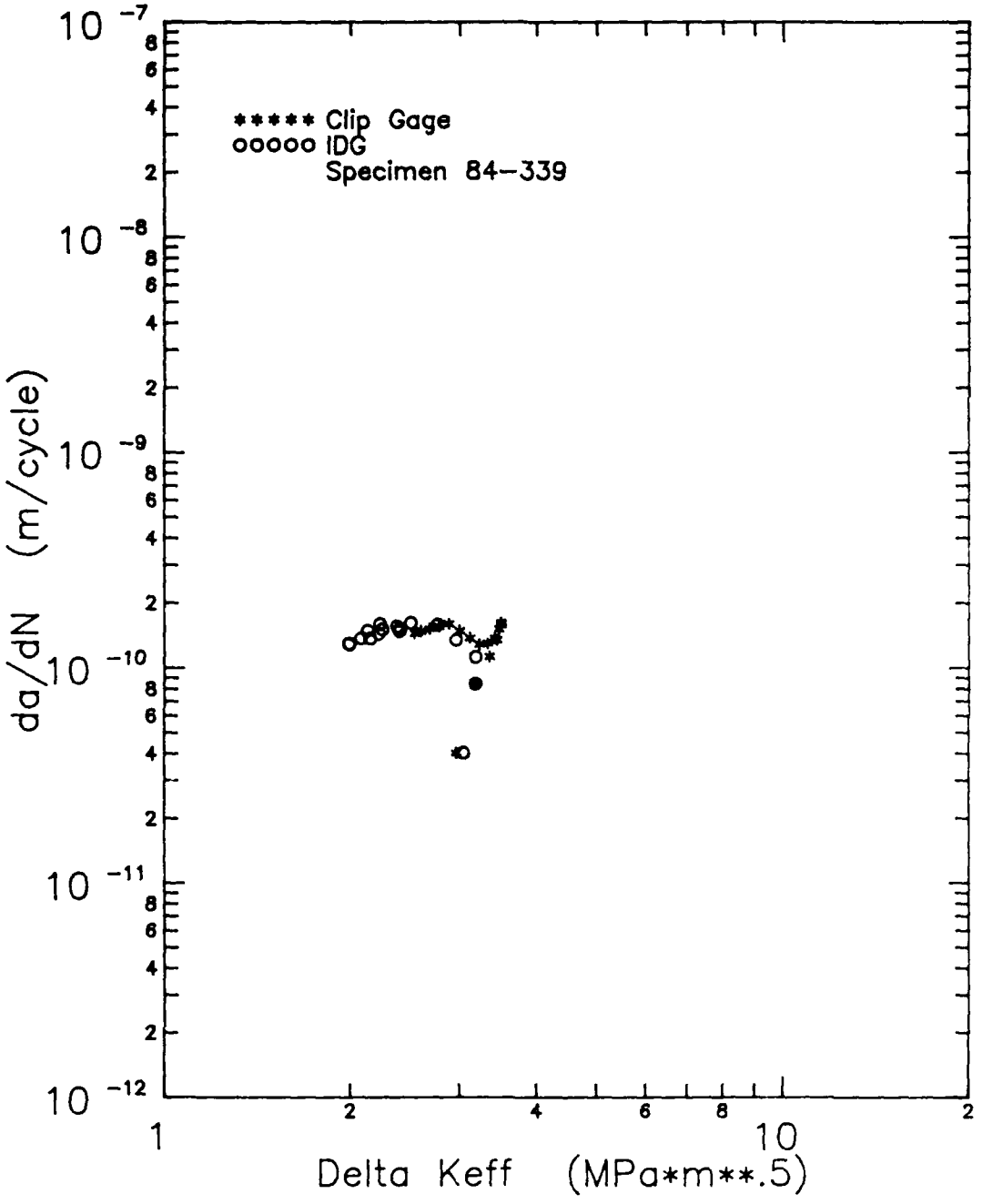

Figure 31. ΔK_{eff} Crack Growth Curves for the Constant K_{max}=6.5 MPa*m**.5 Test

Appendix C: Loading Histories

Since there were three techniques used to measure the closure load, three load histories for each test are included in this appendix. Only two tests, ASTM decreasing K test at R = 0.1 and constant K_{max} = 6.5 MPa$\sqrt{m}$ test, did not have BFS data due to the late arrival of the strain gage amplifier. Thus, the maximum, minimum, and closure (measured either by the clip gage, BFS, or IDG) loads for each test were plotted against the number of cycles.

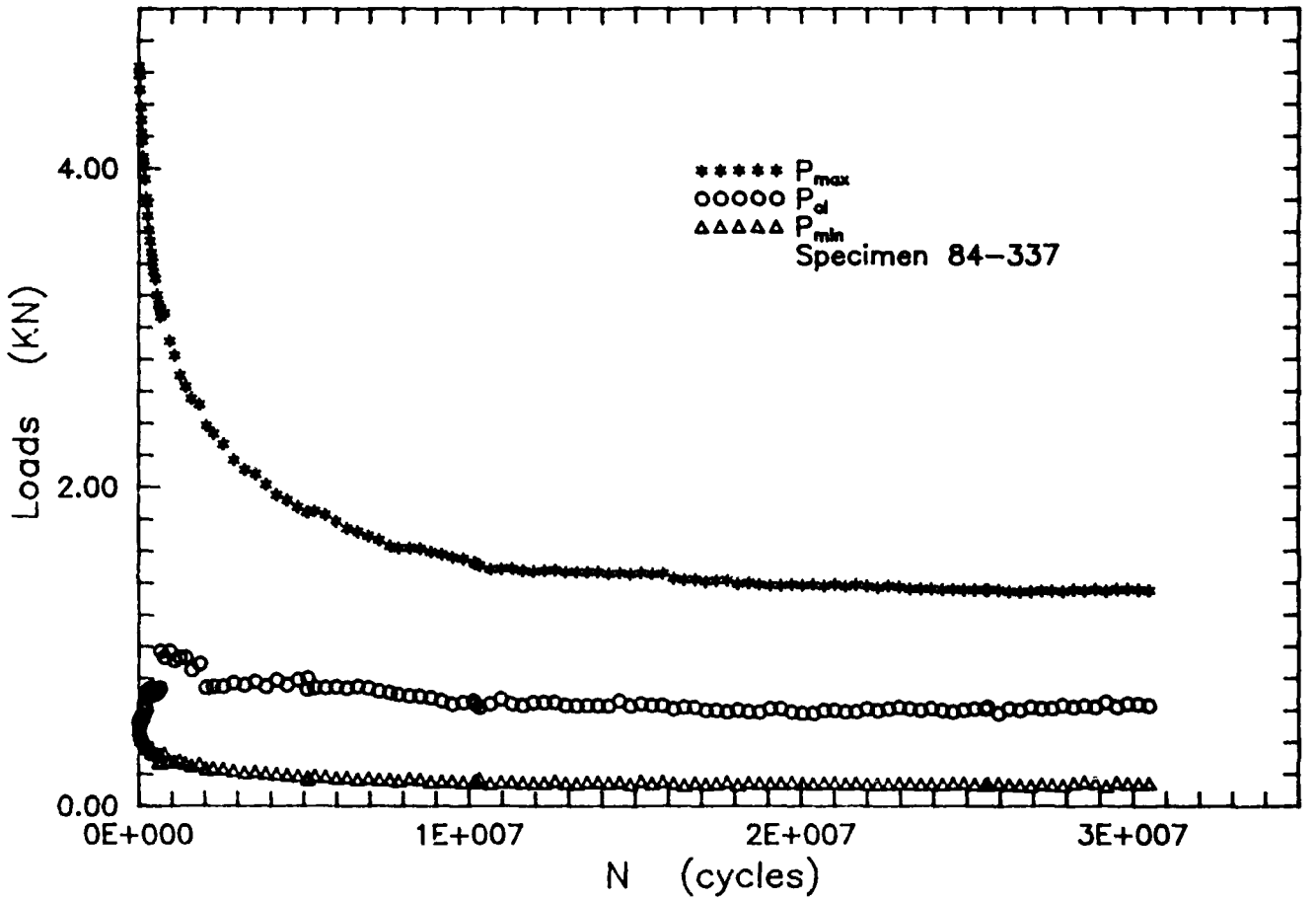

Figure 32. Load History for ASTM Decreasing K Test with Closure from Clip Gage for R=0.1

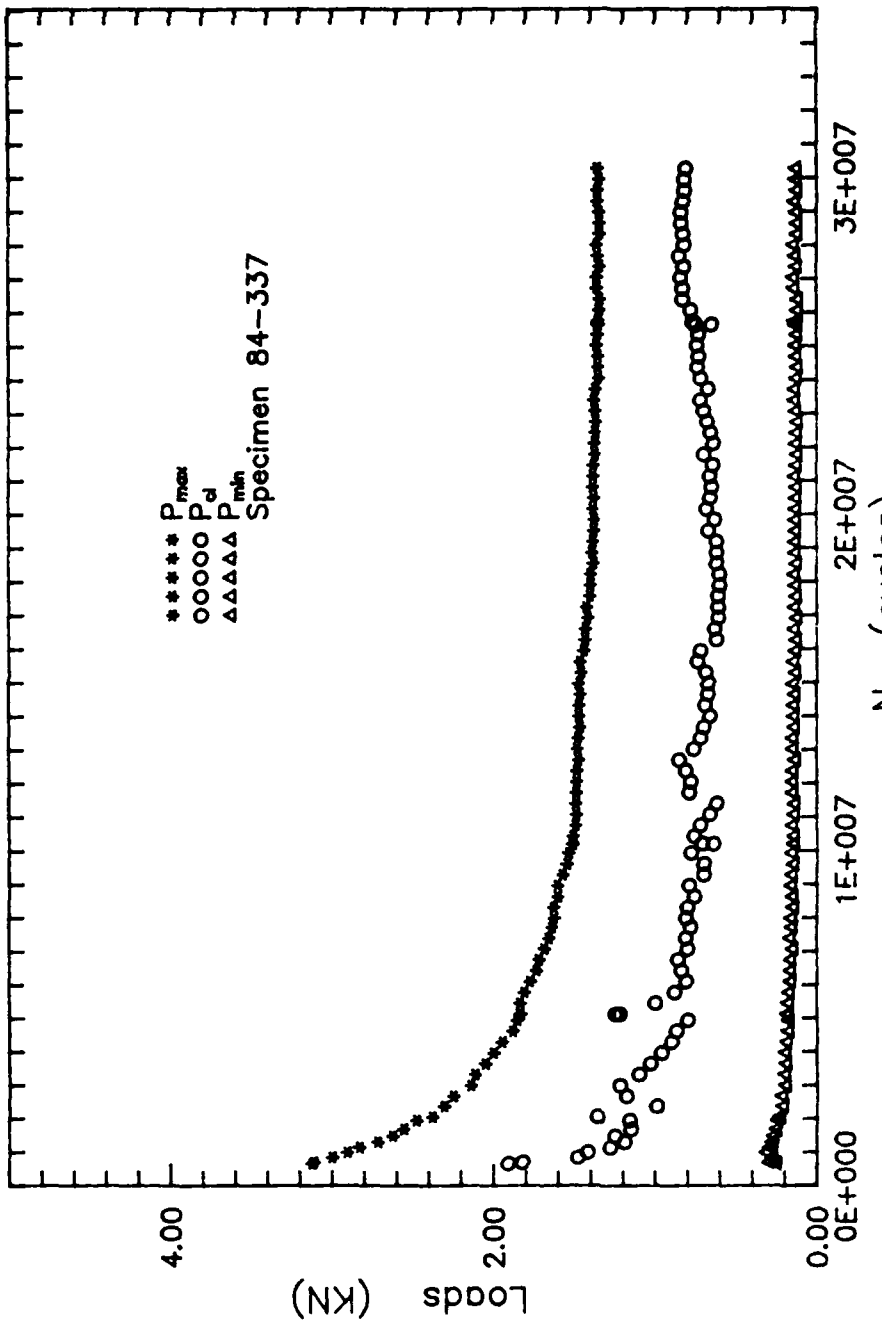

Figure 33. Load History for ASTM Decreasing K Test with Closure from IDG for R=0.1

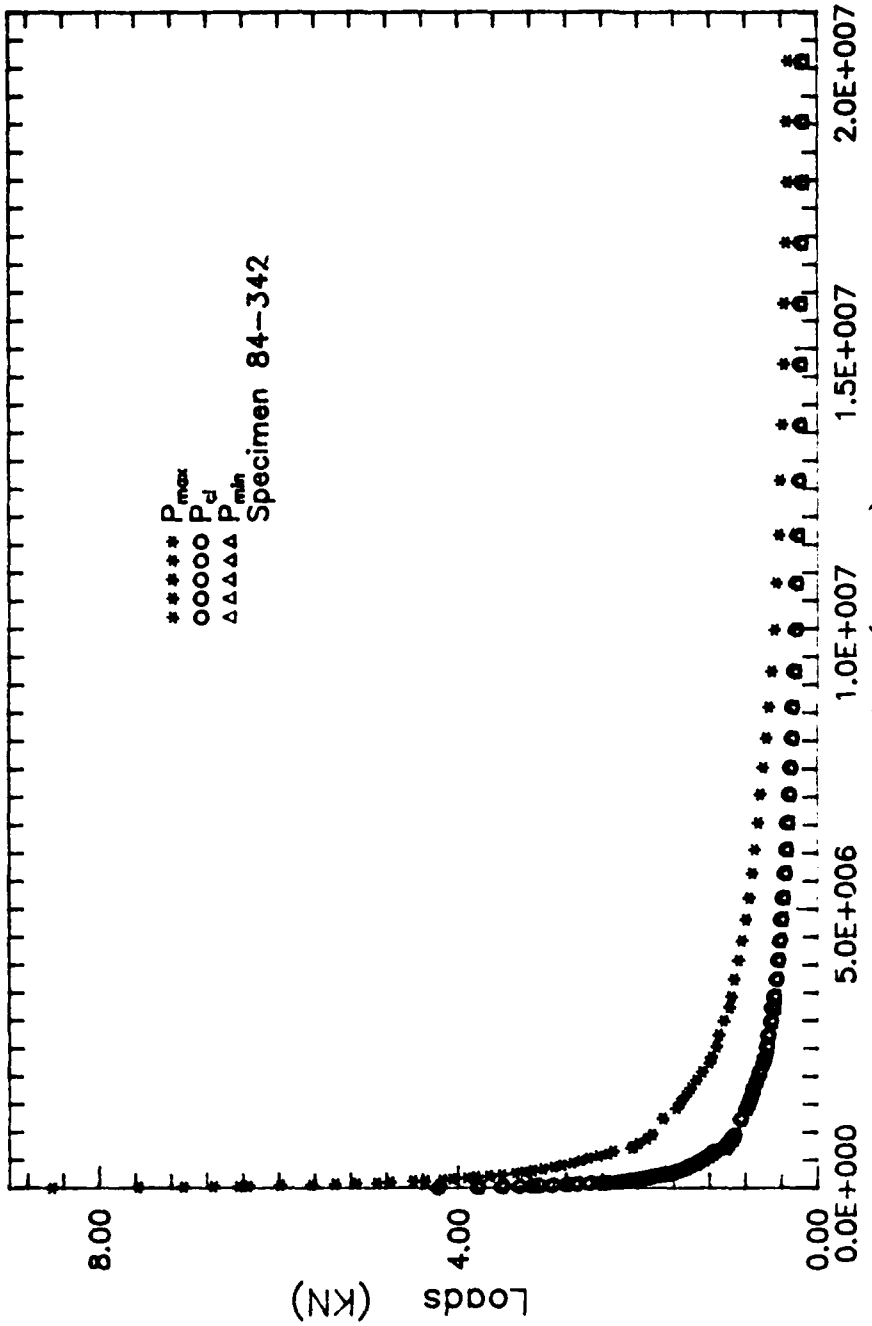

Figure 34. Load History for ASTM Decreasing K Test with Closure from Clip Gage for R=0.5

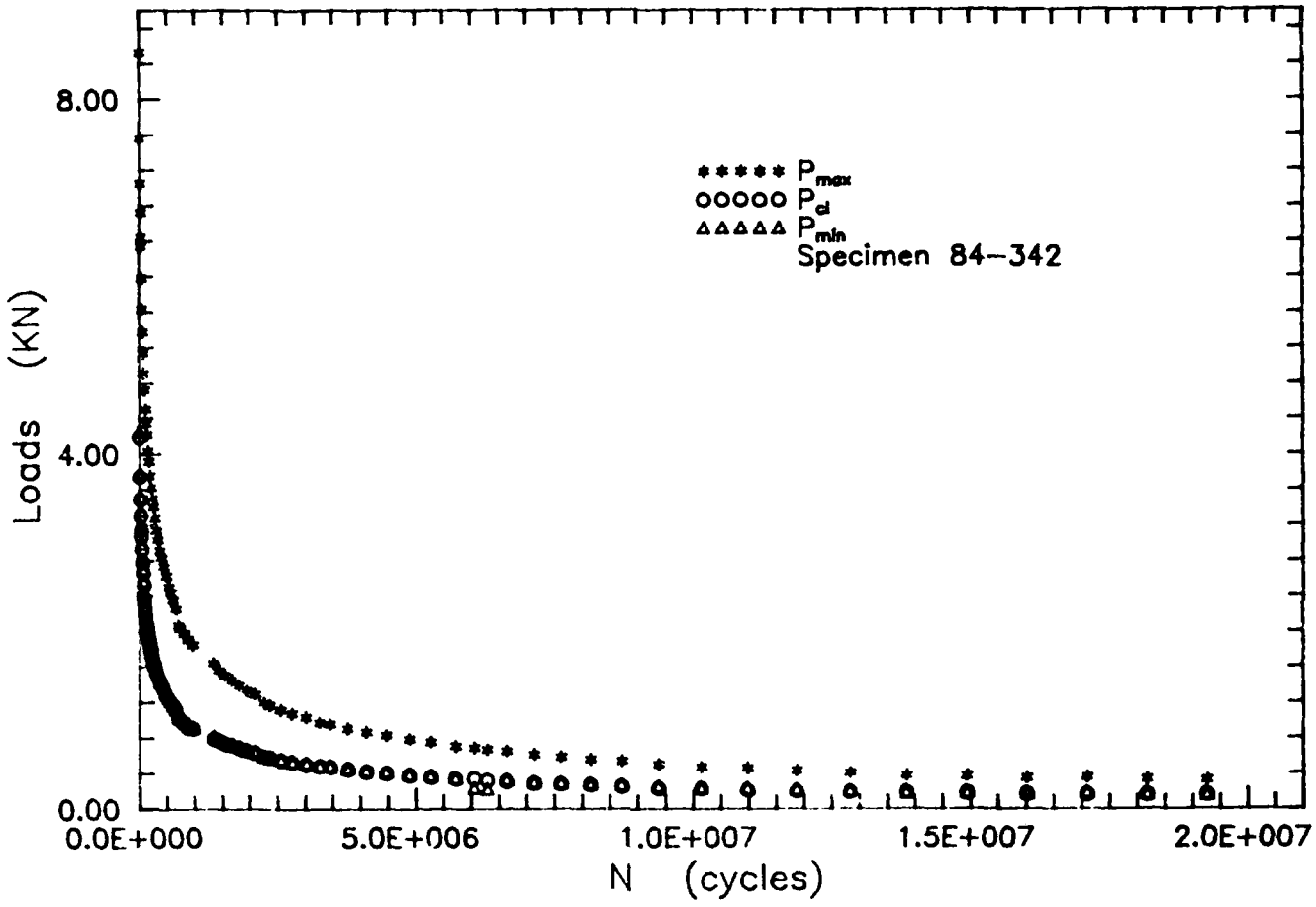

Figure 35. Load History for ASTM Decreasing K Test with Closure from BFS for R=0.5

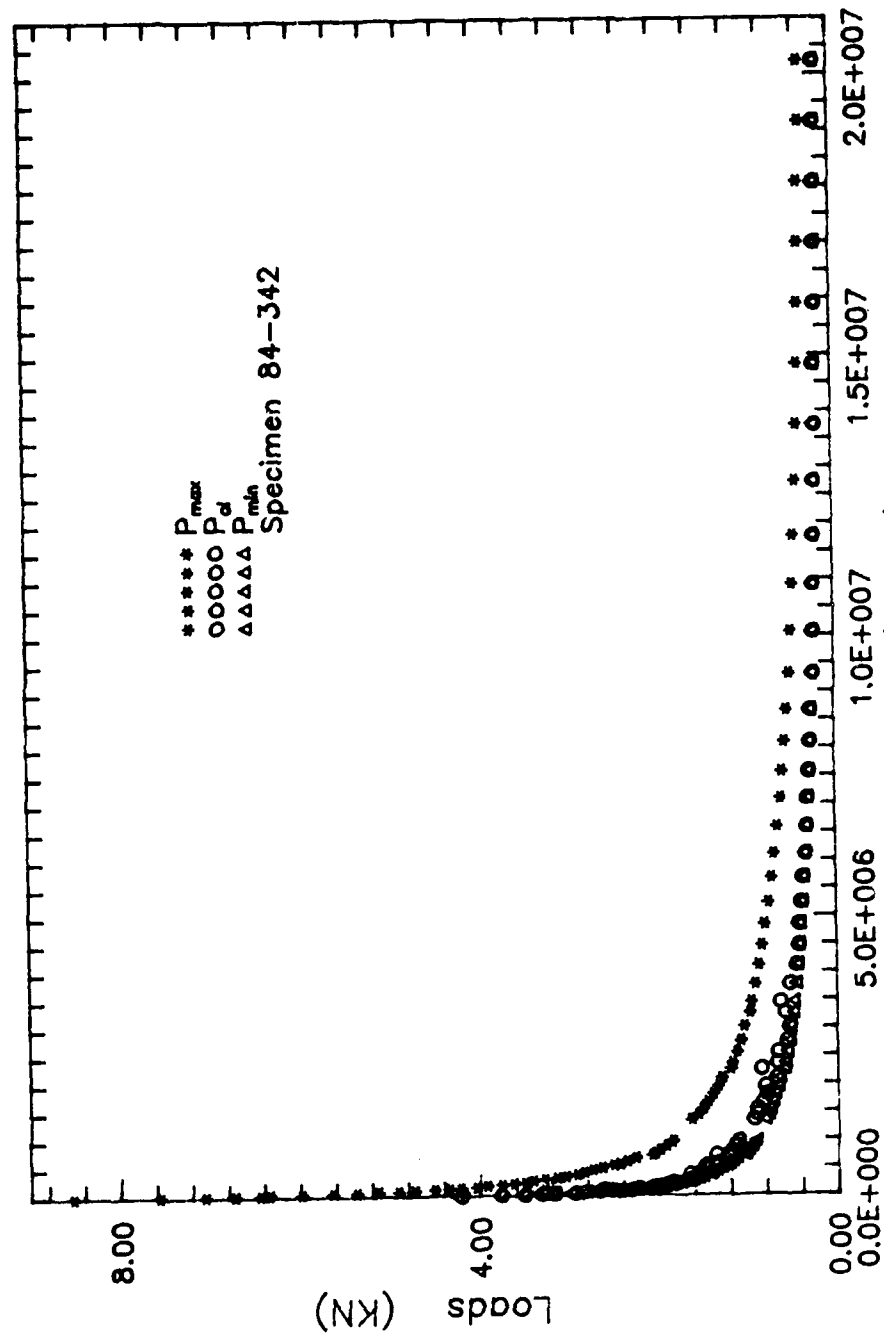

Figure 36. Load History for ASTM Decreasing K Test with Closure from IDG for R=0.5

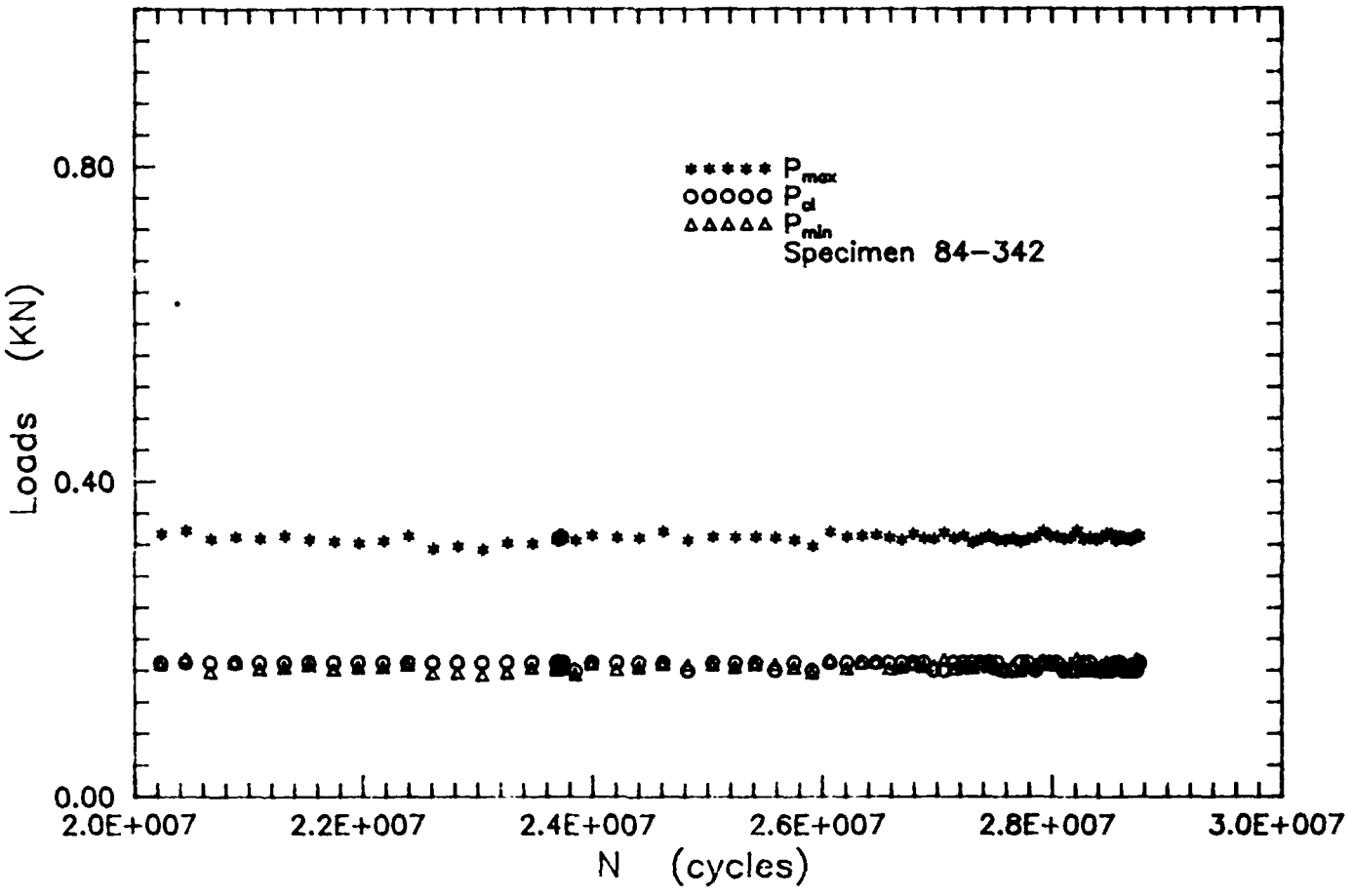

Figure 37. Load History for Constant P_{max} Test with Closure from Clip Gage for R=0.5

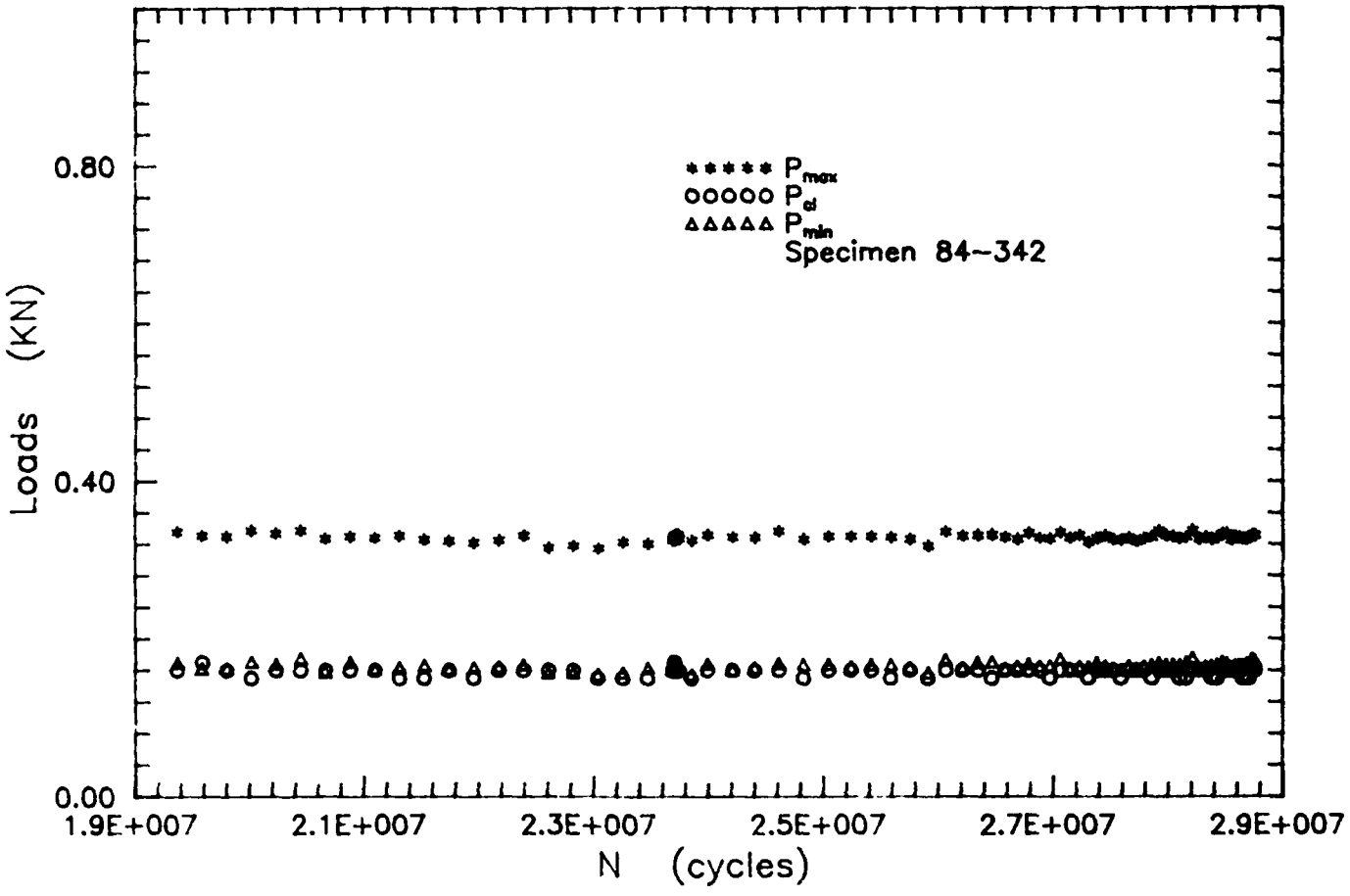

Figure 38. Load History for Constant P_{max} Test With Closure from BFS for R=0.5

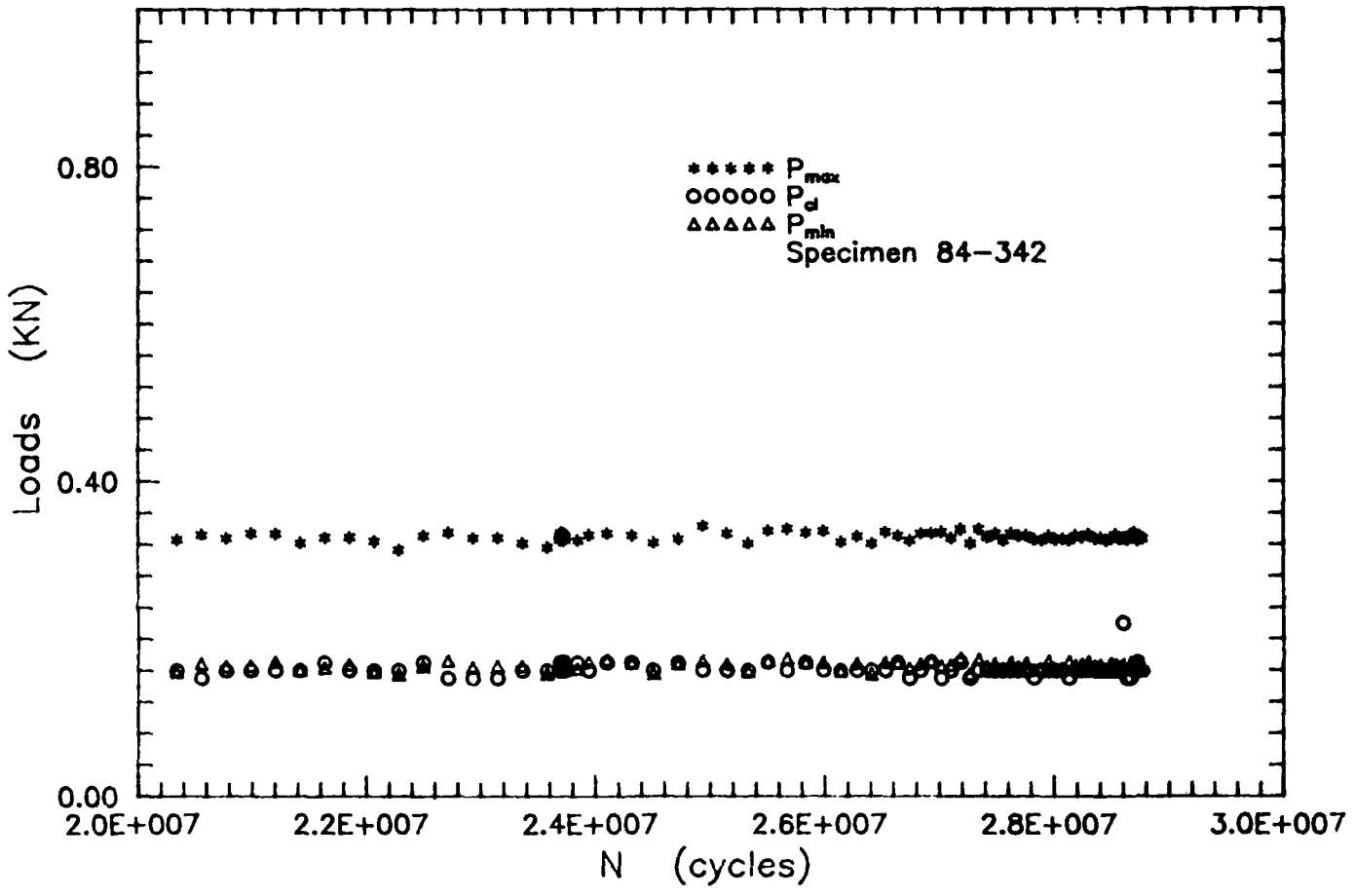

Figure 39. Load History for Constant P_{max} Test with Closure from IDG for R=0.5

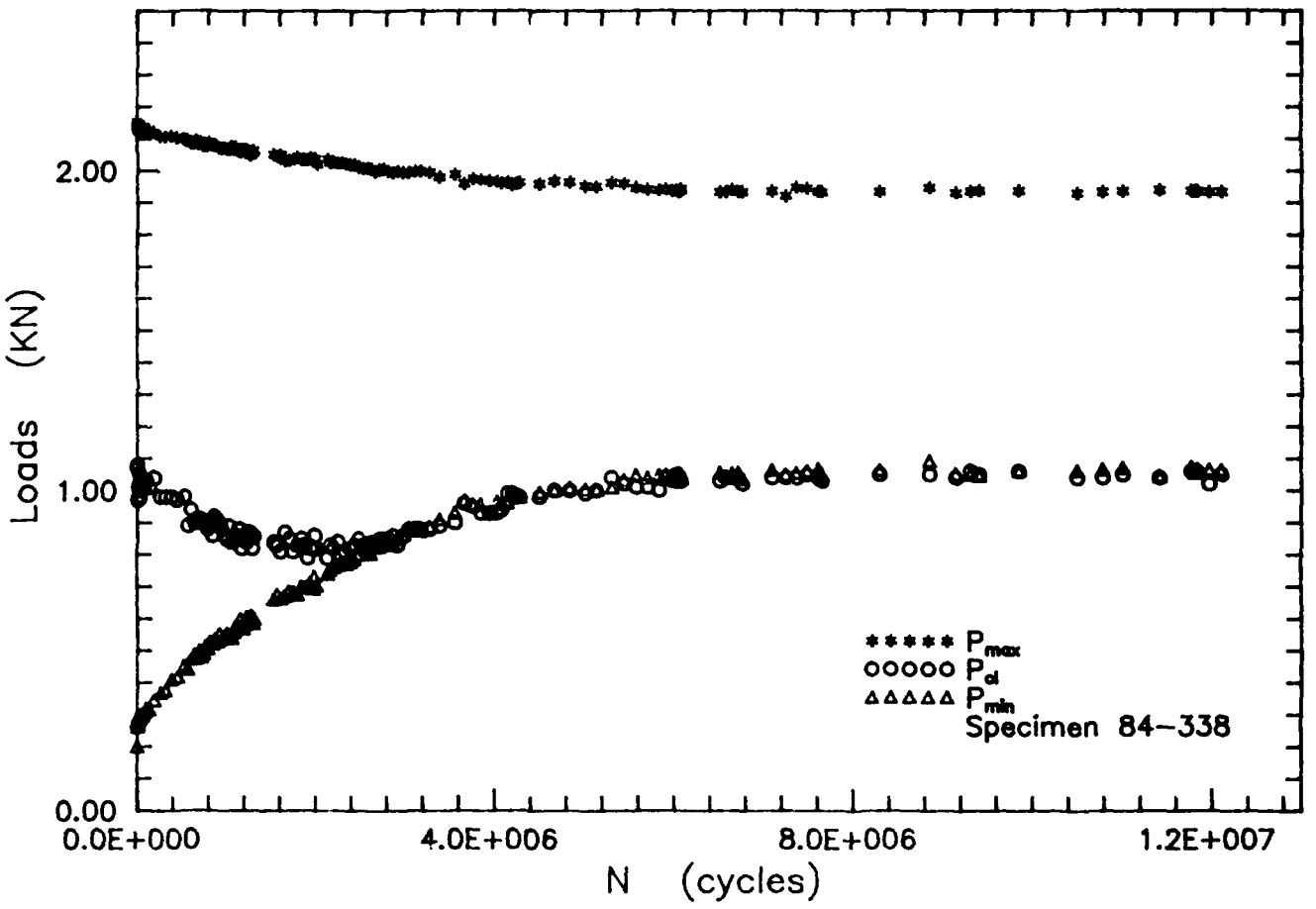

Figure 40. Load History for Constant K_{max}=7 MPa*m**.5 Test with Closure from Clip Gage

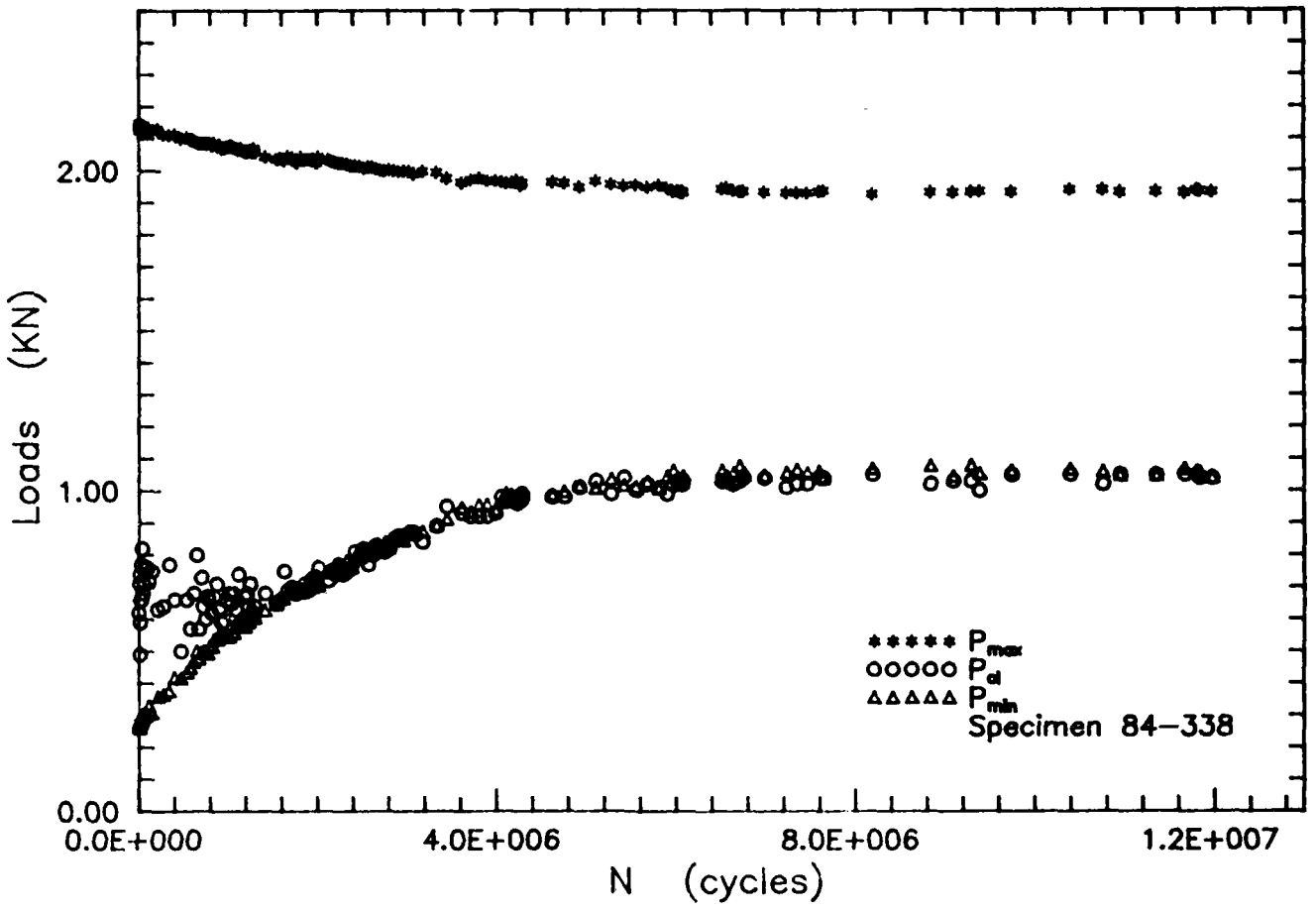

Figure 41. Load History for Constant K_{max}=7 MPa*m**.5 Test with Closure from BFS

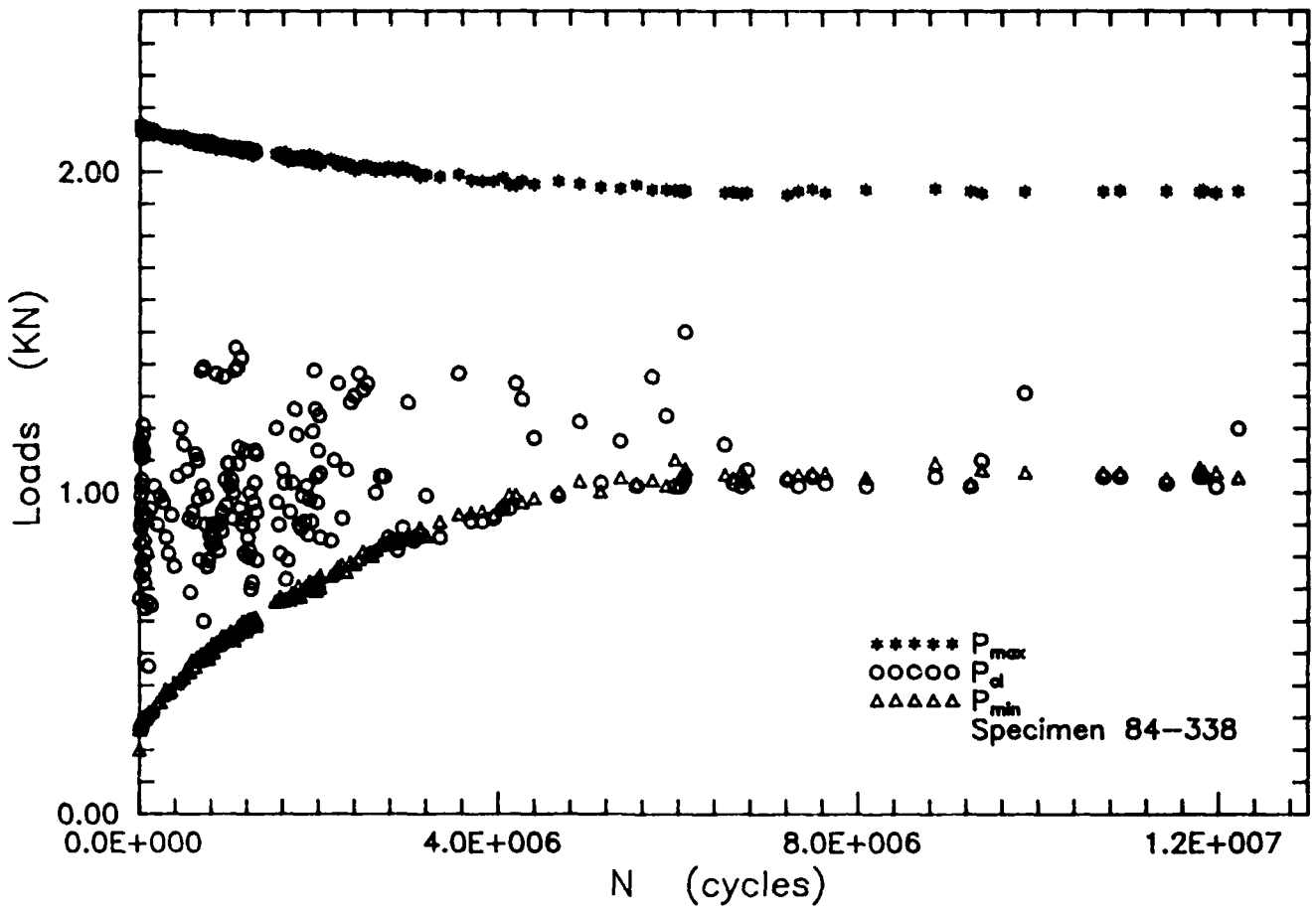

Figure 42. Load History for Constant K_{max}=7 MPa*m**.5 Test with Closure from IDG

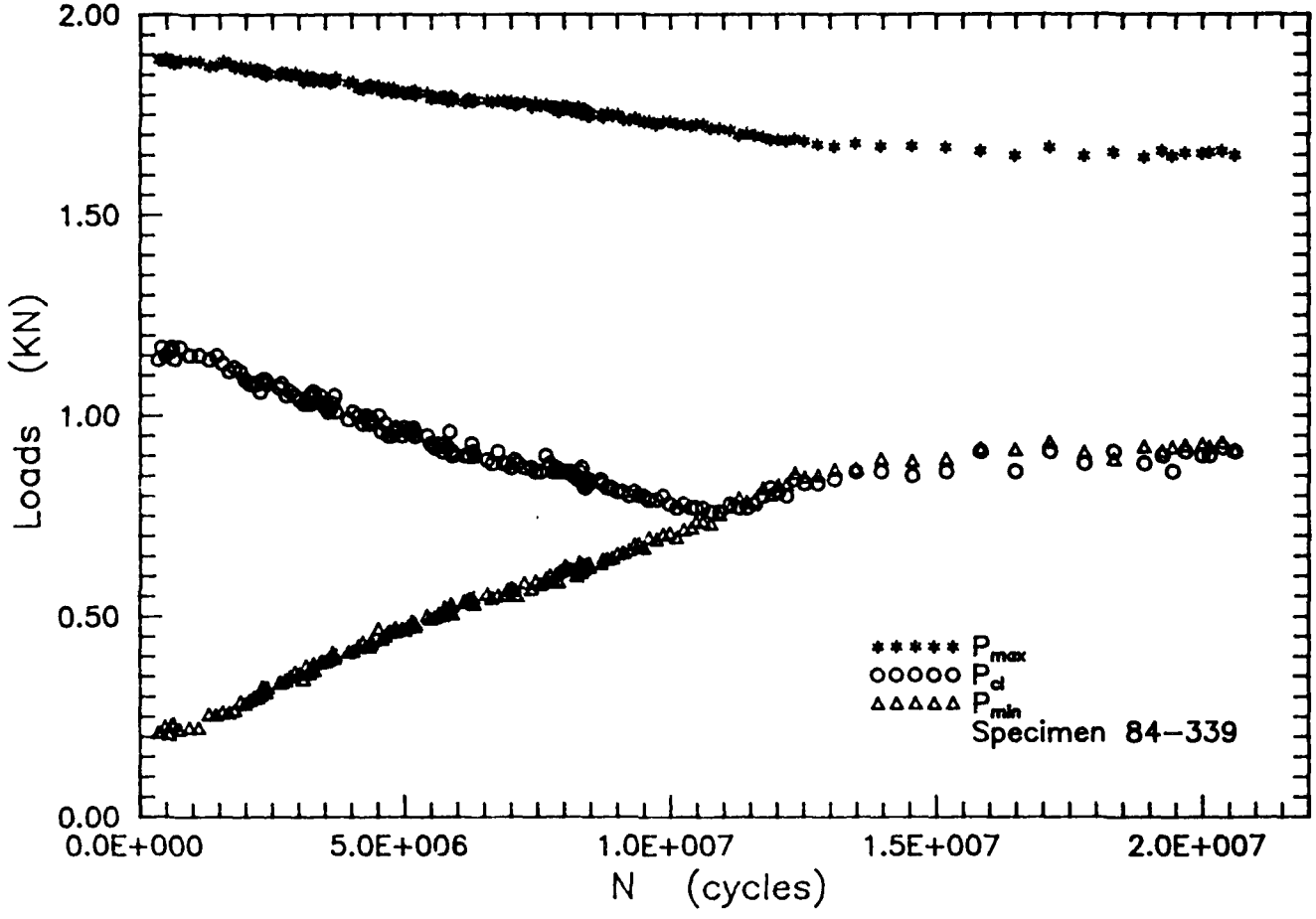

Figure 43. Load History for Constant K_{max}=6.5 MPa*m**.5 Test with Closure from Clip Gage

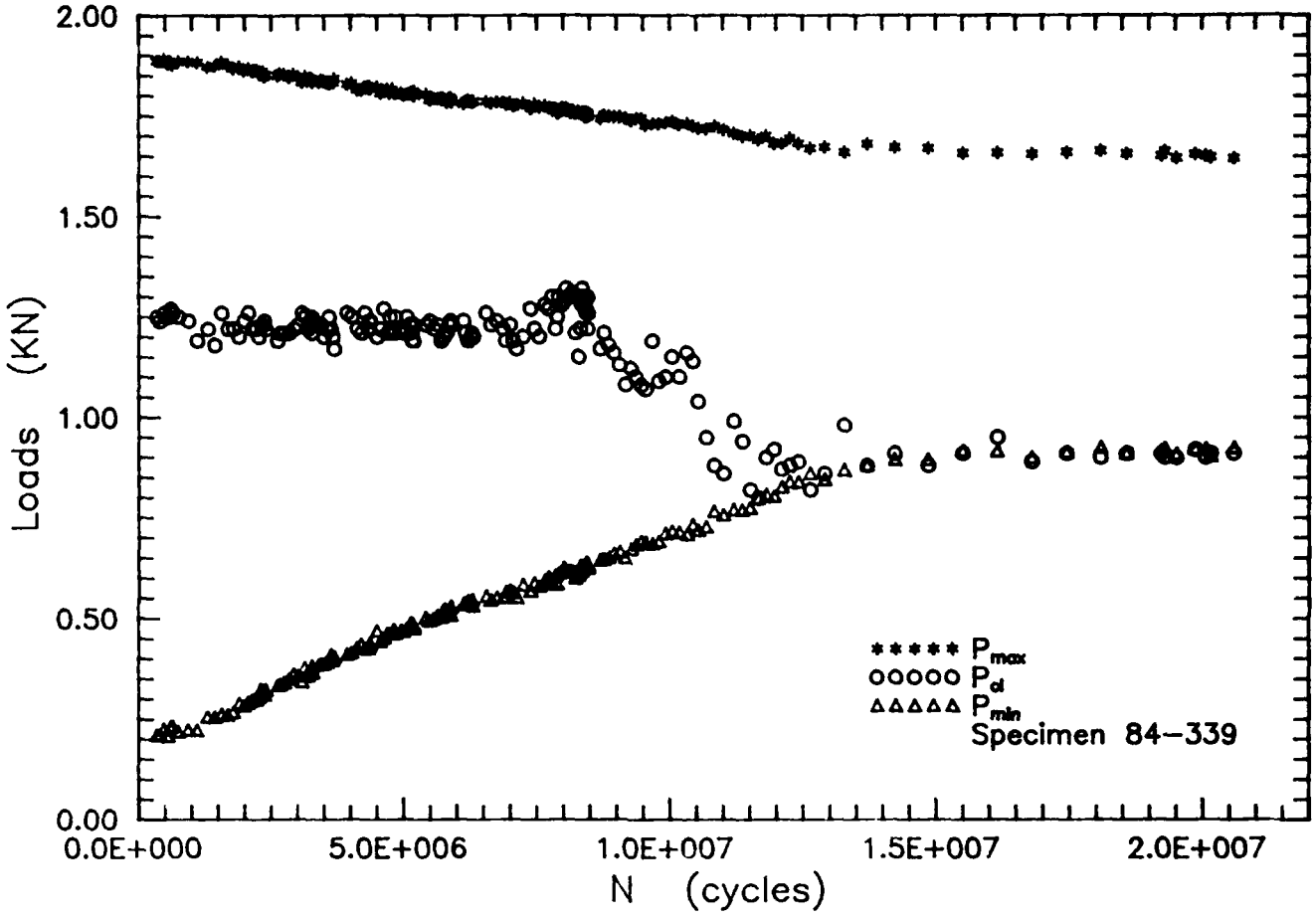

Figure 44. Load History for Constant K_{max}=6.5 MPa*m**.5 Test with Closure from IDG

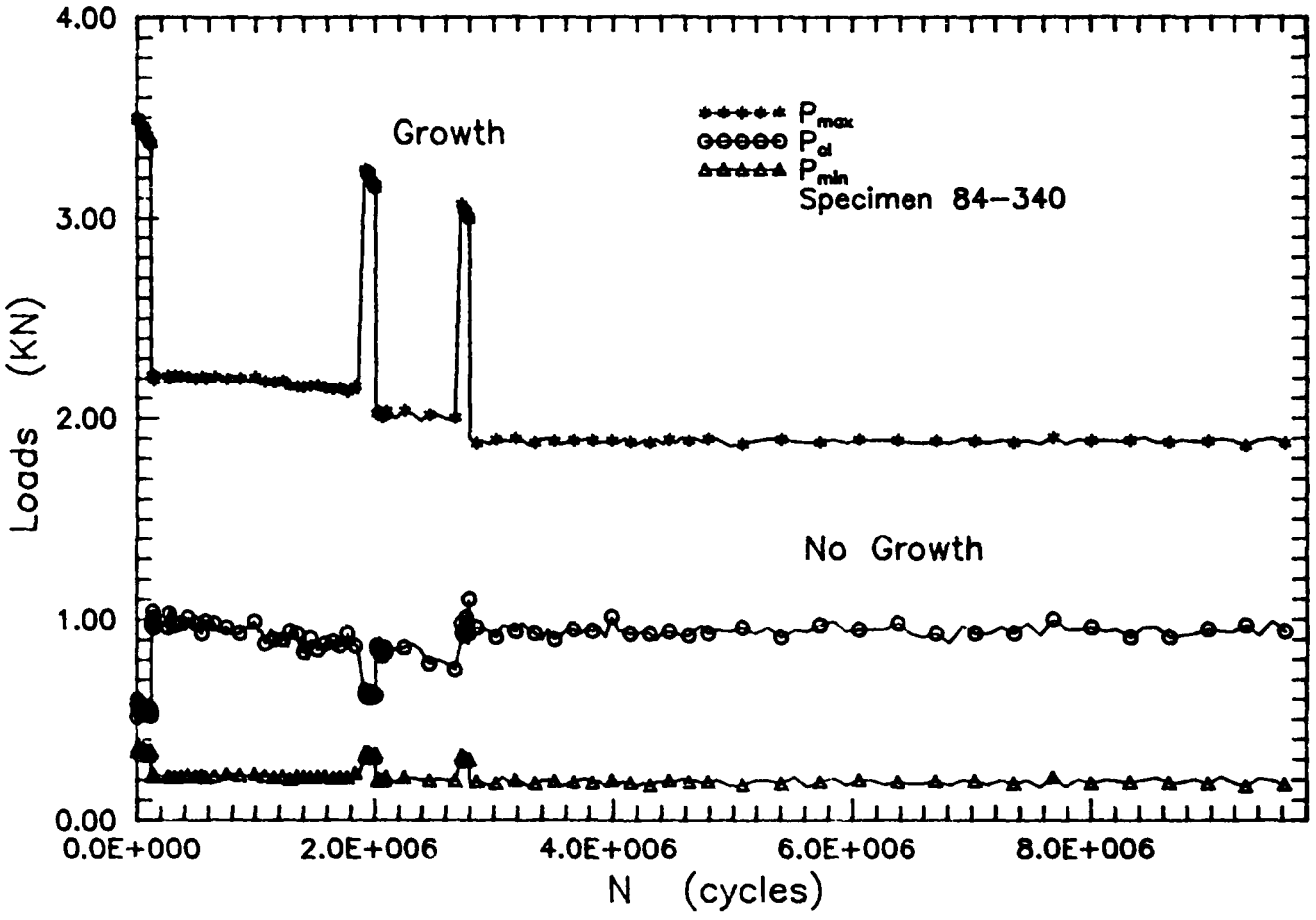

Figure 45. Load History for Varying ΔK Test with Closure from Clip Gage for R=0.1 and K_{max0}=10 MPa*m**.5

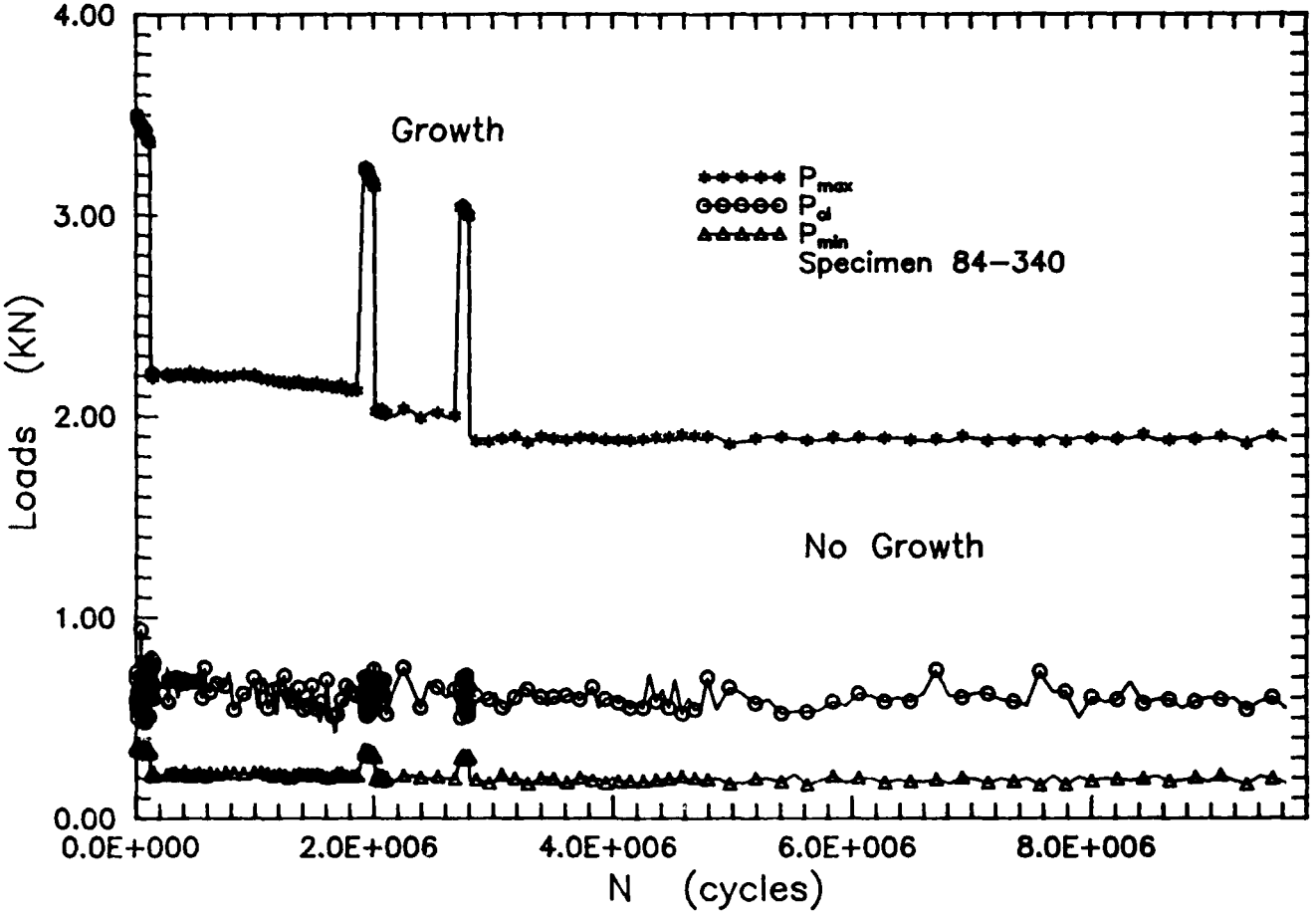

Figure 46. Load History for Varying ΔK Test with Closure from BFS for R=0.1 and K_{max0}=10 MPa*m**.5

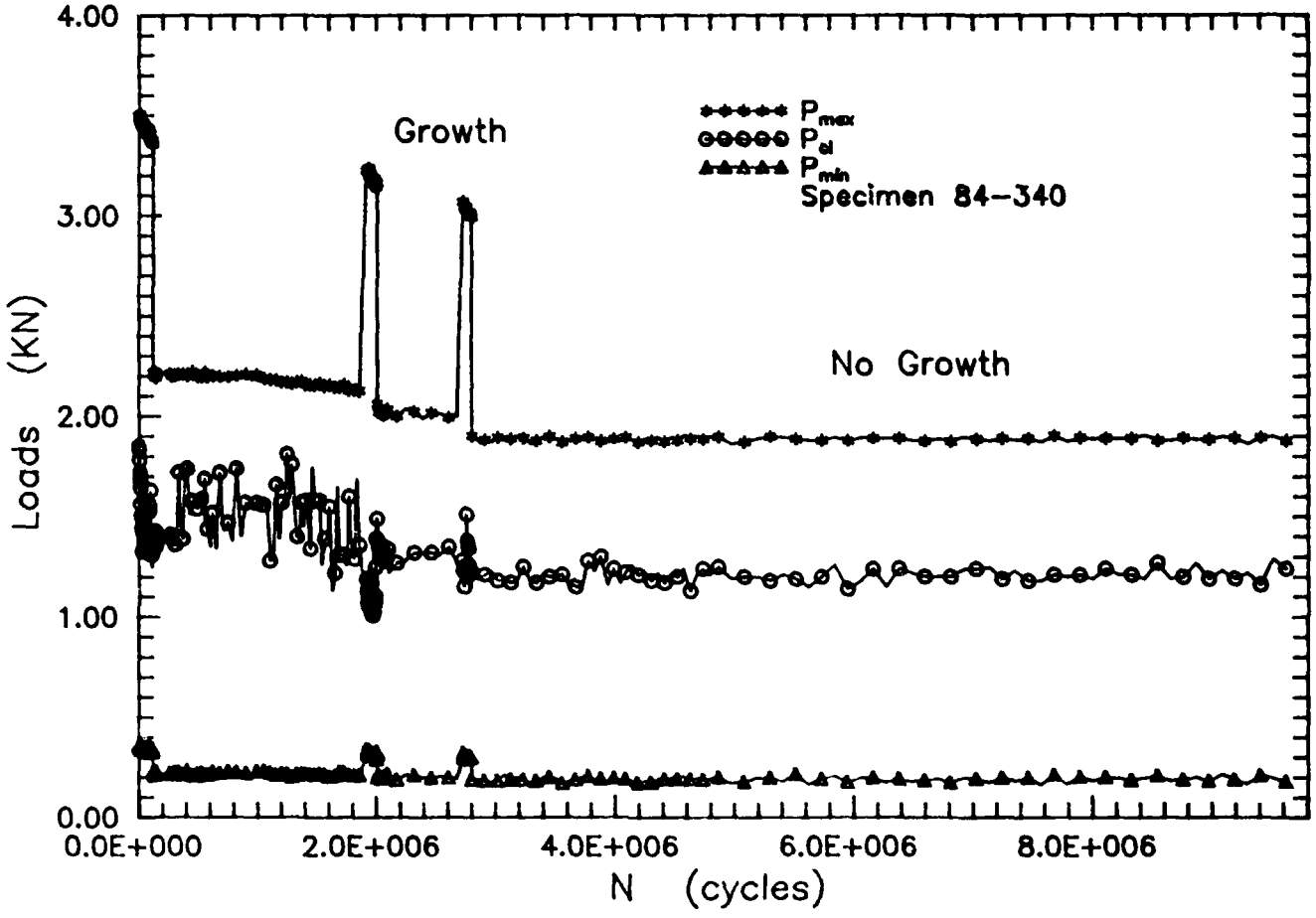

Figure 47. Load History for Varying ΔK Test with Closure from IDG for R=0.1 and K_{max0}=10 MPa*m**.5

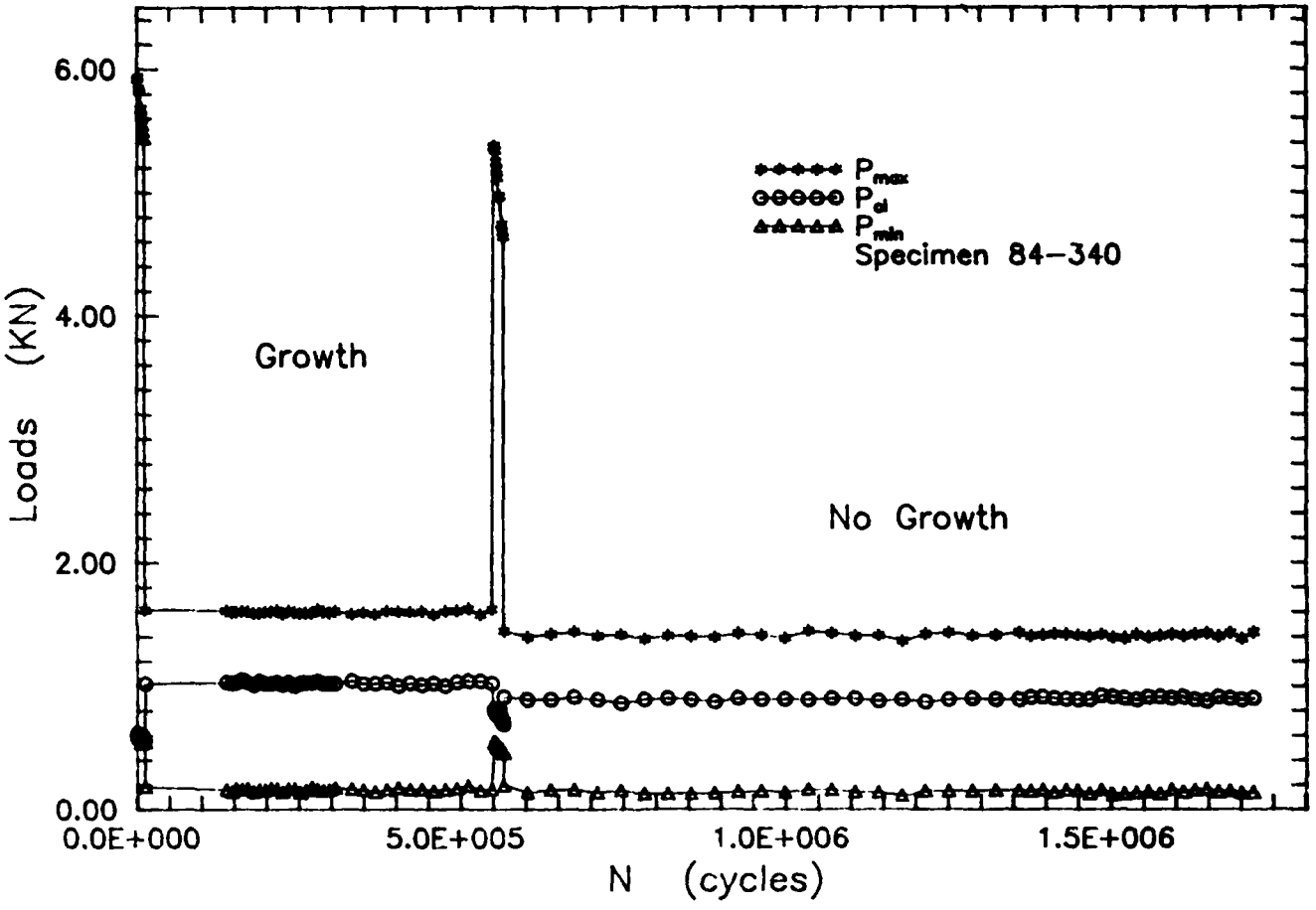

Figure 48. Load History for Varying ΔK Test with Closure from Clip Gage for R=0.1 and K_{max0}=20 MPa*m**.5

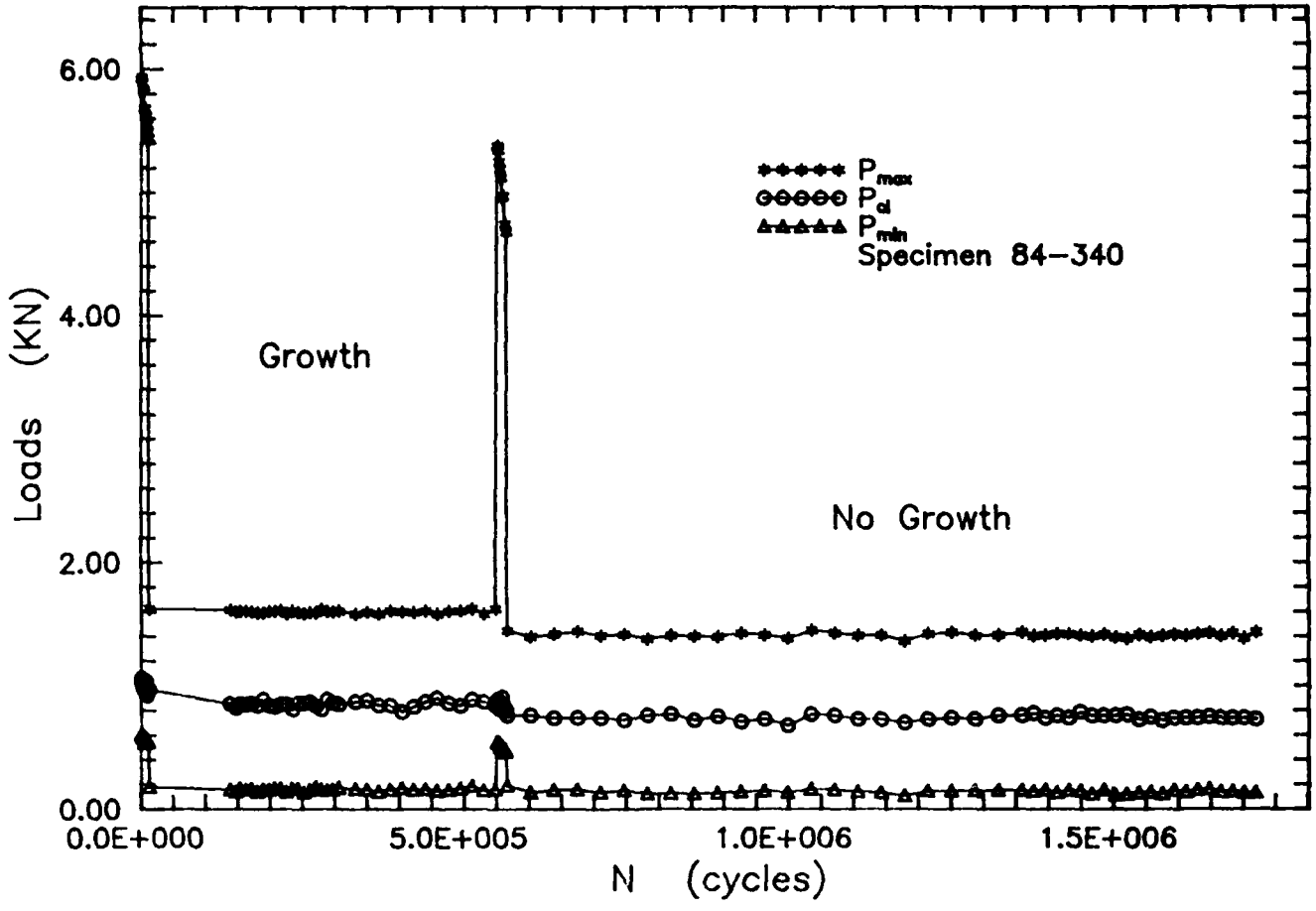

Figure 49. Load History for Varying ΔK Test with Closure from BFS for R=0.1 and K_{max0}=20 MPa*m**.5

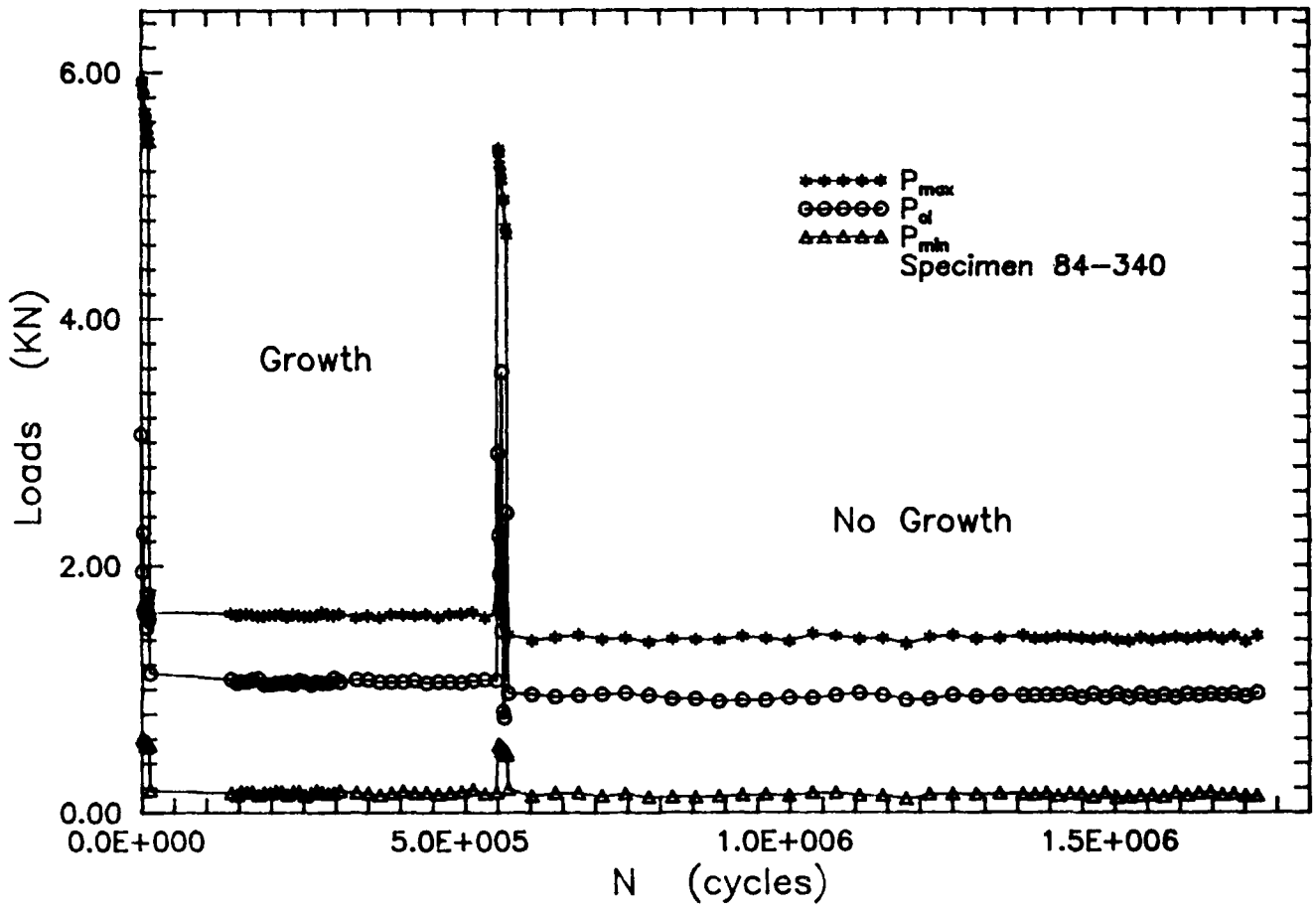

Figure 50. Load History for Varying ΔK Test with Closure from IDG for R=0.1 and K_{max0}=20 MPa*m**.5

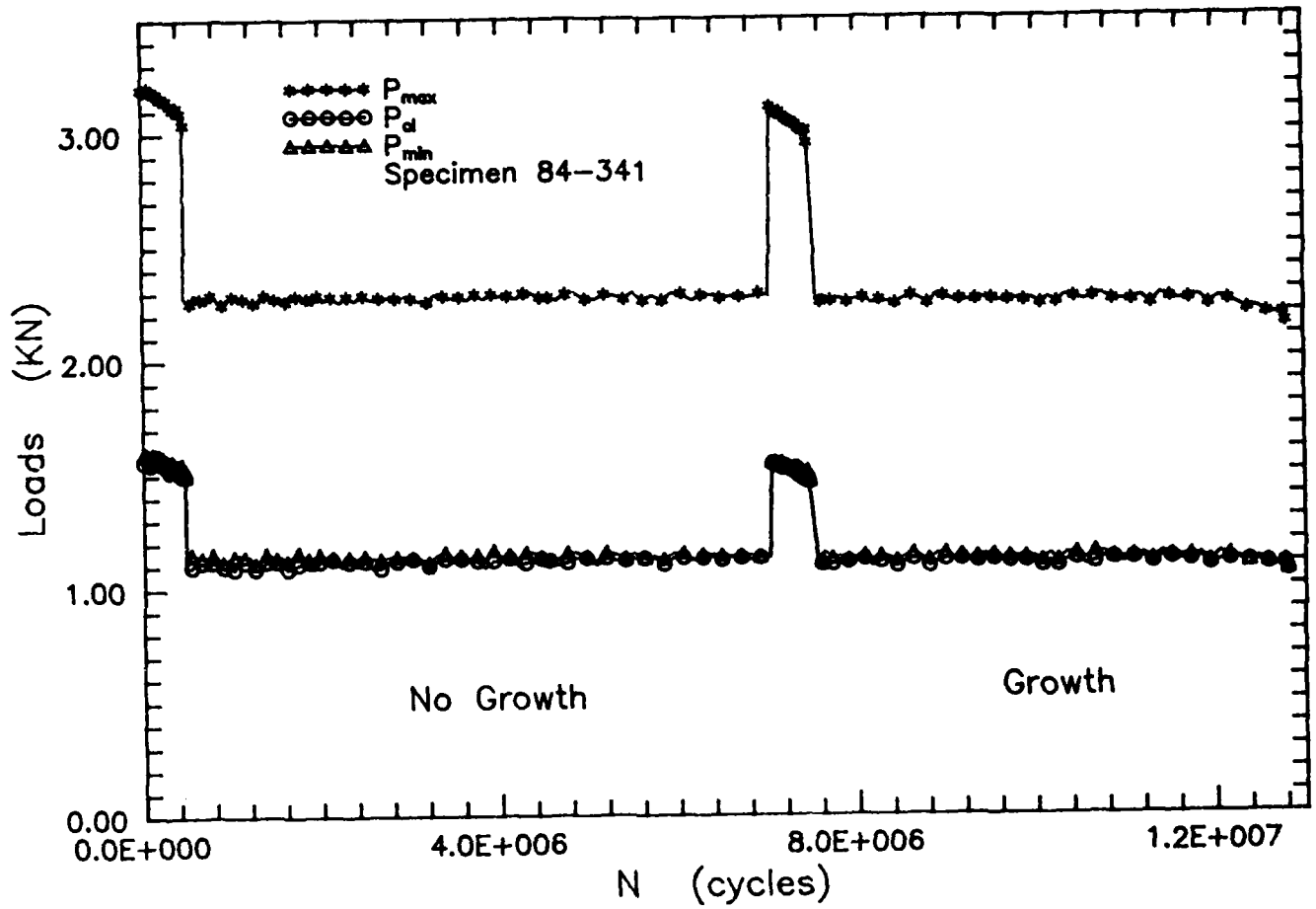

Figure 51. Load History for Varying ΔK Test with Closure from Clip Gage for R=0.5 and K_{max0}=10 MPa*m**.5

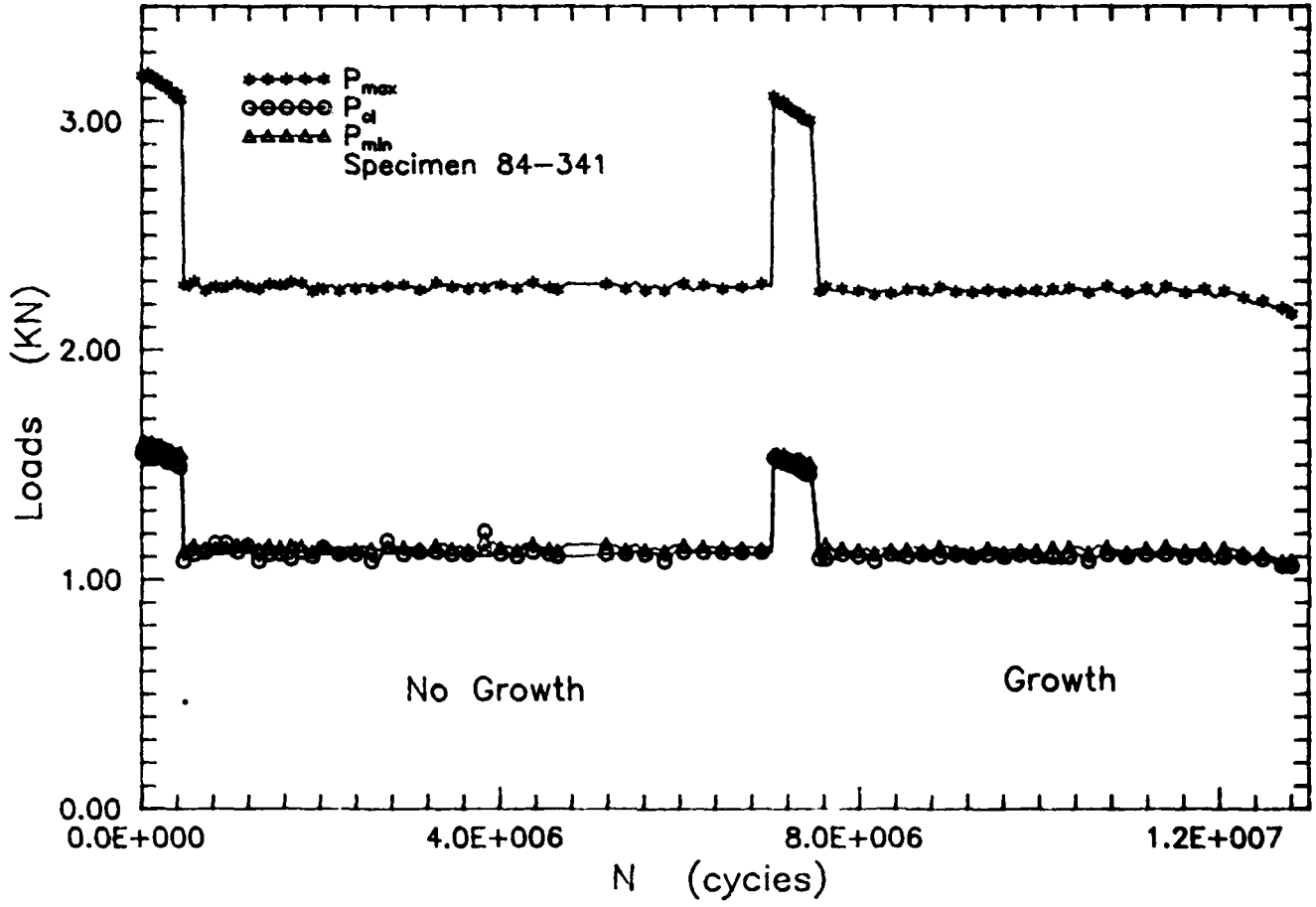

Figure 52. Load History for Varying ΔK Test with Closure from BFS for R=0.5 and K_{max0}=10 MPa*m**.5

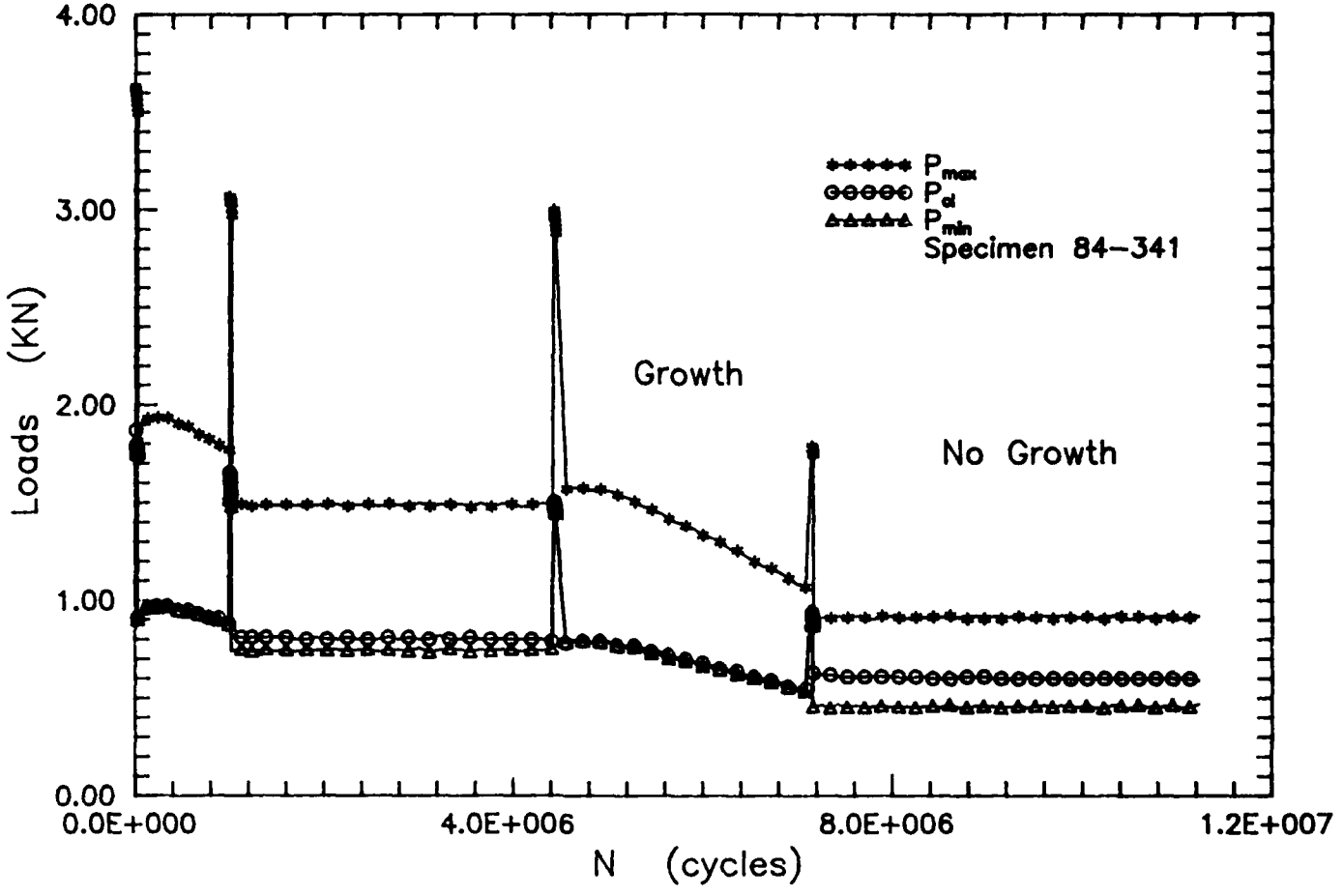

Figure 53. Load History for Varying ΔK Test with Closure from Clip Gage for R=0.5 and K_{max0}=20 MPa*m**.5

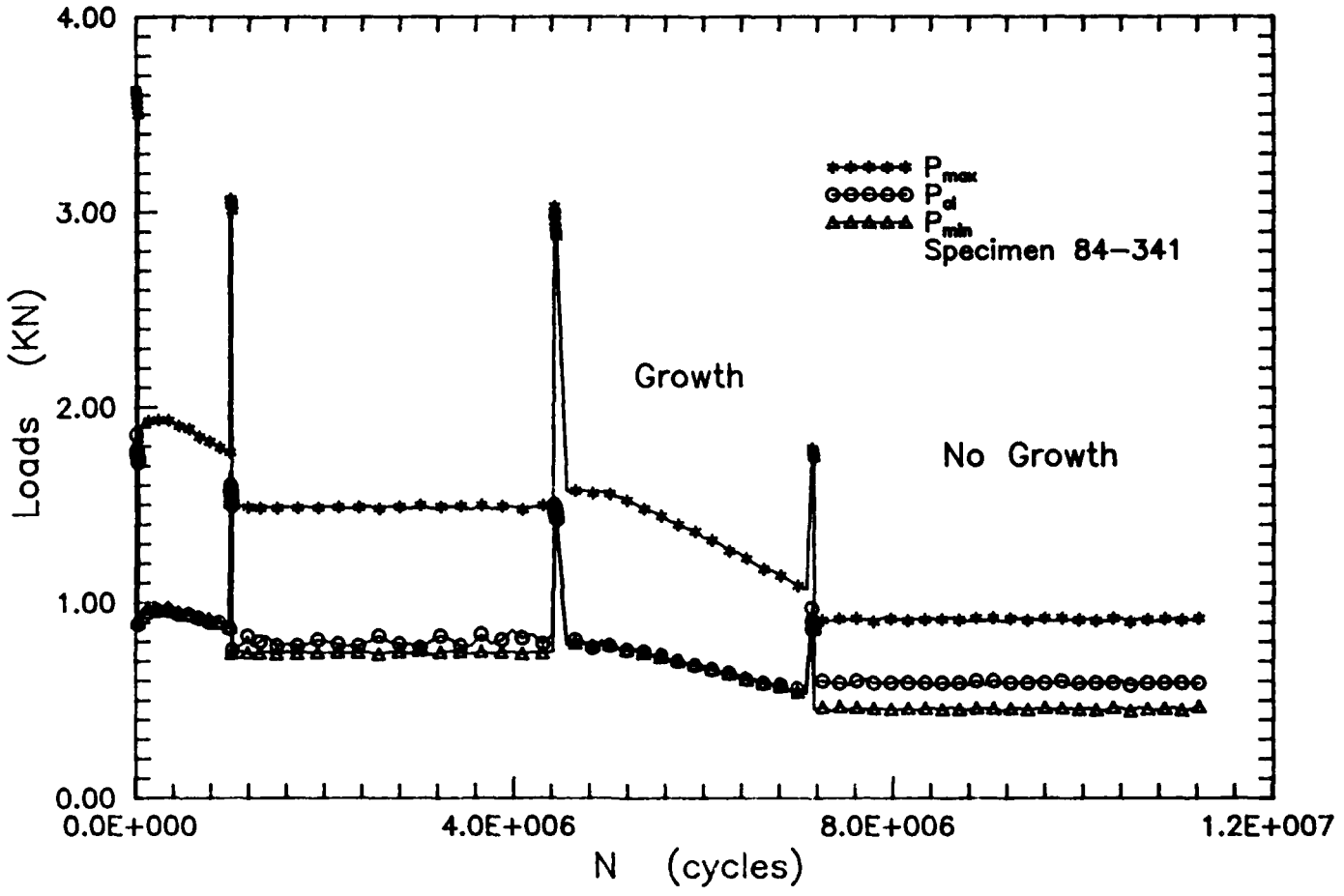

Figure 54. Load History for Varying ΔK Test with Closure from BFS for R=0.5 and K_{max0}=20 MPa*m**.5

Appendix D: Crack Length Histories

The figures showing the actual crack length measurements plotted against the number of cycles run are included in this appendix. The varying ΔK tests have a few discontinuities in the crack length histories because the specimen was removed after each load drop to put a new set of indents at the crack tip.

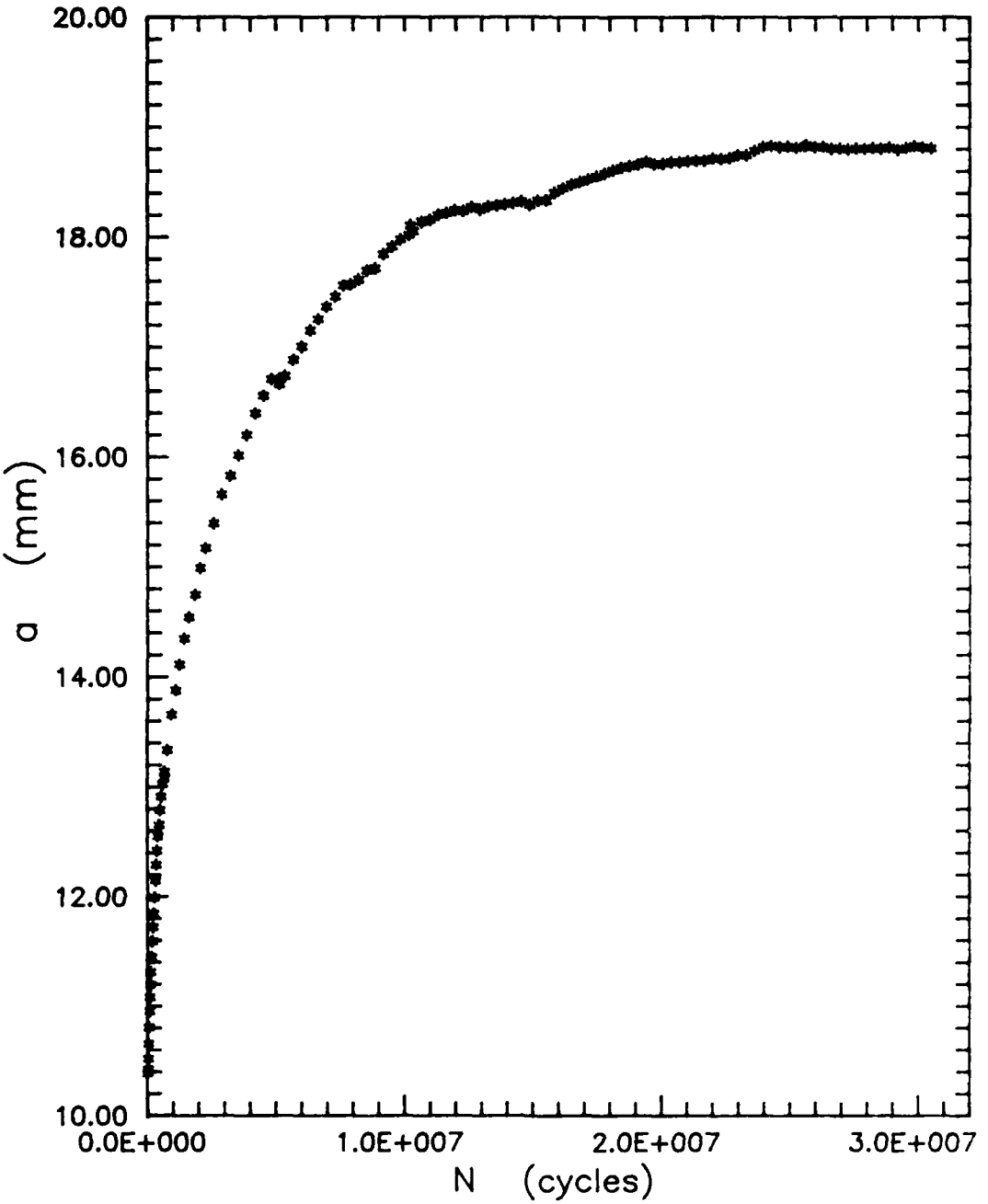

Figure 55. Crack Length History for the ASTM Decreasing K Test with R=0.1

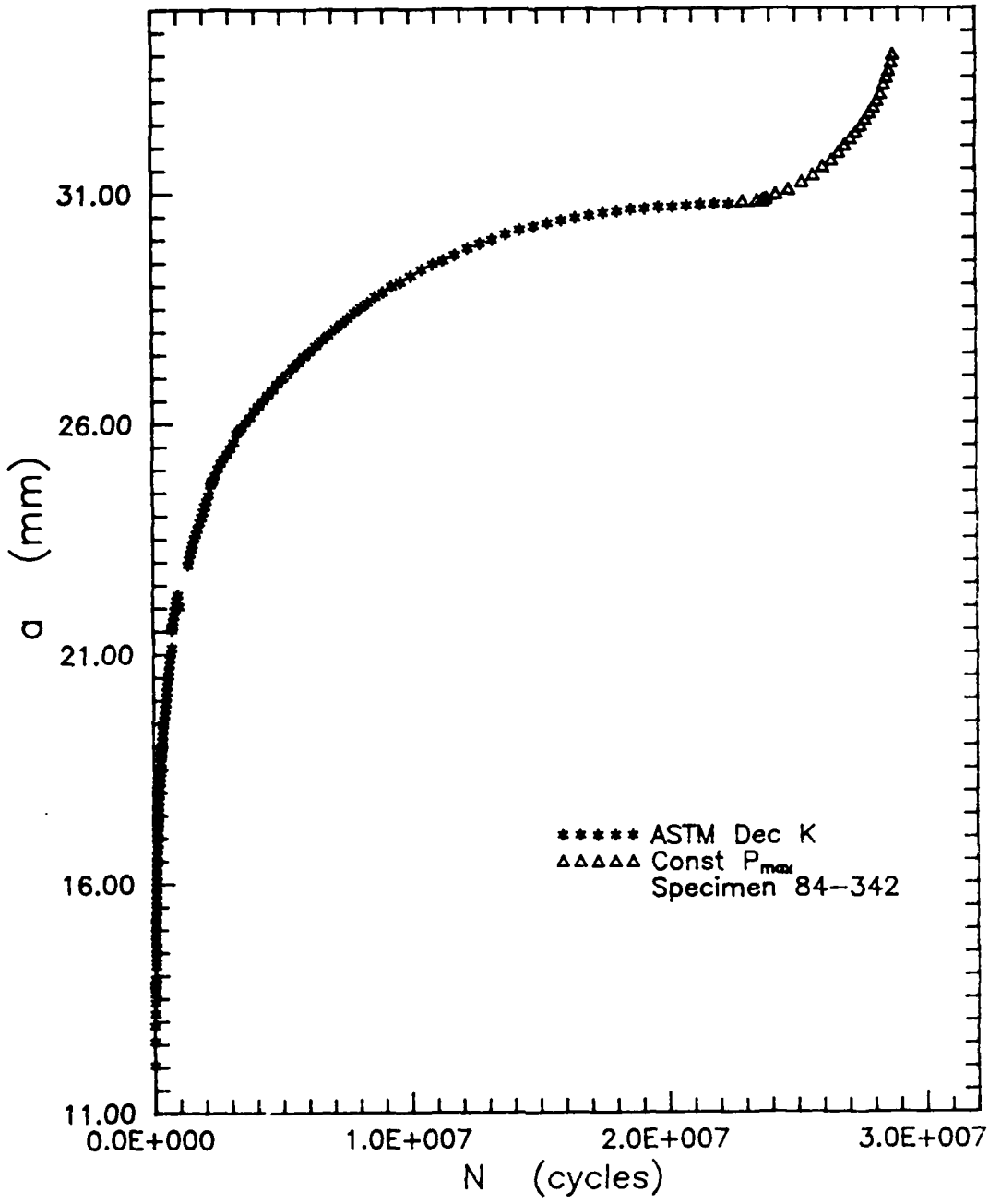

Figure 56. Crack Length History for the ASTM Decreasing K and Constant P_{max} Tests with R=0.5

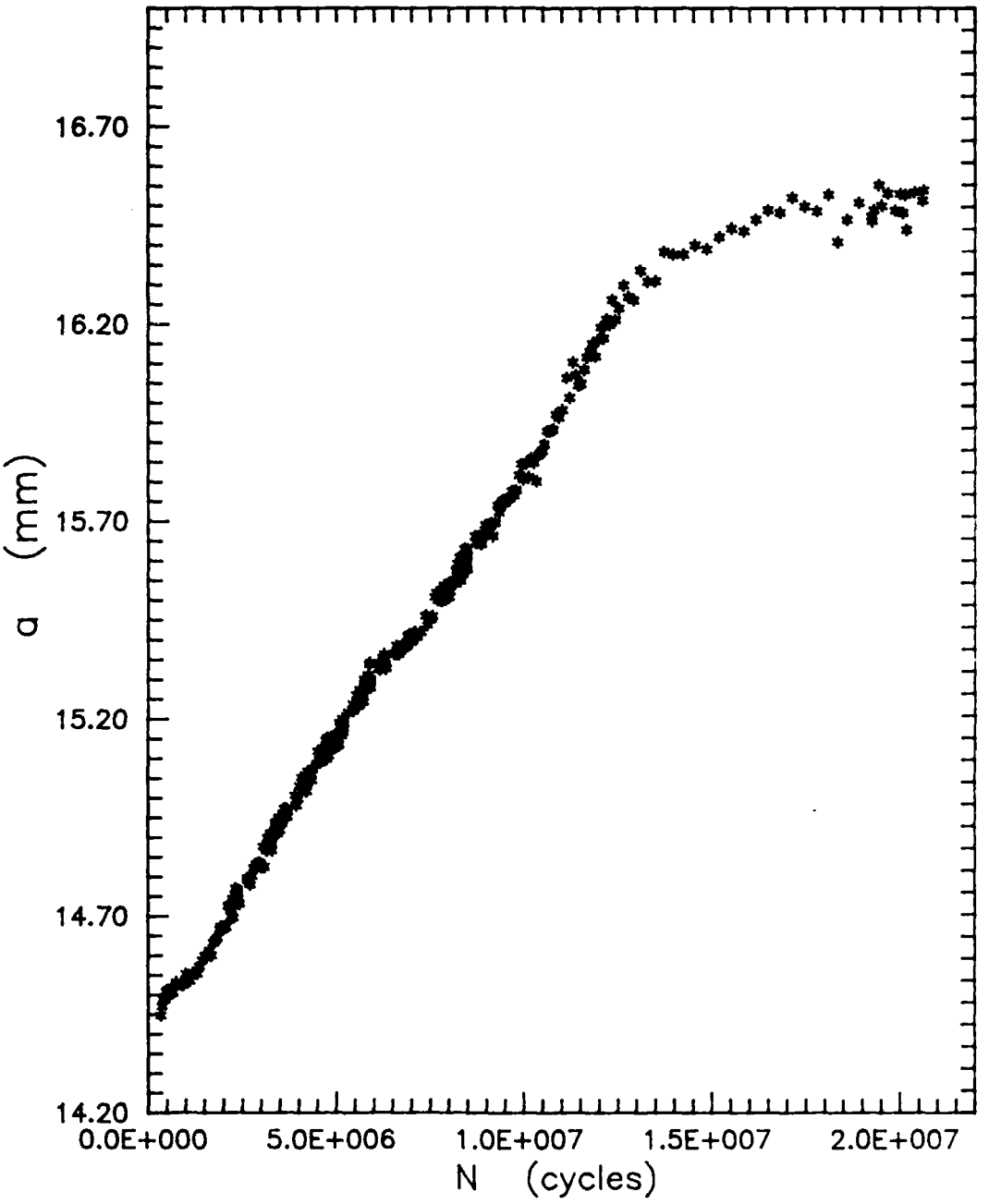

Figure 57. Crack Length History for the Constant K_{max} =6.5 MPa*m**.5 Test

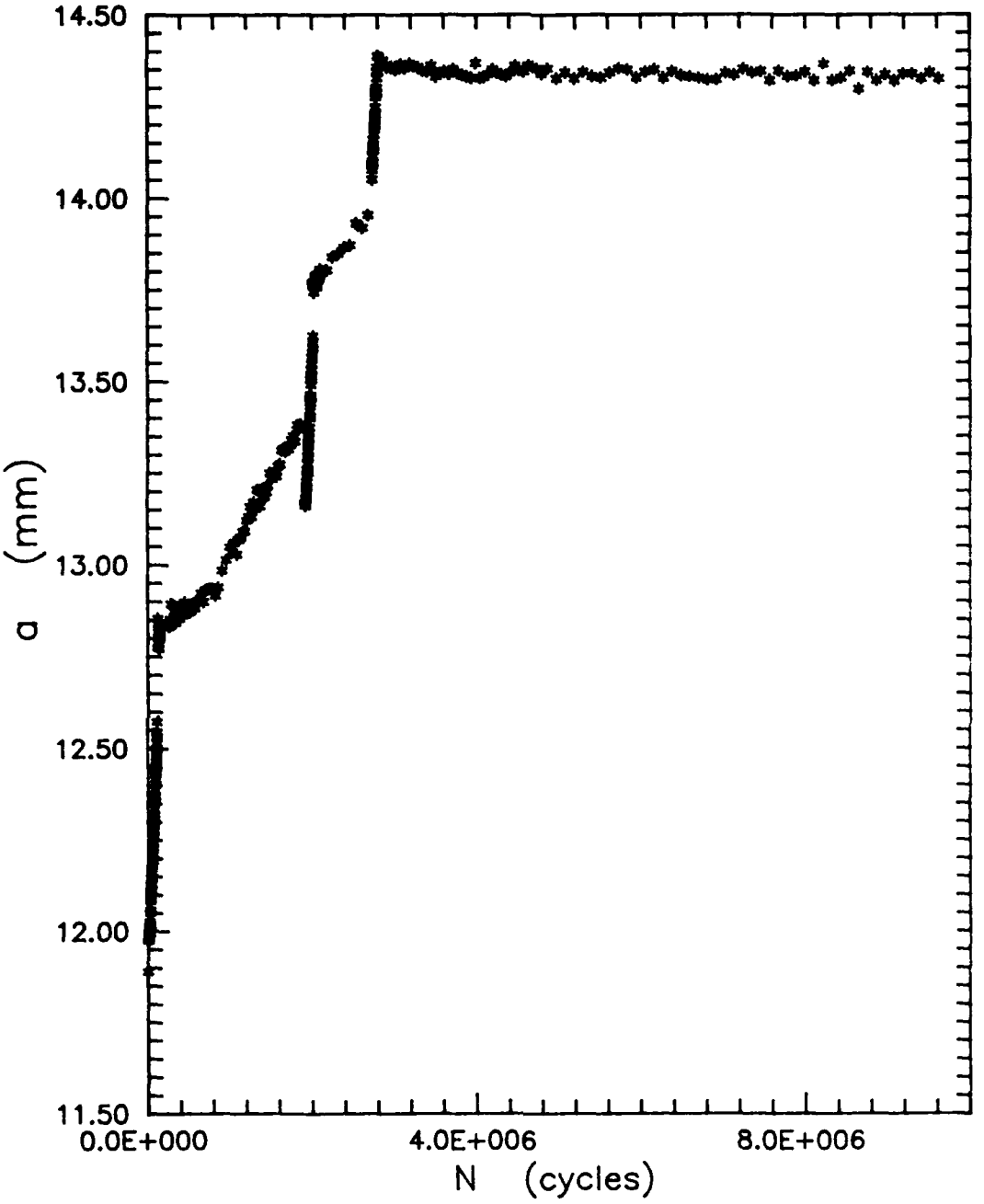

Figure 58. Crack Length History for the Varying ΔK Test with R=0.1 and K_{max0}=10 MPa*m**.5

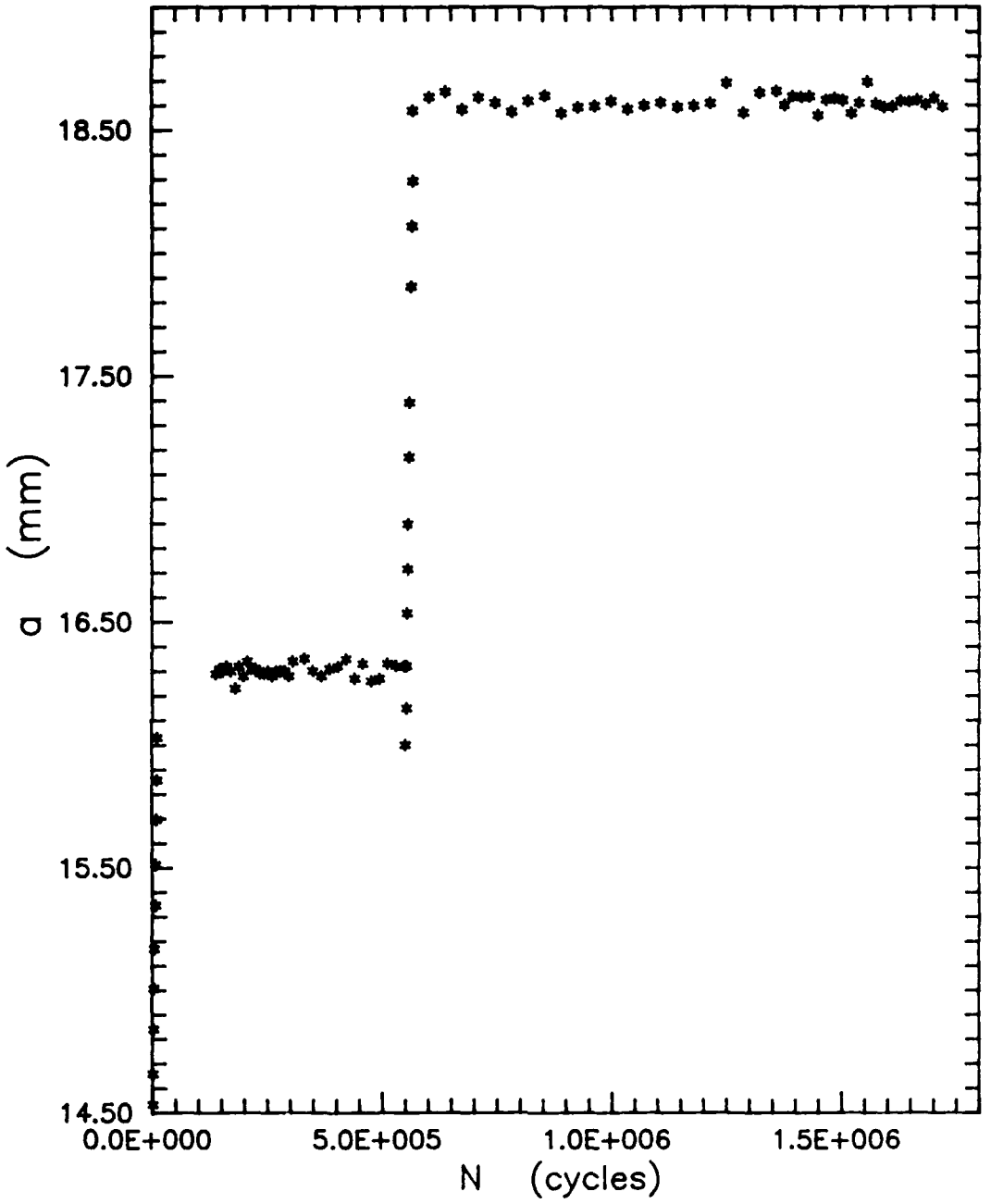

Figure 59. Crack Length History for the Varying ΔK Test with R=0.1 and K_{max0}=20 MPa*m**.5

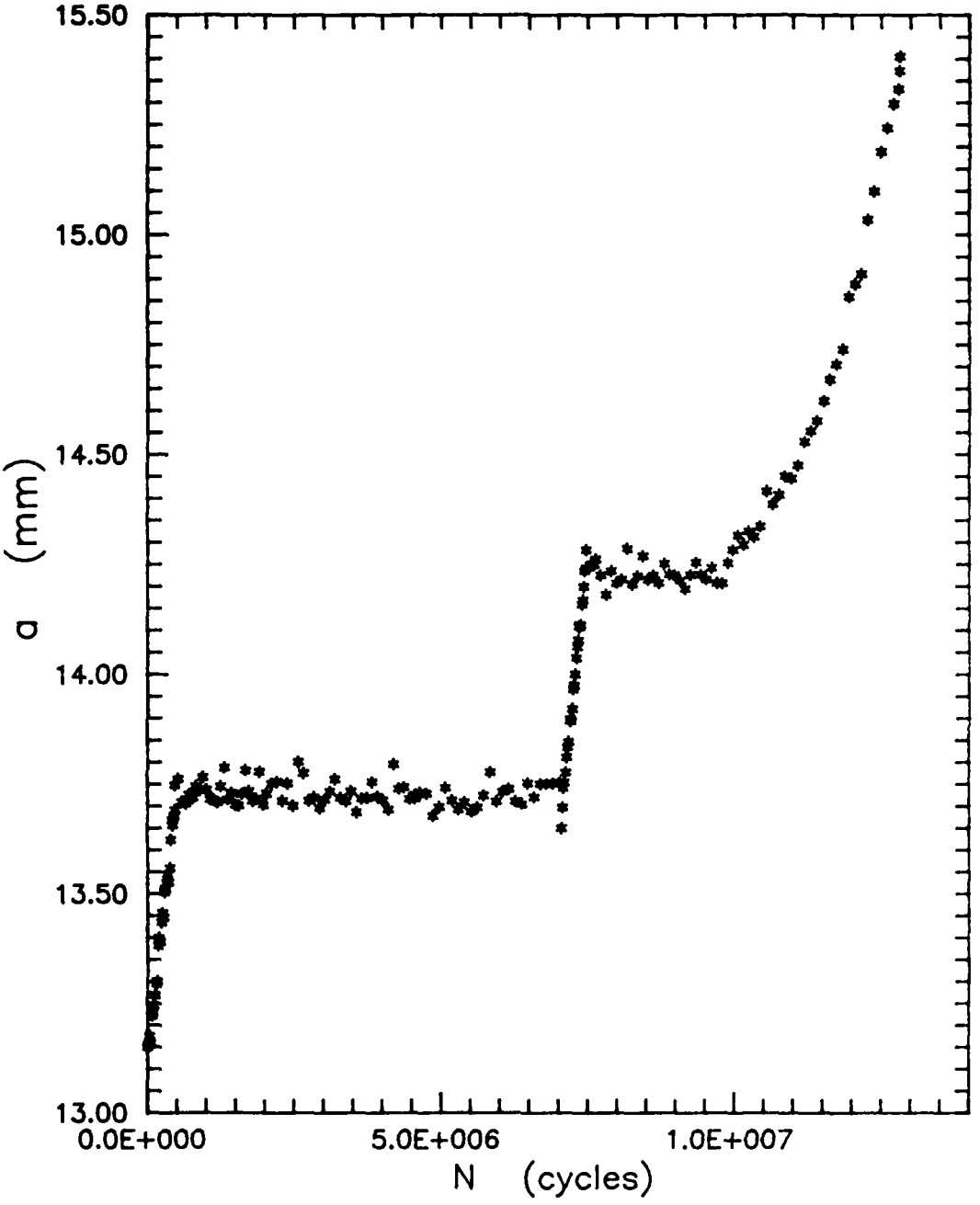

Figure 60. Crack Length History for the Varying ΔK Test with R=0.5 and K_{max0}=10 MPa*m**.5

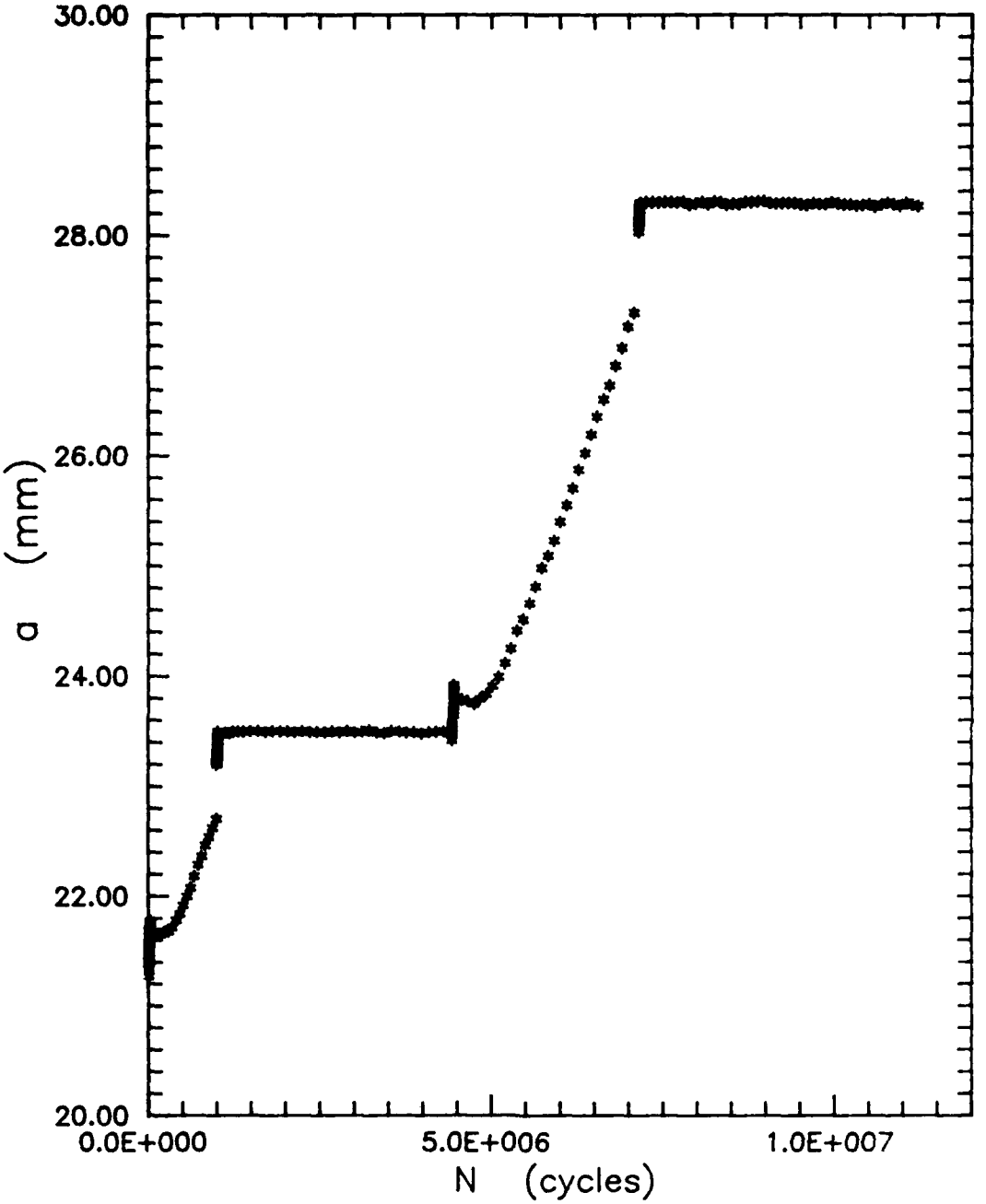

Figure 61. Crack Length History for the Varying ΔK Test with R=0.5 and K_{max0}=20 MPa*m**.5

Appendix E: Crack Growth Rates

The crack growth rates for each test were plotted against the number of cycles run. The figure for the constant K_{max} test at 7 MPa$\sqrt{m}$ is located in Chapter IV. Lines to connect the data points for the varying ΔK tests so that the sequence of loading could be noted.

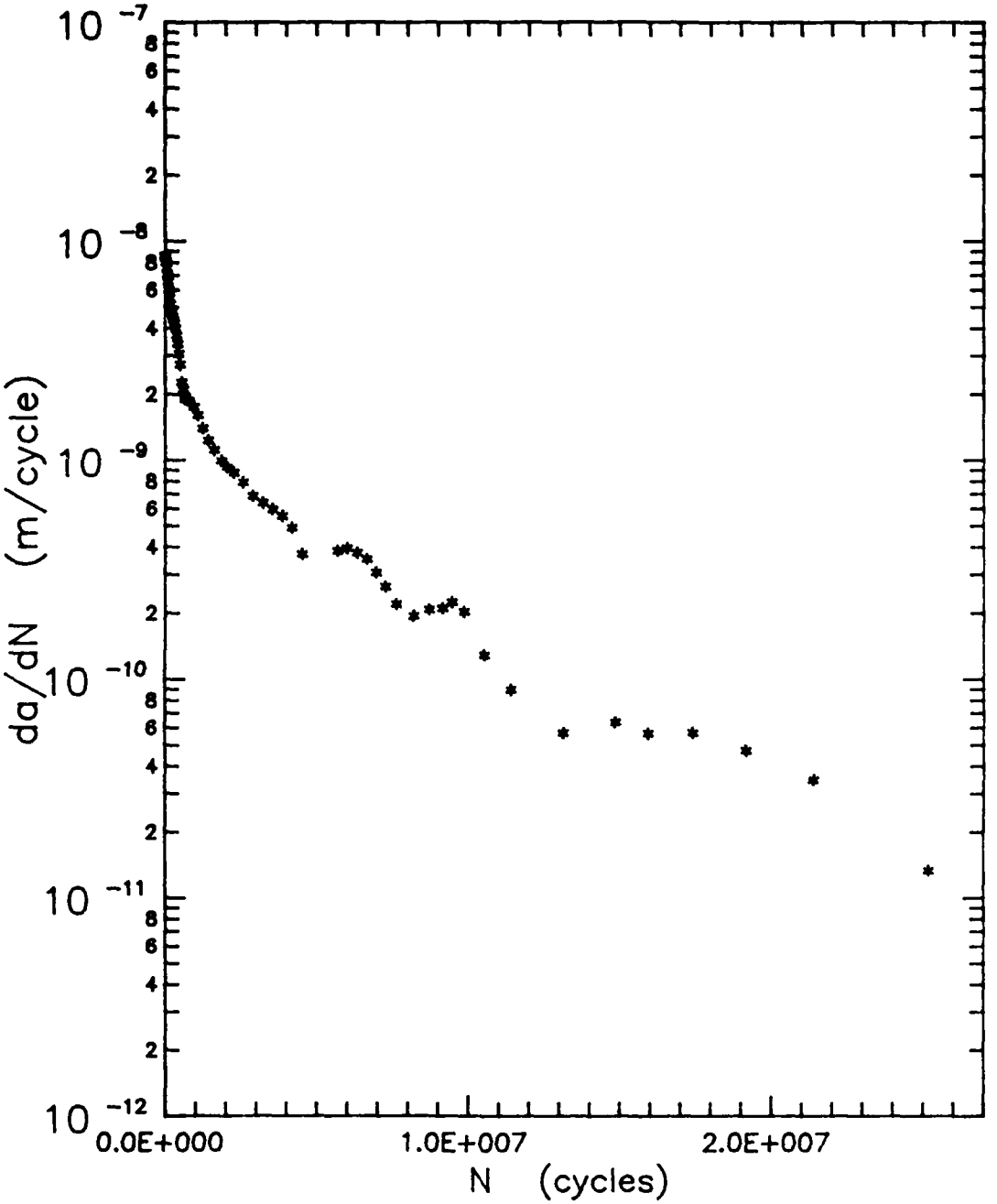

Figure 62. Crack Growth Rates for the ASTM Decreasing K Test with R=0.1

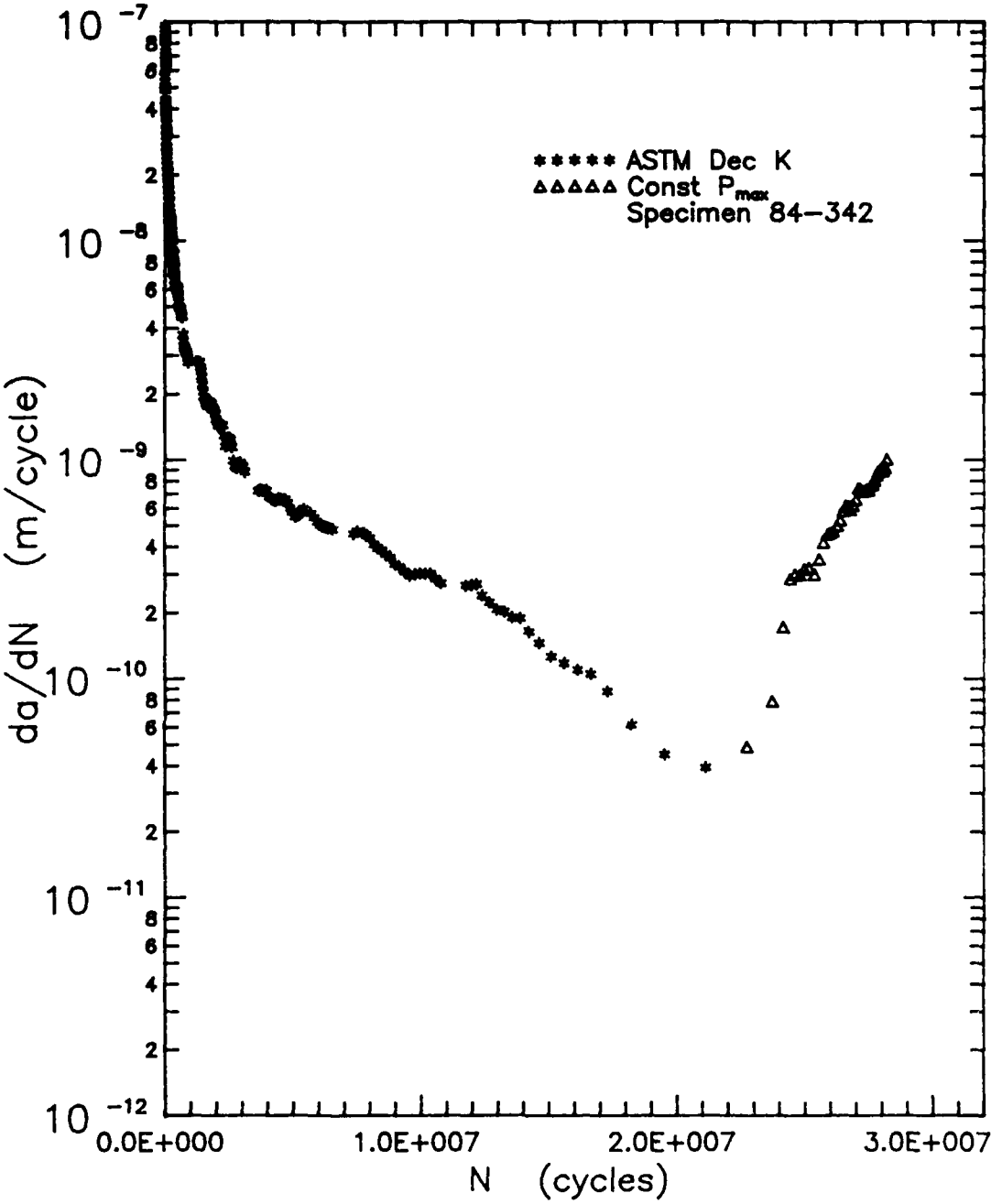

Figure 63. Crack Growth Rates for the ASTM Decreasing K and Constant P_{max} Tests with R=0.5

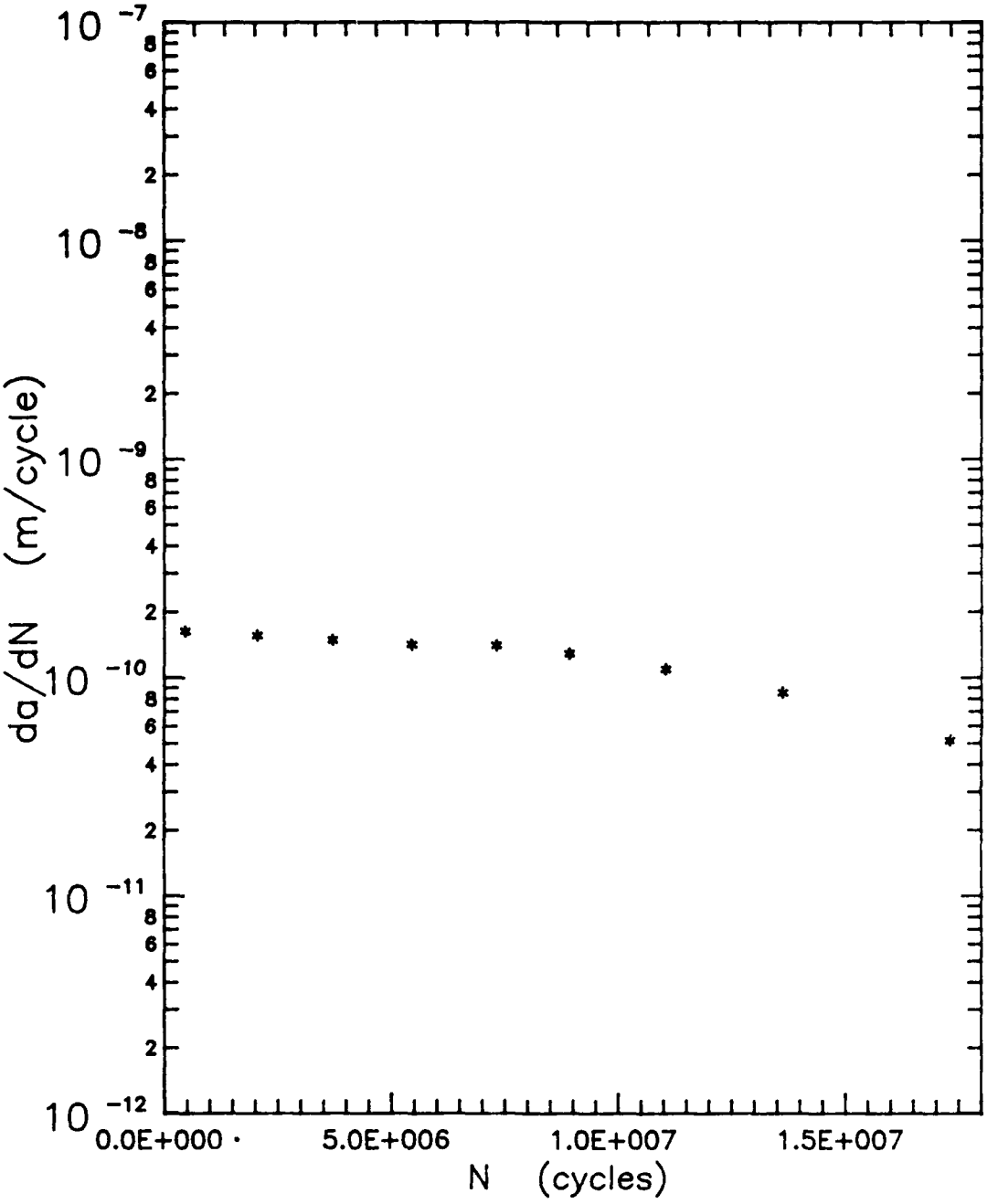

Figure 64. Crack Growth Rates for the Constant K_{max}=6.5 MPa*m**.5 Test

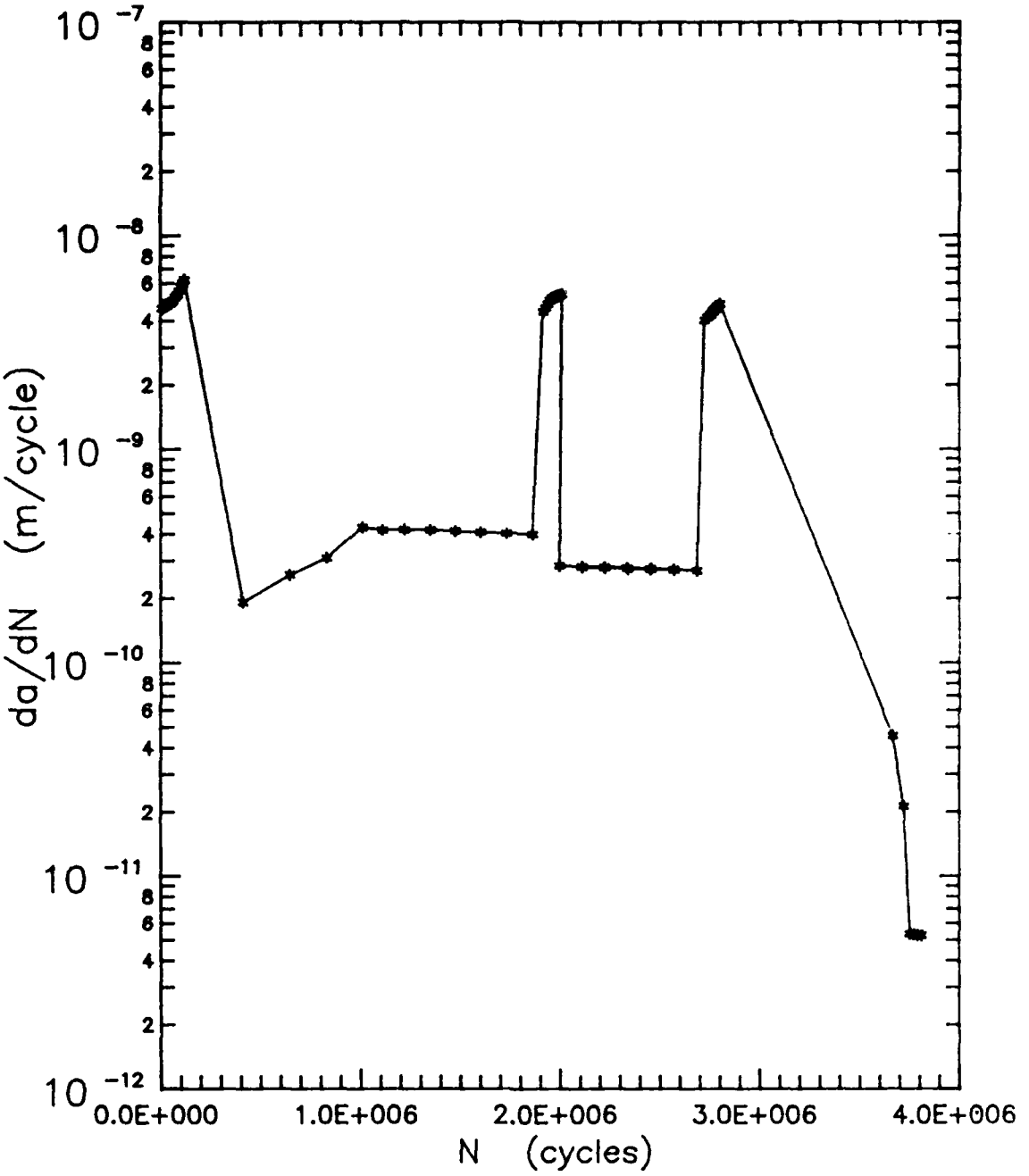

Figure 65. Crack Growth Rates for the Varying ΔK Test with R=0.1 and K_{max0}=10 MPa*m**.5

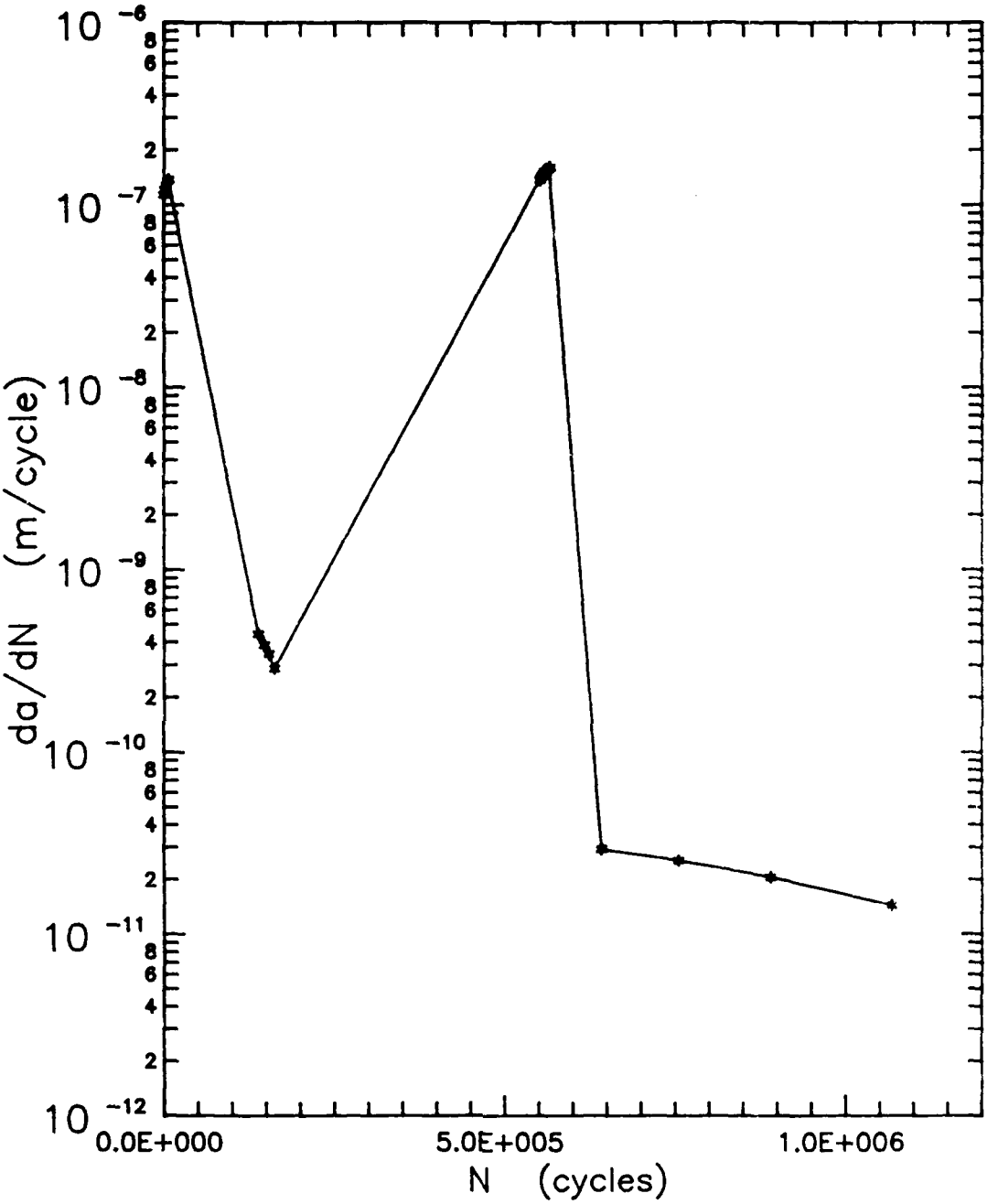

Figure 66. Crack Growth Rates for the Varying ΔK Test with R=0.1 and K_{max0}=20 MPa*m**.5

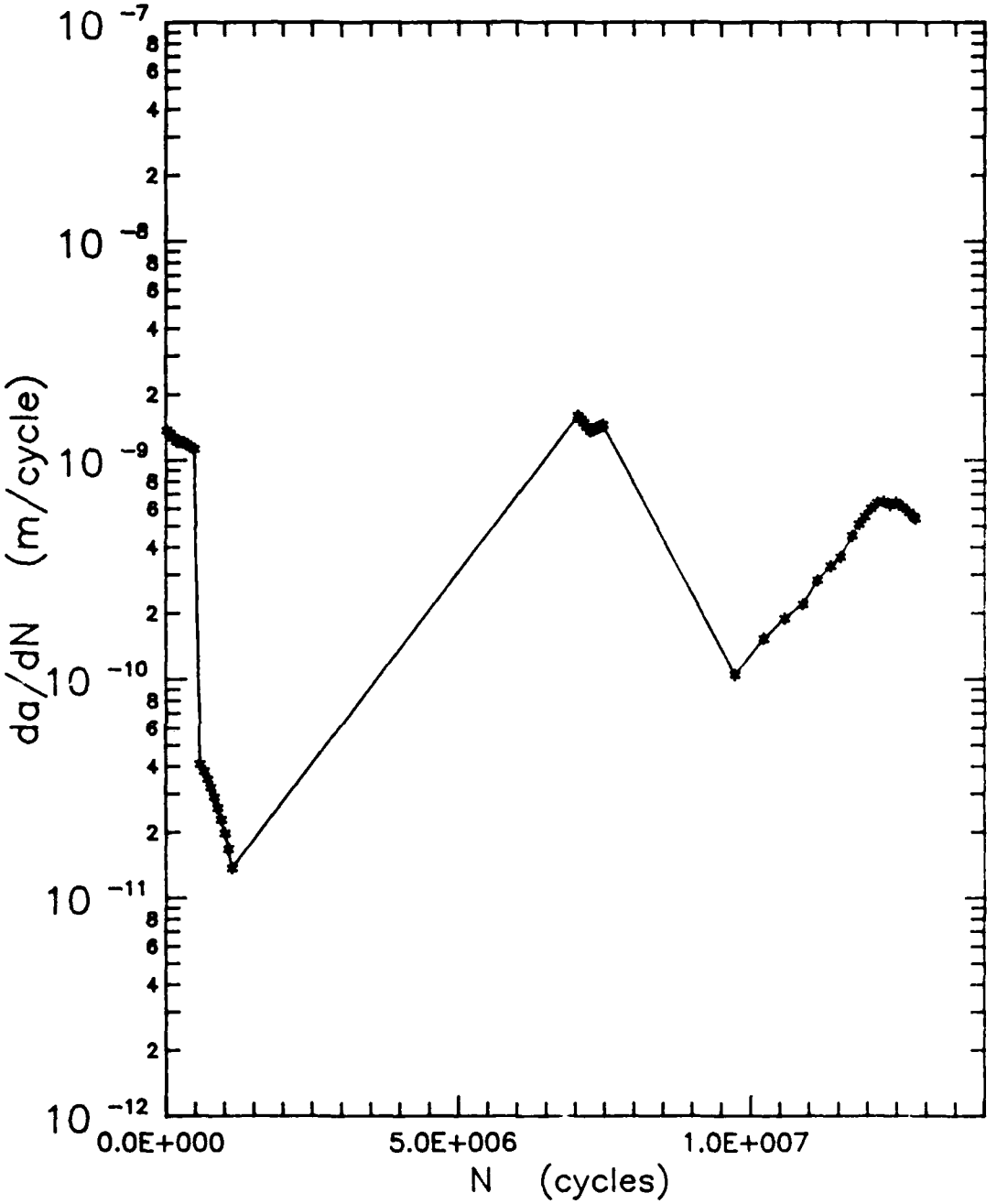

Figure 67. Crack Growth Rates for the Varying ΔK Test with R=0.5 and K_{max0}=10 MPa*m**.5

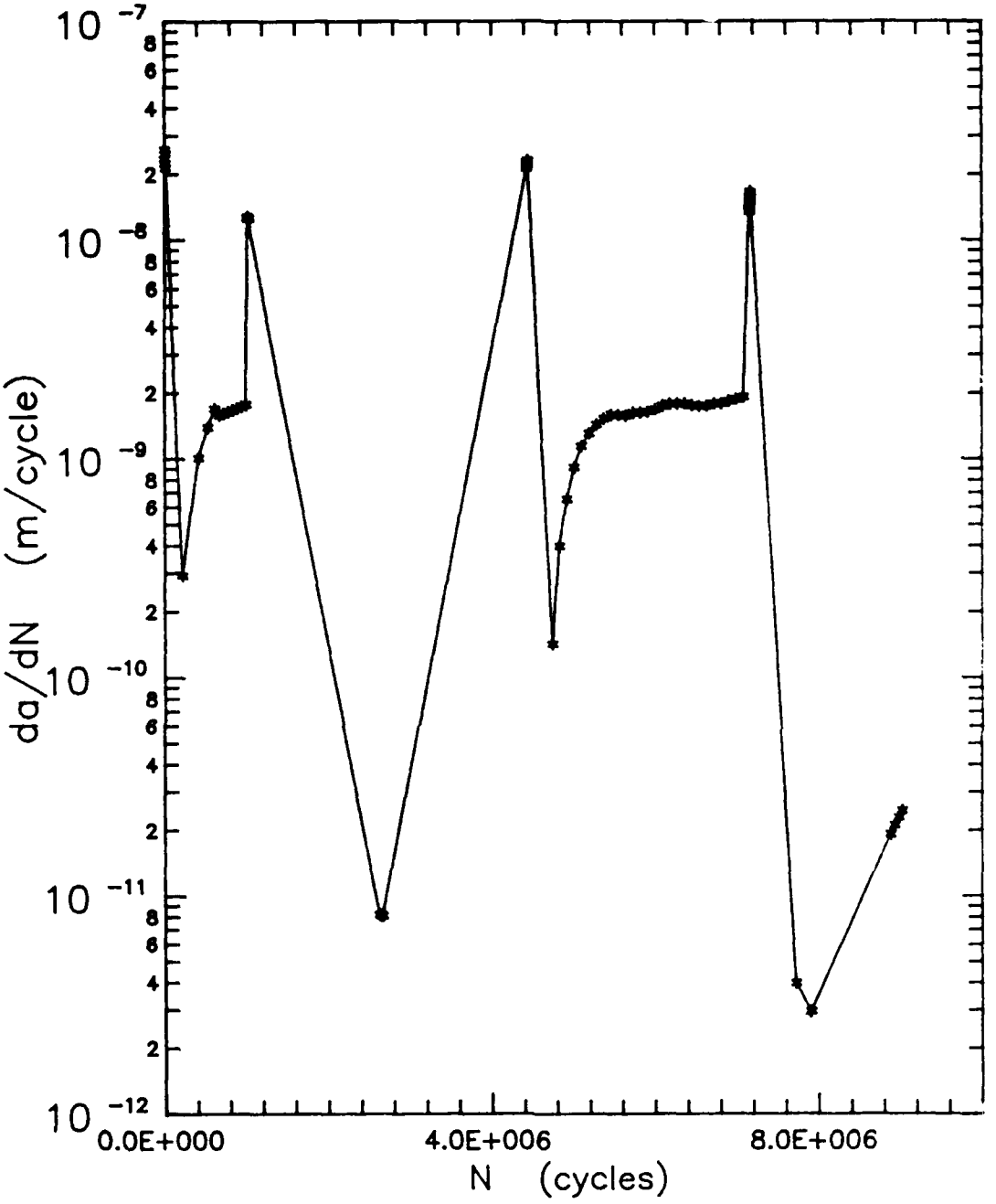

Figure 68. Crack Growth Rates for the Varying ΔK Test with R=0.5 and K_{max0}=20 MPa*m**.5

Vita

Captain Jerardo A. Pérez was born on [redacted] In 1979, he graduated from [redacted] High School in [redacted] He received the degree of Bachelor of Arts in Interdisciplinary Math and Physics from Austin College. Captain Pérez then attended Texas A&M University where he received the degree of Bachelor of Science in Mechanical Engineering in May 1984. Upon graduation, he acquired his commission in the USAF through Officer Training School (OTS). For his first assignment, Captain Pérez worked for the Jet Engine Division, San Antonio Air Logistics Center, Kelly AFB, Texas. He entered the School of Engineering, Air Force Institute of Technology, in May 1987.

[redacted]

UNCLASSIFIED
SECURITY CLASSIFICATION OF THIS PAGE

REPORT DOCUMENTATION PAGE

Form Approved
OMB No. 0704-0188

1a. REPORT SECURITY CLASSIFICATION UNCLASSIFIED	1b. RESTRICTIVE MARKINGS
2a. SECURITY CLASSIFICATION AUTHORITY	3. DISTRIBUTION/AVAILABILITY OF REPORT Approved for public release; distribution unlimited
2b. DECLASSIFICATION/DOWNGRADING SCHEDULE	
4. PERFORMING ORGANIZATION REPORT NUMBER(S) AFIT/GAE/AA/88D-30	5. MONITORING ORGANIZATION REPORT NUMBER(S)
6a. NAME OF PERFORMING ORGANIZATION School of Engineering 6b. OFFICE SYMBOL (If applicable) AFIT/EN	7a. NAME OF MONITORING ORGANIZATION
6c. ADDRESS (City, State, and ZIP Code) Air Force Institute of Technology Wright-Patterson AFB OH 45433-6583	7b. ADDRESS (City, State, and ZIP Code)
8a. NAME OF FUNDING/SPONSORING ORGANIZATION Materials Lab. Air Force Wright Aero. Labs. 8b. OFFICE SYMBOL (If applicable) AFWAL/MLLN	9. PROCUREMENT INSTRUMENT IDENTIFICATION NUMBER
8c. ADDRESS (City, State, and ZIP Code) Materials Laboratory Air Force Wright Aeronautical Laboratories Wright-Patterson AFB OH 45433	10. SOURCE OF FUNDING NUMBERS PROGRAM ELEMENT NO. / PROJECT NO / TASK NO / WORK UNIT ACCESSION NO.

11. TITLE (Include Security Classification)
The Effects of Loading History and Closure on the Fatigue Characteristics of Heat Treated Ti-6Al-2Sn-4Zr-6Mo

12. PERSONAL AUTHOR(S)
Jerardo A. Perez, Capt, USAF

13a. TYPE OF REPORT	13b. TIME COVERED	14. DATE OF REPORT (Year, Month, Day)	15. PAGE COUNT
MS Thesis	FROM _____ TO _____	1988 December	137

16. SUPPLEMENTARY NOTATION

17. COSATI CODES			18. SUBJECT TERMS (Continue on reverse if necessary and identify by block number)
FIELD	GROUP	SUB-GROUP	
11	06	01	Ti 6246, Fatigue Threshold, Crack Closure, Loading History, Laser Interferometric Displacement Gage, (~~IDG~~)

19. ABSTRACT (Continue on reverse if necessary and identify by block number)

Thesis Advisor: Dr. Shankar Mall
Professor
Department of Aeronautics and Astronautics

10 Jan 89

20. DISTRIBUTION/AVAILABILITY OF ABSTRACT	21. ABSTRACT SECURITY CLASSIFICATION
☒ UNCLASSIFIED/UNLIMITED ☐ SAME AS RPT. ☐ DTIC USERS	UNCLASSIFIED

22a. NAME OF RESPONSIBLE INDIVIDUAL	22b. TELEPHONE (Include Area Code)	22c. OFFICE SYMBOL
Dr. Shankar Mall, Professor	(513) 255-3517	AFIT/ENY

DD Form 1473, JUN 86 — Previous editions are obsolete. — SECURITY CLASSIFICATION OF THIS PAGE
UNCLASSIFIED

The purpose of this study was to investigate the effects of loading history and crack closure on the fatigue threshold properties of additionally heat treated Ti-6Al-2Sn-4Zr-6Mo. The crack closure measurements taken by a clip gage, strain gage mounted on the back face (BFS), and laser interferometric displacement gage (IDG) were compared. Also, the effects of heat treatment on the fatigue behavior of Ti 6246 were discussed.

Three tests were run using compact test specimens at a test frequency of 30 hz. Two tests, the ASTM decreasing K and varying ΔK tests, had a constant R, load ratio, throughout the test. For the varying ΔK test, K_{max} was dropped and K_{min} was increased instantaneously after an overload condition. If threshold was not reached, the test was repeated with a larger K_{max} drop after the overload than before. The third test utilized a varying R. For the constant K_{max} test, K_{max} was held constant while K_{min} was gradually increased.

The results from these tests indicated that additionally heat treating Ti 6246 did improve its fatigue threshold characteristics. Also, out of the three measurements techniques used, the IDG measured the highest closure loads. Further, with the constant K_{max} test under tensile cyclic loading, threshold could not be reached for R less than 0.5 as desired for closure studies. The ΔK_{th} was found to be dependent on R, loading history, and crack closure. The $\Delta K_{eff,th}$, on the other hand, was relatively constant for the ASTM decreasing K and constant K_{max} tests. However, since the threshold data for the varying ΔK tests did not coincide with the other tests, $\Delta K_{eff,th}$ should not be considered a material property until further research involving the effects of overloads is conducted.